NUREG/CR-5887
LA-UR-89-2158

Posttest Analysis of MIST Test 3109AA Using TRAC-PF1/MOD1

Prepared by
J. L. Steiner, D. A. Siebe, B. E. Boyack

Los Alamos National Laboratory

Prepared for
U.S. Nuclear Regulatory Commission

AVAILABILITY NOTICE

Availability of Reference Materials Cited in NRC Publications

Most documents cited in NRC publications will be available from one of the following sources:

1. The NRC Public Document Room, 2120 L Street, NW., Lower Level, Washington, DC 20555
2. The Superintendent of Documents, U.S. Government Printing Office, P.O. Box 37082, Washington, DC 20013-7082
3. The National Technical Information Service, Springfield, VA 22161

Although the listing that follows represents the majority of documents cited in NRC publications, it is not intended to be exhaustive.

Referenced documents available for inspection and copying for a fee from the NRC Public Document Room include NRC correspondence and internal NRC memoranda; NRC bulletins, circulars, information notices, inspection and investigation notices; licensee event reports; vendor reports and correspondence; Commission papers; and applicant and licensee documents and correspondence.

The following documents in the NUREG series are available for purchase from the GPO Sales Program: formal NRC staff and contractor reports, NRC-sponsored conference proceedings, international agreement reports, grant publications, and NRC booklets and brochures. Also available are regulatory guides, NRC regulations in the *Code of Federal Regulations*, and *Nuclear Regulatory Commission Issuances*.

Documents available from the National Technical Information Service include NUREG-series reports and technical reports prepared by other Federal agencies and reports prepared by the Atomic Energy Commission, forerunner agency to the Nuclear Regulatory Commission.

Documents available from public and special technical libraries include all open literature items, such as books, journal articles, and transactions. *Federal Register* notices, Federal and State legislation, and congressional reports can usually be obtained from these libraries.

Documents such as theses, dissertations, foreign reports and translations, and non-NRC conference proceedings are available for purchase from the organization sponsoring the publication cited.

Single copies of NRC draft reports are available free, to the extent of supply, upon written request to the Office of Administration, Distribution and Mail Services Section, U.S. Nuclear Regulatory Commission, Washington, DC 20555.

Copies of industry codes and standards used in a substantive manner in the NRC regulatory process are maintained at the NRC Library, 7920 Norfolk Avenue, Bethesda, Maryland, for use by the public. Codes and standards are usually copyrighted and may be purchased from the originating organization or, if they are American National Standards, from the American National Standards Institute, 1430 Broadway, New York, NY 10018.

DISCLAIMER NOTICE

This report was prepared as an account of work sponsored by an agency of the United States Government. Neither the United States Government nor any agency thereof, or any of their employees, makes any warranty, expressed or implied, or assumes any legal liability of responsibility for any third party's use, or the results of such use, of any information, apparatus, product or process disclosed in this report, or represents that its use by such third party would not infringe privately owned rights.

NUREG/CR-5887
LA-UR-89-2158

Posttest Analysis of MIST Test 3109AA Using TRAC-PF1/MOD1

Prepared by
J. L. Steiner, D. A. Siebe, B. E. Boyack

Los Alamos National Laboratory

Prepared for
U.S. Nuclear Regulatory Commission

AVAILABILITY NOTICE

Availability of Reference Materials Cited in NRC Publications

Most documents cited in NRC publications will be available from one of the following sources:

1. The NRC Public Document Room, 2120 L Street, NW., Lower Level, Washington, DC 20555
2. The Superintendent of Documents, U.S. Government Printing Office, P.O. Box 37082, Washington, DC 20013-7082
3. The National Technical Information Service, Springfield, VA 22161

Although the listing that follows represents the majority of documents cited in NRC publications, it is not intended to be exhaustive.

Referenced documents available for inspection and copying for a fee from the NRC Public Document Room include NRC correspondence and internal NRC memoranda; NRC bulletins, circulars, information notices, inspection and investigation notices; licensee event reports; vendor reports and correspondence; Commission papers; and applicant and licensee documents and correspondence.

The following documents in the NUREG series are available for purchase from the GPO Sales Program: formal NRC staff and contractor reports, NRC-sponsored conference proceedings, international agreement reports, grant publications, and NRC booklets and brochures. Also available are regulatory guides, NRC regulations in the *Code of Federal Regulations*, and *Nuclear Regulatory Commission Issuances*.

Documents available from the National Technical Information Service include NUREG-series reports and technical reports prepared by other Federal agencies and reports prepared by the Atomic Energy Commission, forerunner agency to the Nuclear Regulatory Commission.

Documents available from public and special technical libraries include all open literature items, such as books, journal articles, and transactions. *Federal Register* notices, Federal and State legislation, and congressional reports can usually be obtained from these libraries.

Documents such as theses, dissertations, foreign reports and translations, and non-NRC conference proceedings are available for purchase from the organization sponsoring the publication cited.

Single copies of NRC draft reports are available free, to the extent of supply, upon written request to the Office of Administration, Distribution and Mail Services Section, U.S. Nuclear Regulatory Commission, Washington, DC 20555.

Copies of industry codes and standards used in a substantive manner in the NRC regulatory process are maintained at the NRC Library, 7920 Norfolk Avenue, Bethesda, Maryland, for use by the public. Codes and standards are usually copyrighted and may be purchased from the originating organization or, if they are American National Standards, from the American National Standards Institute, 1430 Broadway, New York, NY 10018.

NUREG/CR-5887
LA-UR-89-2158
R4

Posttest Analysis of MIST Test 3109AA Using TRAC-PF1/MOD1

Manuscript Completed: April 1992
Date Published: September 1992

Prepared by
J. L. Steiner, D. A. Siebe, B. E. Boyack

Los Alamos National Laboratory
Los Alamos, NM 87545

Prepared for
Division of Systems Research
Office of Nuclear Regulatory Research
U.S. Nuclear Regulatory Commission
Washington, DC 20555
NRC FIN A7311

For sale by the U.S. Government Printing Office
Superintendent of Documents, Mail Stop: SSOP, Washington, DC 20402-9328
ISBN 0-16-038819-0

CONTENTS

TABLES . . . iv
FIGURES . . . v
ABSTRACT . . . 1
EXECUTIVE SUMMARY . . . 1
I. INTRODUCTION . . . 4
II. TEST DESCRIPTION . . . 5
A. Test Conduct . . . 5
B. Test Phenomena Overview . . . 6
III. TRAC MODEL OF MIST FACILITY . . . 7
IV. CODE DESCRIPTION . . . 8
V. CODE PERFORMANCE . . . 8
VI. COMPARISON OF TEST AND CALCULATED RESULTS . . . 9
A. Steady State . . . 9
B. Transient . . . 9
1. Code-Experiment Comparison Overview . . . 9
2. Detailed Discussion of Transient Results . . . 11
C. Additional Studies . . . 18
1. Studies Related to Knowledge of the Facility . . . 18
2. Studies Related to the Input Model . . . 19
3. Studies Related to Code Models and Correlations . . . 20
VII. LESSONS LEARNED AND CONCLUSIONS . . . 20
A. Knowledge of the Facility . . . 21
B. Input Model . . . 21
C. Code Models and Correlations . . . 21
D. Scaling Implications . . . 22
E. Regulatory Implications . . . 22
1. Background . . . 22
2. MIST SBLOCA Tests . . . 23
3. Conclusions . . . 24
REFERENCES . . . 26
APPENDIX A . . . 48
APPENDIX B . . . 63
APPENDIX C . . . 63
APPENDIX D . . . 65

TABLES

I. STEADY-STATE CONDITIONS FOR TEST 3109AA 28
II. TEST 3109AA TRANSIENT CONTROLS 29
III. EVENT TABLE FOR TEST 3109AA 30
IV. TAG EVALUATION OF ISSUES 31
V. PRIORITY OF SBLOC' EVENTS 32

A-1. COMPONENT DESCRIPTION OF MIST MODEL 52

FIGURES

1. Overview of measured results for MIST Test 3109AA . . . 33
2. Overview of code-experiment comparisons for MIST Test 3109AA . . . 34
3. Primary and secondary pressures . . . 35
4. Total A-loop cold-leg flow . . . 35
5. Total B-loop cold-leg flow . . . 36
6. Pressurizer liquid level . . . 36
7. Core power . . . 37
8. Cold-leg leak and HPI flows . . . 37
9. Leak upstream fluid temperatures . . . 38
10. Full-closed indicators for facility RVVVs . . . 38
11. RVVV flows . . . 39
12. Vapor fraction upstream of RVVVs . . . 39
13. A-loop SG AFW flow . . . 40
14. B-loop SG AFW flow . . . 40
15. Hot-leg U-bend temperatures . . . 41
16. Hot-leg collapsed liquid levels . . . 41
17. A-loop SG collapsed liquid levels . . . 42
18. B-loop SG collapsed liquid levels . . . 42
19. A-loop SG-secondary steam flow . . . 43
20. B-loop SG-secondary steam flow . . . 43
21. Reactor vessel collapsed liquid level . . . 44
22. Downcomer collapsed liquid level . . . 44
23. Cold-leg A1 mass flow . . . 45
24. Cold-leg A2 mass flow . . . 45
25. Cold-leg B1 mass flow . . . 46
26. Cold-leg B2 mass flow . . . 46
27. Primary liquid inventory . . . 47

A-1. MIST facility isometric . . . 55
A-2. TRAC component noding schematic of MIST facility . . . 56
A-3. TRAC reactor vessel noding schematic of MIST facility . . . 57
A-4. TRAC A-loop noding schematic of MIST facility . . . 58
A-5. TRAC A-loop SG noding schematic . . . 58
A-6. TRAC B-loop noding schematic of MIST facility . . . 59
A-7. TRAC B-loop SG noding schematic . . . 59

D-1. CPU time vs real time for Test 3109AA . . . 66
D-2. Time-step size vs real time for Test 3109AA . . . 66
D-3. Number of time steps vs real time for Test 3109AA . . . 67

POSTTEST ANALYSIS OF MIST TEST 3109AA USING TRAC-PF1/MOD1*

by

Donald A. Siebe, James L. Steiner, and Brent E. Boyack

ABSTRACT

We have completed a posttest calculation and analysis of Multi-loop Integral System Test (MIST) 3109AA as the nominal test for the MIST program. It is a test of a small-break loss-of-coolant accident (SBLOCA) with a scaled 10-cm^2 break in the B1 cold leg. The test exhibited the major post-SBLOCA phenomena, as expected, including depressurization to saturation, intermittent and interrupted loop flow, boiler-condenser mode cooling, refill, and postrefill cooldown. Full high-pressure injection and auxiliary feedwater were available, reactor coolant pumps were not available, and reactor-vessel vent valves and guard heaters were automatically controlled. Constant level control in the steam-generator secondaries was used after steam-generator secondary refill and symmetric steam-generator pressure control was used. We performed the calculation using TRAC-PF1/MOD1. We found that agreement between test data and the calculation was generally reasonable. All major trends and phenomena were correctly predicted. We believe that the correct conclusions about trends and phenomena will be reached if the code is used in similar applications.

EXECUTIVE SUMMARY

A TRAC-PF1/MOD1 posttest calculation and data comparison has been completed for the Multi-loop Integral System Test (MIST) nominal test, Test 3109AA. This was the nominal test for the MIST program. It is a test of a small-break loss-of-coolant accident (SBLOCA) with a scaled 10-cm^2 break in the B1 cold leg. During the early test program, several variations of the specified nominal test were run. The test selected for the nominal, Test 3109AA, differs from the pretest specification for Test 310000, the prescribed nominal. A higher initial pressurizer liquid level was used and efforts were made to warm the surge line and maintain the pressurizer liquid at saturation until test initiation. These changes were necessary to compensate for surge-line heat losses that were not prevented by the guard heaters because of too few control zones.

Initiation of the MIST facility in natural circulation rather than pumped flow caused modeling difficulties unique to this facility. An accurate prediction of steam-generator (SG) heat-transfer distribution is necessary to correctly predict steady-state loop flows and, hence,

---

* This work was funded by the US Nuclear Regulatory Commission (NRC), Office of Nuclear Regulatory Research, Division of Reactor and Plant Systems.

initial system pressure and temperatures. Model and code modifications were necessary to achieve this. These are expected to be applicable only to the MIST facility and are used only with the model for it.

The phenomena in the SG secondaries are three dimensional and attempts to model them with one-dimensional components did not yield an adequate steady state. The SG heat transfer was predicted to occur at too low an elevation, and this caused loop flows to be underpredicted at steady state. Input model modifications and code modifications were used to empirically set the auxiliary feedwater (AFW) and heat-transfer distribution so that correct steady-state loop flows and, hence, correct pressures and temperatures were obtained. The transient obtained starting from this steady state gave results that were sufficient for assessing the input model, code models, and correlations used in this application.

Impact on plant calculations for Babcock & Wilcox (B&W) plants should be minimal since these would be initialized in steady state with the reactor coolant pumps controlling loop flows and, hence, system pressure and temperatures. A reduction in the driving potential for natural circulation, caused by predicting the average SG heat transfer at too low an elevation in the SG, would impact the transient calculation by causing loop flow rates to be low and to end early. Thus, primary-to-secondary heat transfer would be underpredicted early in the transient. It would not cause the transient to start from an incorrect steady state. The resulting calculation would be conservative in predicting system depressurization rates during the first few minutes after primary coolant pump coast down since primary-system cooling would be underpredicted.

B&W identified the following major interactions that occurred in Test 3109AA:

1. leak actuation,
2. depressurization to saturation,
3. interruption of Loop A (intact loop, includes the pressurizer),
4. intermittent Loop B (broken-loop) flow,
5. condensation of core-generated vapor passing through reactor-vessel vent valves (RVVVs) by high-pressure injection (HPI),
6. boiler-condenser mode (BCM) heat transfer in SGs,
7. quasi-equilibrium established between leak flow and HPI flow,
8. intermittent spillovers of hot-leg liquid through the U-bend into the SGs during refill, and
9. cooldown to test termination with one loop active.

Depressurization of the primary before the loop flows ceased occurred mainly because of primary-to-secondary heat transfer in the SGs. After the cessation of loop flow, depressurization was the result of condensation by HPI fluid of core-generated steam that passed through the RVVVs into the downcomer and by leak-HPI feed-and-bleed cooling. BCM heat transfer contributed to the primary depressurization after controlled depressurization of the SG secondaries was begun. During refill, primary-to-secondary heat transfer during the spillovers contributed to depressurization.

The TRAC calculation is in reasonable agreement with the test. The phenomena listed, through the establishment of quasi-equilibrium between leak and HPI flow, were predicted. The calculation was terminated before the system refilled sufficiently for the other phenomena to occur. Our lessons learned and key conclusions have been subdivided into areas related to

(1) knowledge of facility configuration and operation, (2) the facility input model used with TRAC, and (3) code models and correlations; we have also considered scaling and regulatory implications.

Knowledge of Facility Configuration and Operation

SG energy losses, whether heat losses or secondary-side steam losses, and possible heat addition to the SG secondaries by the guard heaters were not adequately understood. In the test, the secondary pressures were very stable during a period with no loop flows and no AFW flows. In the calculation, the secondary pressures drifted up as the secondary fluid came to thermal equilibrium with SG metal mass. We believe that the facility had greater energy losses than those included in the calculation such that temperatures and pressures did not rise in response to heat transfer from metal mass. SG-secondary pressures did not decline because of the greater losses since these losses were apparently offset by the guard heaters. A stable pressure response resulted. Our knowledge of the facility and its operation from specifications and from test data has been inadequate to resolve the precise nature of the SG energy balances.

Since this unexpected stability in SG-secondary pressures during periods of no SG activity occurred in other tests, as well as in the nominal test, it would be desirable to understand this phenomenon more fully. The result of this inadequate knowledge of the SG energy balance on the TRAC calculation was that the timing to reach set points was not accurately predicted. This problem is not deemed significant enough to warrant rerunning the calculation.

Input Model

We found the input model to be adequate for the nominal test, a CBLOCA, in the MIST facility. No areas were found that suggested a need to review the input model, including noding.

Code Models and Correlations

We found two areas of concern regarding TRAC constitutive models and correlations. First, the critical flow model during liquid flow shows a sensitivity to subcooling not observed in the data for Test 3109AA. Second, we found that TRAC underpredicted the BCM heat transfer near the start of SG refill. Even though the condensation surface area and AFW flow matched the data, the primary-system depressurization during this event was too small.

Scaling Implications

The issue of scaling is one of the most difficult with which to deal. At the level of TRAC models and correlations, some effort has been made to deal with scaling as part of the TRAC-PF1/MOD1 documentation effort. However, it is difficult to review individual constitutive models and correlations and build a definitive statement about scalability for prediction of transients in a full-size plant. A large effort is currently in progress to quantify the uncertainty of using TRAC-PF1/MOD1 for prediction of large-break loss-of-coolant accidents. Los Alamos supports addressing the scaling question through application of Code Scaling, Applicability, and Uncertainty or similar methodology.

There is one other activity within the MIST Phase-IV test program that will prove helpful in addressing scaling. A counterpart test to the Crystal River event will be conducted. Within the limitations of the MIST test facility, every effort will be made to simulate key events and

phenomena in the transient. TRAC calculations are planned for the MIST plant counterpart transient and for the full-size plant event. These activities should provide direct information about code scalability as the key transient phenomena are calculated in a model of both the full-size plant and the MIST facility with its scale factor of 1/817 for volume and power.

Regulatory Implications

We have concluded that the TRAC-calculated results are in reasonable overall agreement with the data for Test 3109AA. All major trends and phenomena were correctly predicted. The observed differences between the measured and calculated results have been traced and related, in part, to deficiencies in our knowledge of the facility configuration and operation. We have identified two models for which additional review is appropriate. However, in general, the TRAC closure models and correlations appear to be adequate for the prediction of the phenomena expected to occur during SBLOCA in the MIST facility. We believe that the correct conclusions about trends and phenomena will be reached if the code is used in similar applications.

I. INTRODUCTION

The Multi-loop Integral System Test (MIST) facility is a scale model of a Babcock & Wilcox (B&W) nuclear power plant. The facility is located in Alliance, Ohio, and is designed to experimentally investigate transients occurring after reactor trip and primary-pump coast down. Data from the MIST facility are used to help resolve current plant licensing issues and also to assess and refine computer codes used to analyze plant thermal-hydraulic behavior.

A primary goal of our code assessment is to evaluate the adequacy of the correlations and models in the Transient Reactor Analysis Code (TRAC). A related goal is to assist in developing an understanding of the phenomena occurring during the experiment. A secondary goal is to evaluate input modeling practices and develop user guidelines. In order to achieve these goals, it is necessary to understand the reasons for differences between test data and calculated values. These fall into three categories. First, a difference may be the result of an incomplete or inaccurate knowledge of the facility or its operation, including the instrumentation and the resulting data. Although this might seem to be a minor problem, it has not been for many facilities. Differences of this type may be difficult to isolate and can mask problems with the input model or the code. Documentation of the MIST facility, its operation, and data qualification are excellent, although there have been occasional problems as can occur in any complex facility or test sequence. Second, the input model may be inadequate because of modeling compromises, noding, use of one-dimensional instead of three-dimensional models, etc. Third, inadequacies in the code closure models and correlations can cause differences. A major task of an analyst in code assessment calculations is to understand the differences between calculation and test within this framework, and in the case of code deficiencies, to identify the particular code model or correlation causing the difference.

The objective of this report is to document assessment studies performed using TRAC-PF1/MOD1 (Ref. 1) by comparing code-calculated valves to the experimental data for MIST Test 3109AA (Refs. 2–3). MIST Test 3109AA was selected for posttest analysis because of its potential to challenge the predictive capability of TRAC. It exhibited most of the small-break loss-of-coolant accident (SBLOCA) phenomena expected, and as the nominal, forms the basis for comparison for the remainder of the MIST experiments. A pretest analysis of MIST Test

310000, the prescribed nominal, was completed and reported in Ref. 4. Differences between the as-run nominal, Test 3109AA and the prescribed nominal, as well as an inadequate steady state caused by steam-generator (SG) model inadequacies, were sufficient to warrant running a posttest calculation for Test 3109AA as well as the pretest calculation for Test 310000.

II. TEST DESCRIPTION

Test 3109AA is the as-run nominal test for the MIST program. It represents a SBLOCA and exhibited the major post-SBLOCA phenomena. It is the reference transient for the MIST program. The phenomena include depressurization to saturation, intermittent and interrupted loop flow, boiler-condenser mode (BCM) cooling, refill, and postrefill cooldown.

The break modeled was a scaled 10-cm^2 (0.01076-ft^2) break in the B1 cold-leg pump discharge. High-pressure injection (HPI) and auxiliary feedwater (AFW) flow were available. Reactor coolant pumps were not available. The reactor-vessel vent valves (RVVVs) were automatically controlled on differential pressure throughout the transient. Guard heaters and SG-secondary liquid levels were automatically controlled, with the SG-secondary levels maintained at a constant level after refill.

A. Test Conduct

The primary system was initialized in single-phase natural circulation in Test 3109AA. The transient was initiated from this natural-circulation steady state with hot- and cold-leg average thermocouple readings of 584.4 K (592.3°F) and 561.4 K (550.9°F), respectively. Primary pressure was at 11.99 MPa, yielding 13.3 K (23.9°F) subcooling in the hot legs. These values were within specification. During the steady state, the guard heaters were in automatic operation, the RVVVs were manually closed, and the core power was 3.9% of scaled full power. The pressurizer level was 1.57 m (5.2 ft) above the bottom of the pressurizer, and the A and B SG-secondary pressures and levels were 6.991 and 6.998 MPa (1014 and 1015 psia) and 1.42 and 1.44 m (4.65 and 4.74 ft), respectively, during steady-state initialization of Test 3109AA. Again, these were within specification. Steady-state test conditions are summarized in Table I.

The initiating event in Test 3109AA was a scaled 10-cm^2 (0.01076-ft^2) leak in the cold-leg pump discharge piping; this event defined the beginning of the transient part of the test. The steady-state control functions were preserved into the transient until the pressurizer level decreased to 0.305 m (1 ft). At that time, the following five control actions were taken: (1) change the SG-secondary level control set point to 9.63 m (31.6 ft), (2) activate full HPI flow, (3) start core power decay, (4) transfer RVVV control from closed to automatic/independent operation with open/close set points of 862 Pa (0.125 psi) and 276 Pa (0.04 psi), and (5) begin abnormal transient operator guidelines (ATOG)-based SG-secondary pressure control (Ref. 5). These are the major transient-control actions specified for Test 3109AA that are listed in Table II.

The SG-secondary pressure was automatically controlled during the test with a control scheme based on the ATOG. The ATOG-based set-point pressure was determined from the core-exit temperature and the two saturation temperatures corresponding to the SG-secondary pressures. Depending on these three temperatures, the ATOG-based set-point pressure could be (1) held constant, (2) reduced by 0.345 MPa/min (50 psi/min), or (3) reduced such that the corresponding saturation temperature is reduced by 55.56 K/h (100°F/h). The logic for

selecting which of these three pressure-control modes is to be used is explained in detail in Ref. 5. The ATOG-based set-point pressure was determined automatically during Test 3109AA and applied to both SGs.

Manual-control actions for Test 3109AA were also specified. These would have been necessary during the transient depending on system conditions. Actions and their criteria for initiation are discussed in detail in Ref. 5. The manual-control actions included (1) manually opening the power-operated relief valve (PORV) if the system pressure reached 16.2 MPa (2350 psia), (2) isolating the core flood tank (CFT), depending on core-exit subcooling, (3) opening the high-point vents (HPVs), depending on system conditions or time, and (4) throttling the HPI flow according to pressurizer level and core-exit subcooling if the PORV was closed. None of these conditions were met during the part of the transient that was calculated with TRAC.

B. Test Phenomena Overview

Test 3109AA, the as-run nominal for the MIST program, was initiated at time zero from the steady state reported in Table I by initiating the scaled 10-cm^2 (0.01076-ft^2) break in the B1 cold leg. At time zero, the primary was liquid full and coolant was being driven by natural circulation. As the pressurizer level fell below 0.305 m (1 ft) at 150 s, several actions were taken. The core-power decay was started, HPI begun, and RVVV automatic control was initiated, allowing the RVVVs to open. Refill of the SG secondaries was also started as the level set point was changed from 1.52 m (5 ft) to 9.63 m (31.6 ft). An overview of the resultant test transient is shown in Fig. 1. Only test data are presented in Fig. 1.

Figure 1.a gives the primary and secondary pressure traces from the test data. Saturation first occurred in the intact-loop hot leg at 185 s. Liquid from the pressurizer warmed the liquid in the intact-loop hot leg so that flashing first occurred in the intact-loop U-bend. A vapor bubble grew rapidly as primary inventory decreased as the hot-leg liquid level dropped away from the intact-loop U-bend (Fig. 1.b). Natural-circulation flow in the intact loop (Fig. 1.c) ended at 240 s as the liquid level in the hot leg dropped too low for spillovers to occur. This effectively decoupled the intact-loop SG as a heat sink. Broken-loop flows, shown by Fig. 1.d, continued.

As the SG secondaries (levels given by Figs. 1.e and 1.f) were refilled by AFW (flow rates given by Figs. 1.g and 1.h), the liquid level in the intact-loop SG primary dropped so that condensing surface was exposed in tubes cooled by the AFW. This resulted in intermittent NCM heat transfer from about 565 to 1000 s as the intact-loop SG-secondary liquid level reached the high set point, and some AFW was required as the liquid level settled in on the set point. This was a threshold event that had an impact on the early course of the transient (it did not occur in a repeat of the as-run nominal test).

The condensation in the intact-loop SG reduced the pressure in the intact-loop U-bend, raising the liquid level in that SG. This shifting of primary inventory contributed to voiding in the broken-loop U-bend. Starting at about 900 s, broken-loop flow (Fig. 1.d) decreased rapidly. At about 1000 s the broken-loop flow reached a minimum.

With the decrease in broken-loop flow, primary-to-secondary heat transfer was reduced. This caused the primary to begin to repressurize at about 1000 s (Fig. 1.a). Voiding in the upper head of the reactor vessel began to push more liquid into the hot legs, causing the broken-loop flow to increase. At 1150 s, the RVVVs closed (Fig. 1.i) as different draining rates in vessel and downcomer exposed the downcomer side of the RVVVs to liquid and the

upper-plenum side to vapor. With the RVVVs closed, steam production in the reactor vessel forced more liquid up the broken-loop hot leg and over the U-bend. This flow occurred in surges. At 1575 s, the RVVVs reopened as draining of the vessel and downcomer exposed the RVVV nozzles. Reopening the RVVVs allowed steam to flow from vessel to downcomer. Flow over the broken-loop U-bend ended because core-generated steam was no longer forcing liquid up the hot legs. With this steam passing through the RVVVs, the repressurization ended as cold HPI liquid condensed some of this core-generated steam in the downcomer.

After the cessation of broken-loop flow, the system entered a relatively inactive period. The system was slowly cooling and depressurizing because the enthalpy of the HPI was less than the enthalpy of the leak flow, and the core power was decreasing along the decay curve. AFW was off in both SGs as the ATOG-based secondary-pressure set point was above the SG secondary pressures. SG-secondary pressures remained nearly constant until the set point decreased to the actual pressures.

The ATOG-based set point was reached at 3600 s. The level in the intact-loop SG primary (Fig. 1.e) was well below the AFW nozzle elevation so that a large surface area was available for condensation when AFW was restarted. This BCM heat transfer caused a significant increase in the depressurization rate. Primary pressure was reduced sufficiently for HPI flow (Fig. 1.j) to exceed leak flow, marking the beginning of refill. The liquid level in the reactor vessel stayed near the elevation of the hot legs (Fig. 1.k) and did not approach the top of the core during the transient.

Condensation in the intact-loop SG reduced the pressure in the U-bend so that the level rose in the intact-loop SG and hot leg. This caused the level in the broken-loop SG to drop. In the test, the level dropped below the 15.48-m (50.8-ft) AFW nozzle elevation, and BCM heat transfer then occurred in the broken-loop SG as the level changed. These BCMs produced a large depressurization rate, which increased the refill rate. A primary repressurization started at about 5500 s because the primary-system inventory (Fig. 1.l) had increased so that SG levels were sufficiently high to preclude BCM heat transfer. The repressurization ended at about 9000 s. During this period, the leak flow rate increased to near the HPI flow rate, resulting in a near-equilibrium condition that lasted for about 3 h. A series of five spillover events started at about 17000 s as the refill raised the liquid level in one of the hot legs to the U-bend. Each of these caused core subcooling and a consequent throttling of HPI, which reduced the hot-leg level below the U-bends. At about 25000 s (~7 h), refill was sufficient to restart natural circulation on a continuous basis in the B loop. The primary pressure then stabilized around 1.4 Mpa. The test was terminated after 12 h on the maximum time criteria.

III. TRAC MODEL OF MIST FACILITY

The TRAC-PF1/MOD1 input model of the MIST facility is constructed entirely of one-dimensional components. The model consists of 77 components that have been subdivided into 276 fluid cells. A detailed description of the input model is provided in Appendix A. Archival information related to the input mode used in the calculation of MIST Test 3109AA is found in Appendix B. Model development was based on information found in Refs. 6–7.

IV. CODE DESCRIPTION

The calculations reported herein were performed with TRAC-PF1/MOD1, version 12.7, with a MIST-specific update. TRAC-PF1/MOD1 code (Ref. 1) was developed at Los Alamos National Laboratory to provide best-estimate predictions of postulated accidents in light-water reactors. The code features a two-phase, two-fluid nonequilibrium hydrodynamics model with a noncondensable gas field; flow-regime-dependent constitutive equation treatment; either one- or three-dimensional treatment of the reactor vessel; complete control-systems modeling capability; a turbine component model; and a generalized SG component model.

Code modifications were necessary for this application. We made changes in the TRAC-PF1/MOD1 code to improve the calculation of falling-film heat transfer on the secondary side of the SG tubes when the AFW is active. The falling-film heat transfer from the AFW was calculated in the updated code version by redistributing the liquid in the single-channel secondary to the heat slabs connected to the three-tube primary channel (see Appendix A for a description of the SG model). In addition to the liquid redistribution, a multiplier was applied to the Chen correlation heat-transfer coefficient for the wetted-channel heat slabs. These code changes resulted in a more accurate calculation of the heat-transfer distribution and the thermal-center elevation in the SG. We note that the code update produced (see Appendix B) is specific to the MIST facility and not for general application.

Archival information about the TRAC-PF1/MOD1 version used for this study is presented in Appendix B. A draft document describing the TRAC-PF1/MOD1, version 14.3 models and correlations has been prepared.[8] In addition, a TRAC-PF1/MOD1 user's manual[9] is available.

V. CODE PERFORMANCE

There are several measures of code performance that are of interest to the user of a particular code. These measures are used to assign value to the code-calculated result. As used here, value is a combination of the quality of the technical result produced and the cost required to produce that result. First, the user is interested in the degree to which the code predicts phenomena occurring in nature (test facility or full-size plant). In this report we have attempted to characterize the degree to which the TRAC-calculated results agree with the test results. To better communicate this information, we use the standard set of code assessment descriptor definitions found in Appendix C. The defined assessment descriptors are "excellent," "reasonable," "minimal," and "insufficient" agreement. The reader's understanding of the analyst's judgments will be enhanced if the definitions in Appendix C are reviewed before proceeding further.

Second, the user is interested in performance parameters or run statistics that provide an indication of how much it costs to produce the result. Several parameters are generally used to convey this information. These include the central processing unit (CPU) time versus real time, the number of calculational steps required versus real time, the time-step size versus real time, and a single-value "grind" parameter indicative of the entire calculation. Identification of the machine used to perform the calculation is also required. For the calculation of MIST Test 3109AA, a CRAY-1S computer was used. The reader is referred to Appendix D for information about the performance parameters specific to the calculation of MIST Test 3109AA.

Third, the user is interested in any performance failures encountered during the calculation. No such failures occurred during the calculation of MIST Test 3109AA.

VI. COMPARISON OF TEST AND CALCULATED RESULTS

The TRAC-PF1/MOD1 posttest calculation for Test 3109AA was performed for the first 7000 s of the experiment. During this time, all of the major phenomena took place and the automatic safety systems and emergency operating procedures were activated. At the end of the 7000-s calculational period, the HPI flow exceeded the leak flow and refilling of the primary system was well under way. The assessment descriptors appearing in Appendix C are used to characterize the degree of agreement between measured and calculated results.

A. Steady State

The TRAC-PF1/MOD1 steady-state calculation for Test 3109AA was performed for 2000 s, corresponding to approximately five loop transits. At the end of the steady-state calculation, the primary- and secondary-system fluid conditions had stabilized within the uncertainties of the measured values. The measured and calculated steady-state conditions are summarized in Table I. The calculated steady state provides the initial conditions for the transient calculation. Our posttest assessment studies conducted to date for the MIST facility have shown that accurate calculation of MIST transient performance requires that the calculated steady state be in reasonable-to-excellent agreement with the test data. Similar sensitivities to small differences in the facility "initial conditions and boundary system controls" have been observed and reported.[3]

B. Transient

We describe the measured and calculated transient results in two ways. We first provide an overview discussion, which will focus on the major phenomena occurring in the test, both measured and calculated. This discussion (1) identifies major phases that occurred during the test, (2) provides an overview of measured and calculated phenomena occurring in the test, and (3) identifies major areas of agreement and disagreement between the measured and calculated results. We next provide a detailed discussion of the transient results, with a more extensive examination of the calculated phenomena that diverge from the phenomena observed and measured in the test. Additional studies needed to clarify the reasons for the divergence are identified, and the results of these studies are summarized. The detailed discussions of the additional studies are presented in Section VI.C.

1 Code-Experiment Comparison Overview. MIST Test 3109AA, the as-run nominal for the MIST program, was initiated at time zero from the steady state reported in Table I by initiating the scaled 10-cm^2 break in the B1 cold leg. An overview of the resultant test and calculated transients are shown in Fig. 2. At time zero, the primary was liquid full and coolant was being driven by natural circulation. The transient calculation was started at time zero by the initiation of a scaled 10-cm^2 (0.01076-ft^2) break just downstream of the HPI nozzle in the B1 cold leg. As the pressurizer level fell below 0.305 m (1 ft) at 150 s in the test and 160 s in the calculation, several actions were taken. The core-power decay was started, HPI begun, and RVVV automatic control was initiated, allowing the RVVVs to open.

Figure 2.a gives the primary and secondary pressures for the test and calculation. Saturation first occurred in the intact-loop hot leg at 185 s in both calculation and test. Liquid from the pressurizer warmed the liquid in the intact-loop hot leg so that flashing first occurred in the intact-loop U-bend (Fig. 2.b). A vapor bubble grew rapidly as primary inventory decreased, causing the hot-leg liquid level to drop away from the intact-loop U-bend. Natural-circulation

flow in the intact loop (Fig. 1.c) ended at 240 s in the test and 310 s in the calculation as the liquid level in the hot leg dropped too low for spillovers to occur. This effectively decoupled the intact-loop SG as a heat sink. Figures 2.c and 2.d show the intact-loop and broken-loop flows, respectively.

As the SG secondaries (levels given by Figs. 2.e and 2.f) were refilled by AFW (flow rates given by Figs. 2.g and 2.h), the liquid level in the intact-loop SG primary dropped so that the condensing surface was exposed in tubes cooled by the AFW. This resulted in a BCM heat-transfer event as the intact-loop SG-secondary liquid level reached the high set point and some AFW was required as the liquid level settled in on the set point. This was a threshold event that had an impact on the early course of the transient (it did not occur in a repeat of the as-run nominal test). To capture this event in the calculation, the actual SG-secondary-level data were used as the set point for the controller in the TRAC model. This occurred from 565 to 1000 s.

The condensation in the intact-loop SG reduced the pressure in the intact-loop U-bend, raising the liquid level in that SG. This shifting of primary inventory contributed to voiding in the broken-loop U-bend. Starting at about 900 s, broken-loop flow (Fig. 2.d) decreased rapidly in the test. The calculation predicted this occurring at about 940 s. At about 1000 s in the test and 1040 s in the calculation, the broken-loop flow reached a minimum.

With the decrease in broken-loop flow, primary-to-secondary heat transfer was reduced. This caused the primary to begin to repressurize (Fig. 2.a) at about 1000 s in both test and calculation. Voiding in the upper head of the reactor vessel began to push more liquid into the hot legs causing broken-loop flow to increase. At 1150 s in the test and 1480 s in the calculation, the RVVVs closed (Fig. 2.i) in response to draining in vessel and downcomer. This occurred when uneven draining rates apparently exposed the downcomer and reactor vessel ends of the RVVV lines to different phases. With the RVVVs closed, steam production in the reactor vessel forced more liquid up the broken-loop hot leg and over the U-bend (Fig. 2.d). This flow occurred in surges, which were more pronounced in the test than in the calculation. At 1575 s in the test and 1840 s in the calculation, the RVVVs reopened as draining of the vessel and downcomer exposed the RVVV nozzles. Reopening the RVVVs allowed steam to flow from vessel to downcomer. Flow over the broken-loop U-bend ended because core-generated steam was no longer forcing liquid up the hot legs. With this steam passing through the RVVVs, the repressurization (Fig. 2.a) ended as cold HPI liquid condensed some of this core-generated steam in the downcomer.

After the cessation of broken-loop flow, the system entered a relatively inactive period. The system was slowly cooling and depressurizing because the enthalpy of the HPI was less than the enthalpy of the leak flow and the core power was decreasing along the decay curve. AFW was off in both SGs as the ATOG-based secondary pressure set point was above the SG-secondary pressures. In the test, the SG-secondary pressures remained nearly constant until the set point decreased to the actual pressures. In the calculation, inadequate losses from the SG secondaries allowed the secondary fluid to be heated by stored energy from the metal mass and thus increase in pressure. Also, calculated leak flow (Fig 2.j) was less than the leak flow in the test. Thus, the depressurization rate in the calculation was less than in the test.

The increase in pressure in the intact-loop SG secondary caused the ATOG-based set point to be reached at 3400 s in the calculation (Fig. 2.a), while in the test it was reached at 3600 s. In both, the level in the intact-loop SG primary was well below the 15.48 m (50.8 ft) AFW nozzle elevation so that a large surface area was available for condensation when AFW was restarted. This BCM heat transfer caused a significant increase in the depressurization rate in both test and calculation. In both, primary pressure was reduced sufficiently for HPI flow to exceed leak flow (Fig. 2.j), marking the beginning of refill. The liquid level in the reactor vessel stayed near the elevation of the hot legs (Fig. 2.k) and did not approach the top of the core during the transient.

In both test and calculation, the condensation in the intact-loop SG reduced the pressure in the U-bend so that the level rose in the intact-loop SG and hot leg. This caused the level in the broken-loop SG to drop (Figs. 2.e and 2.f). In the test, the level dropped below the AFW nozzle elevation; in the calculation it did not. In the test, BCM heat transfer then occurred in the broken-loop SG as the level changed. These BCMs produced a larger depressurization in the test and a correspondingly larger increase in refill rate than seen in the calculation. In the test, a primary repressurization started at about 5500 s. This occurred because the primary-system inventory (Fig. 2.l) had increased so that SG levels were high enough that BCM heat transfer no longer occurred. In the calculation, the depressurization during refill was more gradual and HPI flow did not exceed leak flow by the margin seen in the test. By the end of the calculation at 7000 s, the system had not refilled sufficiently to end BCM heat transfer in the calculation. The rate of repressurization in the test declined such that most of the pressure increase occurred before 7000 s, even though the repressurization continued to about 9000 s. The primary continued to refill throughout this period and it became apparent that the point of minimum primary inventory had indeed been reached earlier.

2. **Detailed Discussion of Transient Results.** The observed and calculated thermal hydraulic phenomena and system interactions are discussed in detail in this section. The discussion is divided into four transient phases; these phases are defined with reference to Fig. 3, the primary- and secondary-pressure response. Phase 1, subcooled decompression, covers the period from the start of the transient to 185 when the intact-loop hot leg saturates and the depressurization rate is reduced. Phase 2 intermittent circulation, covers the period of continued depressurization, repressurization, and termination of repressurization from 185 s to 1870 s when natural circulation is terminated in the loops. Phase 3, loop stagnation, covers the period of gradual depressurization from 1875 s to approximately 3900 s when primary-system refill begins. Phase 4, refill, extends from the beginning of refill at 3900 s to the end of the calculation at 7000 s. A summary of the major events for Test 3109AA is presented in Table III.

Phase 1—Subcooled Decompression. Phase 1 is the first part of the transient from leak initiation until the saturation pressure was reached in the hot legs at 185 s. During Phase 1, the fluid in the primary system was subcooled liquid, and the primary-system pressure decreased rapidly as the liquid expanded because of the leak flow. At the end of Phase 1, the primary-system depressurization rate was reduced by the flashing of liquid in the hot legs.

At the beginning of the transient, the primary system was in steady-state single-phase natural circulation. The driving force for natural circulation was the density difference between the hot liquid in the hot legs and vessel, and colder liquid in the SG tubes, cold legs, and

downcomer. The test was initiated at time zero by opening a scaled 10-cm^2 leak in the B1 cold leg just downstream of the HPI injection port. This caused an immediate reduction in the calculated primary-system pressure (Fig. 3) and pressurizer level because of the flow of liquid through the leak. The liquid initially in the pressurizer was near saturation temperature, and as this liquid was discharged into the intact-loop hot leg, it mixed with the hot-leg fluid resulting in a higher fluid temperature in the intact-loop hot leg relative to the broken-loop hot leg. Since the density of the liquid in the intact-loop hot leg was thereby reduced, the intact-loop natural-circulation flow increased at the beginning of the transient, as shown in Fig. 4. Broken-loop flows are shown by Fig. 5.

The level in the pressurizer (Fig. 6) drained down to the 0.305-m (1-ft) level at 150 s in the test and at 160 s in the calculation. At these times the following control actions were taken: core-power decay (Fig. 7) was started, HPI flow was started, the RVVVs were transferred to automatic control, the AFW level control set point was changed from 1.52 m (5 ft) to 9.63 m (31.6 ft), and the ATOG-based pressure control logic was initiated for the SG secondaries. The pressurizer low-level trip was reached 10 s earlier in the test because of the higher measured leak flow at the beginning of the transient (Fig. 8). Figure 9 gives the fluid temperatures just upstream of the leak site.

The effect of the core-power decay after the pressurizer low-level trip was to increase the measured and calculated primary depressurization rates, as shown in Fig. 3. The depressurization rate was high at this time because all of the primary fluid was still subcooled and expanding because of the leak flow. Also, at the time of the low-level trip, the RVVVs were switched from manually closed to automatic control based on differential pressure. Figures 10 and 11 show that the vent valves opened immediately, causing a brief reduction in both loop flows at 150 s in the calculation and 160 s in the test. Figure 12 gives the calculated void fraction on the reactor vessel side of the vent valves. The reduction in the loop flows was then followed by a recovery in both loops with the sharpest recovery in the intact loop. This increase in the loop flows was a result of the increased AFW flow (Figs. 4, 5, 13 and 14) in response to the AFW set point change at 150 s in the calculation and 160 s in the test. The loop flows were increased by the AFW flow because the AFW raised the thermal center in the SGs; the intact-loop flow was increased more since the pressurizer was still discharging hot fluid into the intact loop at this time.

Figure 4 shows that the increase in the intact-loop flow was abruptly terminated at approximately 185 s in both the calculation and in the experiment. At this time, the primary-system pressure (Fig. 3) had decreased to the saturation pressure of the intact-loop hot-leg fluid (Fig. 15). Flashing of the hot-leg fluid then created a vapor bubble in the intact-loop hot-leg U-bend (Fig. 16) and the natural-circulation flow in the intact loop was interrupted, as shown in Fig. 4. The intact-loop saturation marked the end of Phase 1 at 185 s. Subsequent depressurization of the primary system was then inhibited by flashing of the fluid in the intact-loop hot leg, as shown in Fig. 3, which indicates a reduction in the measured and calculated primary-system depressurization rates at 185 s.

Differences between the calculation and the experiment during Phase 1 resulted primarily from the higher measured leak flow (Fig. 8). This caused a slightly higher depressurization rate (Fig. 3) and an earlier occurrence of the pressurizer low-level trip in the test.

Phase 2—Intermittent Circulation. Phase 2 covers the period of intermittent circulation in the loops after the first saturation of loop fluid occurred in the intact-loop hot leg. During Phase 2, the natural-circulation flow in each loop was governed by the liquid level in the hot leg of that loop. As the hot-leg liquid level receded, the U-bend was uncovered and the loop flow quickly terminated. Also during Phase 2, the SG AFW and steam flows responded to the control procedures started during Phase 1 when the pressurizer level decreased to 0.305 m (1 ft). At the beginning of Phase 2, the AFW was on in both SGs as the levels were being raised to the 9.63-m (31.6-ft) set point; throughout Phase 2, the secondary pressures were controlled to a variable set point based on ATOG. The ATOG-based set point is determined from the core-exit temperature and the saturation temperatures corresponding to the SG-secondary pressures as described in Ref. 5. Depending on these three temperatures, the set-point pressure may be (1) held constant, (2) reduced by 0.345 MPa/min (50 psi/min), or (3) reduced such that the corresponding saturation temperature is reduced by 55.6 K/hr (100°F/hr). The logic for determining which of these pressure-control modes is to be used is explained in detail in Ref. 5. Phase two extends to 1575 s in the test and 1870 s in the calculation, when the flow in the broken loop was terminated by the uncovery of the broken-loop hot-leg U-bend.

After the saturation of the intact-loop hot-leg fluid at the end of Phase 1, the liquid level in the intact-loop hot leg decreased rapidly (Fig. 16) because of continued flashing. Figure 4 shows that as a result, the intact-loop natural-circulation flow was terminated by 240 s in the test and 310 s in the calculation and was not re-established. Heat transfer in the intact-loop SG then ceased because of the loss of natural circulation in the intact loop. In the absence of heat transfer from the primary, the intact-loop SG-secondary pressure decreased from the ATOG-based set point in both the test (at 240 s) and in the calculation (at 310 s), as shown in Fig. 3. This decrease, caused by the AFW flow into the intact-loop SG (Fig. 13), continued until the level (Fig. 17) reached the 9.63-m (31.6-ft) set point at 565 s in both the test and the calculation, and the AFW flow decreased (Fig. 13). With continuing natural-circulation flow through the broken loop, AFW in the broken-loop SG (Fig. 14) caused a more gradual secondary depressurization (Fig. 3) as the broken-loop SG filled (Fig. 18). After the intact-loop SG-secondary pressure fell below the ATOG-based set point, the steam flow in the intact-loop secondary was terminated (Fig. 19) by the pressure controller. Steam flow in the broken-loop secondary (Fig. 20) was also terminated by the pressure controller during refill. Unlike in the intact-loop SG, steam flow was restarted shortly after refill in the broken-loop SG.

When the intact-loop SG secondary was refilled to the 9.63-m (31.6-ft) level in the experiment, the AFW controller was switched into a constant-level control mode, and a proportional-integral controller was used to maintain the SG level at the 9.63-m (31.6-ft) set point. This control mode change affected the AFW flow after the intact-loop SG was refilled at 565 s. Figure 13 shows that after 565 s, the AFW flow was briefly terminated and then restarted from 800 to 1500 s while the SG level settled in on the 9.63-m (31.6-ft) set point. When the AFW was restarted in the intact-loop SG, vapor was present in the primary side of the tubes at the 15.48-m (50.8-ft) AFW elevation (Fig. 17), and condensation heat transfer began immediately. This BCM heat transfer began in both the test and the calculation at 565 s, resulting in a more rapid primary depressurization (Fig. 3). The BCM was terminated at

1000 s in both the test and the calculation when the intact-loop SG-primary level (Fig. 17) increased to the AFW elevation and condensation in the primary was terminated.

Without steam flow, AFW flow was not required to maintain the level in the intact-loop SG after the 9.63-m (31.6-ft) set point was achieved, and Fig. 13 shows that the AFW flow was completely terminated in the intact loop after 1500 s in both the test and the calculation. The intact-loop SG, therefore, remained inactive after 1500 s while its pressure was below the ATOG-based set point.

The system interactions in the broken loop during Phase 2 were similar to the intact-loop behavior just described. However, the timing of events in the broken loop was delayed because the broken-loop hot-leg fluid was cooler than the fluid in the intact-loop hot leg at the beginning of Phase 2. Figure 16 shows that the broken-loop hot leg was maintained liquid full until 1000 s as the intact-loop hot-leg level receded because of local flashing. Beginning at approximately 850 s, however, the intact-loop level fell at a slower rate as it approached the liquid level in the primary side of the intact-loop SG (Fig. 16). With the slower draining in the intact-loop hot leg, the broken-loop hot-leg level eventually began to recede at 1000 s, as indicated in Fig. 16. The natural-circulation flow in the broken loop (Fig. 5) then began to decrease rapidly at approximately 1000 s, in both the test and the calculation, in response to the decrease in the broken-loop hot-leg level. This reduction of flow in the broken loop had two effects. First, the heat transfer in the broken-loop SGs started to decrease, leading to an increase in the primary-system pressure and corresponding decrease in broken-loop secondary pressure beginning at 1000 s (Fig. 3). Second, the core outlet flow was diverted into the upper head and through the RVVVs, as shown in Fig. 11. The repressurization of the primary system retarded the flashing in both the intact and broken loops. At the same time, flashing increased in the upper head because of the diverted core outlet flow. As a consequence, both the measured and calculated intact-loop hot-leg levels started to increase at 1000 s while the vessel level decreased more rapidly, as shown in Figs. 16 and 21.

The final sequence of events in Phase 2 started at 1000 s with the intact-loop hot-leg levels increasing and the vessel levels decreasing as described above. The increased rate of upper-head voiding in both the test and the calculation at 1000 s was sufficient to terminate the reduction in the broken-loop natural-circulation flow (Fig. 5), which then began to increase. As flashing continued in the upper head, the vessel level receded, as shown in Fig. 21, and at 1250 s in the test (1295 s in the calculation), the RVVV nozzles were uncovered. As a result, the RVVV flow began to decrease rapidly at this time and was completely terminated at 1150 s in the test and at 1480 s in the calculation, as shown in Figs. 10 and 11. The broken-loop spillover flows (Fig. 5) were sharply increased by the RVVV closures at these times in both the test and the calculation. Shortly afterward, however, the broken-loop U-bend uncovered (Fig. 16) as the primary system continued to drain and the natural-circulation flow in the broken loop started to decrease rapidly, as shown in Fig. 5. The broken-loop natural-circulation flow then continued to decrease and was completely interrupted at 1575 s in the test and at 1870 s in the calculation. During this final decrease in broken-loop natural-circulation flow, Figs. 10 and 11 show that the RVVVs reopened at 1575 s in the test and at 1840 s in the calculation when the downcomer drained to the RVVV elevation (Fig. 22) and remained open thereafter.

During the period when the RVVVs were closed, Fig. 5 shows a strong natural-circulation flow in the broken loop. The effect of this flow was to increase the heat transfer in the broken-loop SG and also to mix cold HPI fluid with hotter fluid in the primary system. As a result, the primary-system repressurization, which began at 1000 s was terminated at 1575 s in the test and 1875 s in the calculation.

The termination of spillover circulation in the broken loop at 1575 s in the test and 1870 s in the calculation marks the end of Phase 2. Major events during Phase 2 occurred slightly earlier in the test than in the calculation because of the higher leak flow in the test from test initiation to 1080 s. At the end of Phase 2, in both the test and the calculation, the primary system was depressurizing, the broken-loop SG-secondary pressure was being controlled to the decreasing ATOG-based set point, and AFW was controlling the SG level in the broken loop. The intact-loop SG was inactive at the end of Phase 2 since its pressure was below the ATOG-based set point.

Phase 3—Loop Stagnation. Phase 3 is the period of stagnated natural-circulation flow in the loops after the final spillover in the broken loop. During Phase 3, the primary system was cooled by the HPI-leak feed and bleed and by AFW in the broken-loop SG. The primary-system pressure decreased during Phase 3 because of core-power decay and the HPI-leak cooling. Phase 3 ended at 3900 s in the test and 3400 s in the calculation when AFW was restarted in the intact loop and the primary-system depressurization rate was increased.

During most of Phase 3, the primary was cooled by the HPI-leak feed and bleed and by AFW in the broken loop (Fig. 14). Most of the cooling was done by the feed and bleed: at 3000 s, for example, Fig. 8 shows that in the test, the HPI flow was approximately 0.074 kg/s (0.1628 lb/s), and the leak upstream temperature (Fig. 9) was 524.9 K (485.2°F). The energy required to heat this HPI flow to the temperature at the leaksite, 72 kW, was greater than the 59-kW core power at this time. In the calculation at 3000 s, the HPI flow was slightly lower (0.0716 kg/s), 71 kW was needed to heat this flow to the leak upstream temperature in the calculation, and the core power was also 59 kW at 3000 s. The primary-system pressure decreased during Phase 3 as a result of the decreasing core power and excess energy removal by the HPI-leak cooling.

Figures 23–26 show the cold-leg flows for the individual cold legs. At the beginning of Phase 3, a circulation flow developed in the broken-loop cold legs (Figs. 25 and 26) in both the test and the calculation. The cold-leg circulation flow began immediately after the broken-loop U-bend spillover flow was terminated at the end of Phase 2. Flow through the B2 cold leg continued after flow ceased in the hot leg with a reverse flow starting in the B1 cold leg. At this time, fluid from the downcomer was drawn toward the leak site and the flow in the B1 cold leg reversed. The cold-leg circulation flow was then maintained by the density difference between the B1 and B2 cold legs resulting from the flow of warmer fluid from the downcomer into the B1 cold leg. The circulation flow was important because it affected the leak upstream temperature (Fig. 9) in both the test and the calculation. A similar flow also occurred in the A cold legs with positive flow in the A1 cold leg and reverse flow in the A2 cold leg. The calculation had this natural circulation flow beginning at about the same time the flow began in the B cold legs (Figs. 23 and 24). The data show this flow starting at about 2300 s, which is about 400 s later.

Figure 9 shows that the broken-loop cold-leg circulation flow caused a reduction of approximately 30 K (54°F) in the fluid subcooling upstream of the leak in the test as well as in the calculation. The corresponding reduction in the leak flow (Fig. 8) at 1930 s in the calculation, however, was larger than the reduction observed in the test at 1660 s. After the initial decrease in leak flow at the beginning of Phase 3, Figs. 8 and 9 show that the calculated leak flow gradually recovered toward the measured value as the subcooling increased in the calculation.

The lower calculated leak flow during Phase 3 resulted in a lower depressurization rate in the calculation (Fig. 3) and slower loop draining (Fig. 16). Figure 16 shows that after the broken loop interrupted in the test, the broken-loop hot-leg level remained above the intact loop level, and both loops drained at approximately the same rate. The difference in hot-leg levels resulted from a temperature difference between the intact and broken loop in the hot-leg piping. After the flow in each U-bend voided and the loop flow interrupted, the U-bend piping temperature was maintained by the guard heaters at approximately the saturation temperature at the time of the interruption. Since the intact loop interrupted earlier when the saturation temperature was higher, the intact-loop U-bend piping temperature stayed higher after both loops had interrupted. The higher piping temperature created a higher vapor pressure in the intact-loop U-bend relative to the broken-loop U-bend; and because of this pressure difference, the intact-loop hot leg level remained below the broken-loop hot-leg level during Phase 3.

The same draining behavior, with the higher level in the broken-loop hot leg, occurred in the calculation during Phase 3. However, after 2600 s in the calculation, the draining in the broken loop was halted and the leak was then fed by accelerated draining of the intact loop (Fig. 16). This transition at 2600 s in the calculation is currently under further study; it appears that a change occurred in the calculation at this time, which affected the heat transfer from the piping to the vapor in one of the U-bends. The difference in the observed and calculated hot-leg draining rates after 2600 s, however, did not cause other calculated parameters to diverge from the measured values. Figures 9, 8, and 3 show no change in the calculated leak upstream temperature, leak flow, or primary-system pressure at 2600 s.

During Phase 3, the primary and secondary conditions were such that the ATOG-based set point pressure was approximately equal to the saturation pressure corresponding to a temperature 27.78 K (50°) below the core exit temperature. This is evidenced in Fig. 3, which shows that during Phase 3, the calculated ATOG-based set point pressure decreased at the same rate as the primary pressure. The difference in the corresponding saturation temperatures during this decrease was approximately 27.78 K (50°F); Fig. 3 shows that the difference between the primary and ATOG-based pressures was nearly constant during Phase 3 in the test and in the calculation.

The SG-secondary pressure control is important because it affects the AFW flow in each SG. The AFW flow depends on the pressure control because AFW is used to control the secondary levels: if the secondary pressure is being reduced, then AFW will be required to maintain the secondary level. During Phase 3, the broken-loop AFW was on (Fig. 14) in both the test and the calculation because the broken-loop SG-secondary pressure was controlled to the decreasing ATOG-based set point (Fig. 3). The intact-loop AFW was off (Fig. 13), however, since the intact-loop SG-secondary pressure was below the ATOG-based set point (Fig. 3), and therefore the intact-loop steam flow was controlled to zero (Fig. 19).

Figure 3 shows that in the test the intact-loop SG pressure remained constant during Phase 3 when the AFW and steam flows were off. The calculated intact-loop SG pressure, however, increased slightly during Phase 3 because the steam line heat losses modeled (1.5 kW per steam line) were too low. The increase in the intact-loop SG pressure during Phase 3 caused the decreasing ATOG set-point pressure to be reached at 3400 s in the calculation (3900 s in the test), as shown in Fig. 3. At these respective times, AFW was restarted in the intact loop leading to BCM, which marked the end of Phase 3 in both the test and the calculation.

Phase 4—Refill. Phase 4 covers the period from the beginning of the BCM in the intact loop until the end of the calculation at 7000 s. During Phase 4 the primary-system pressure was reduced by AFW BCM heat transfer in the intact-loop SG, causing the HPI flow to exceed the leak flow. The calculation was terminated at 7000 s, since at this time it was evident that the point of minimum primary-system inventory had been reached.

At the end of Phase 3, the ATOG-based set-point pressure decreased to the intact-loop SG-secondary pressure (Fig. 3), causing the steam and AFW flows to be restarted in the intact loop at 3900 s in the test and at 3400 s in the calculation. This caused extensive condensation heat transfer in the primary side of the intact-loop SG tubes because the level in the tubes was well below the 15.48-m (50.8-ft) AFW injection elevation (Fig. 17) at this time. As a result, the primary-to-secondary heat transfer in the intact-loop SG was increased at these times and the primary system began to depressurize rapidly in the test and the calculation (Fig. 3).

When the AFW was restarted in the intact loop, the pressure of the vapor inside the SG tubes was reduced by condensation. The liquid level in the intact-loop SG and hot leg then rose rapidly while the levels in the broken loop fell. This occurred in both the test and in the calculation, as shown in Fig. 16. However, the level in the broken-loop SG (Fig. 18) fell below the 15.48-m (50.8-ft) AFW elevation in the test but not in the calculation. Therefore, the intact-loop BCM in the test was immediately followed by a BCM in the broken loop, and the overall reduction in the primary pressure (Fig. 3) was greater in the test than in the calculation.

The effect of the primary-system depressurization at 3900 s in the test and 3400 s in the calculation was to increase the HPI flow above the leak flow, as shown in Fig. 8. This event marks the beginning of the refill period. After the start of refill, the levels in the intact and broken loops started to increase, as shown in Figs. 17 and 18. The refill rate (excess of HPI flow over leak flow) was higher in the test because of the larger BCM depressurization in the test (Fig. 3). The higher refill rate (Fig. 27) in the test resulted in correspondingly higher primary-system level increases after refill began in the test, as shown in Figs. 8 and 16. The primary system continued to depressurize rapidly in the test (Fig. 3) until the SG primaries were filled above the upper tube sheets (Figs. 17 and 18) and the condensation heat transfer was terminated at approximately 5200 s. This event still had not been reached by the end of the calculation at 7000 s because of the lower refill rate in the calculation.

The differences between the test and the calculation discussed above involved three separate phenomena. First, the critical flow model in TRAC apparently did not properly account for the changes in the leak upstream temperature. Consequently, the calculated leak flow and primary depressurization rates were too low during Phase 3. Second, the TRAC input model

did not include enough heat losses for the steam lines. This allowed the intact-loop SG to pressurize slightly during Phase 3 in the calculation and thereby reach the ATOG-based set point too soon. Phase 3 was, therefore, terminated 600 s early in the calculation. Third, the magnitude of the BCM heat transfer was apparently too low at the beginning of Phase 4 in the calculation. Even though the condensation surface area and AFW flow during this BCM in the calculation matched the data, the primary-system depressurization during the BCM was too low in the calculation. This then caused a lower refill rate during Phase 4 in the calculation.

The overall comparison of the TRAC-PF1/MOD1 calculation for Test 3019AA with measured data from the test was reasonable; this means that the major trends were predicted correctly in the calculation, although TRAC values were frequently outside the range of data uncertainty because of minor code/model deficiencies. With reasonable agreement, correct conclusions will still be reached when the code is used in similar applications.

C. Additional Studies

During the course of our analysis of MIST Test 3109AA, we either identified or performed additional studies with the objective of resolving issues and answering questions. We have collected and grouped the resultant information in three categories. In some instances, additional studies cover two or even three of the categories. For instance, the work discussed below on SG heat transfer involves all three categories. The facility data are not sufficient to resolve the liquid and SG distribution in the SG. This complicates efforts to develop an input model and to determine the adequacy of code models and correlations for SG-secondary heat transfer.

The first category provides information about our understanding of facility configuration and operation. Ideally, the analyst would have a perfect knowledge of facility configuration and operation. However, it has been our experience that problems often occur in this area for tests performed in integral systems. We document our efforts for MIST Test 3109AA in the hope that this information will assist other analysts of MIST Tests and other TRAC users. The second category provides information developed regarding the adequacy of the TRAC input model of the MIST facility. We believe that the results of our studies in this area will assist other TRAC users. The third category provides information regarding the adequacy of the closure models and correlations in the TRAC code. We hope that this information will assist those involved in the development and improvement of TRAC.

1. Studies Related to Knowledge of the Facility. During the process of reviewing the results from the calculation of MIST Test 3109AA, several deficiencies in our knowledge of the facility were identified. These include inadequate knowledge of two-phase-flow multipliers for the leak orifice, the liquid and vapor distribution in the SG secondaries, and the energy losses and gains for the SG secondaries.

Several runs were necessary to determine the two-phase-flow multipliers that best matched the data for flow out the leak orifice. Since these multipliers are not known a priori, and the course of the calculated transient is sensitive to system inventory, it was necessary to determine what values gave the best comparisons. This was done by a trial and repeat approach.

As stated above, the lack of knowledge about the distribution of flows and heat transfer in the SG secondaries made determining the adequacy of the input model and code models and correlations difficult. This problem is inevitable for an integral facility where the capability

to determine fine detail in flows and heat transfer cannot be practically achieved. The studies that provide some insight into this are discussed below since they more directly relate to the input model.

During the period of inactivity in the intact-loop SG from about 1300 s to about 3100 s, the secondary pressure stayed constant in the test, but rose in the calculation when the fluid mass in the secondary warmed in coming to equilibrium with the SG metal mass. A possible explanation for this result is that the secondary-side heat losses were greater than determined by B&W so that pressure did not rise as the metal mass came to equilibrium with the secondary-side fluid, and the guard heater operation was sufficient to prevent a decrease in the pressure. No studies have been performed in an attempt to more thoroughly understand this phenomenon. Since this phenomenon occurred in other tests as well, it would seem desirable to understand why it happened, however.

2. Studies Related to the Input Model. Most of the model development work performed in this study is reported in this section although it relates to an inadequate knowledge of the multidimensional flows in the SGs and to possible inadequacies in the code models and correlations as well. The pretest calculation for steady-state conditions showed loop flows of about 0.32 kg/s per loop. The test data gave values of about 0.42 kg/s. The low values for loop flows for the pretest steady-state calculation gave primary-system pressures and temperatures that were too high. This in turn caused the path of the calculated transient to be different than the as-run nominal. When coupled with changes in initial conditions between pretest specifications and the as-run nominal, the as-run nominal test was sufficiently different from the pretest calculation that it was deemed necessary to run the transient calculation with the new initial conditions and a correct steady state.

The prediction of lower-loop flows than actually occurred was an indication that the predicted heat-transfer distribution in the SGs did not provide sufficient heat transfer at high elevations of the SG, *i.e.*, that the predicted thermal center was too low. The model used for the pretest calculation had two channels for the secondary, one to represent the portion that is nominally wet and one for the portion that is nominally dry. Two PIPE components on the primary side were used to represent the tubes that are nominally wet and those that are nominally dry. The first attempts to raise the thermal center of the SG involved increasing the heat transfer in the wetted channel by applying a multiplier to the Chen correlation for the upper cells. When that approach failed to work, the multiplier was applied to the final heat-transfer coefficients for liquid and vapor (h_l and h_v). A total of nine runs, including some needed to resolve numerical difficulties, made it possible to investigate the increase in natural circulation that can be obtained by increasing the heat transfer in the secondary side. The flow increases obtained were much less than desired.

Two runs were then made to compare the predicted primary-system flow losses for the TRAC model to the losses from Test 000420, a pumped isothermal test performed to determine irrecoverable pressure drops in the facility. These runs did not indicate any abnormal losses in the TRAC model. The results of the calculations with increased secondary-side heat transfer in the wetted channel and the irrecoverable pressure loss tests led to the conclusion that there was insufficient mass flow and heat transfer in the dry channel of the SG secondaries.

As a consequence, we decided to renode the SG secondary to a single channel with a code update to apply the AFW heat transfer to the three wetted tubes only. This allowed more

steam flow to reach the dry tubes. Four runs were made in the process of debugging these changes. Four more runs were then made with varying parameters for the wetted portion. Even with the increased steam flow in the dry portion of the SG secondary, the natural-circulation flow did not increase to the data value. The conclusion from these runs was that some liquid needed to be introduced to the nominally dry portion of the SG secondary to increase the heat transfer so that the natural-circulation flows of the data could be achieved.

Eight more runs were made with small amounts of liquid introduced to the nominally dry portion of the SG secondary and multipliers applied to the wetted side heat-transfer coefficients. The steady state that was used to start the transient calculation used a void fraction of 0.9965 to calculate heat-transfer coefficients for the upper cells on the nominally dry side, and a subsequent multiplier for h_i of 1.8. Several transient runs were then required to get all of the controls working properly before the final, full run was made.

3. **Studies Related to Code Models and Correlations.** There are two areas where additional studies would be desirable if sufficient experimental data can be found. The critical flow model used in TRAC did not show the subcooling dependence seen in the leak-flow data. It would be desirable to understand this because inaccuracies in predicting leak flow and, hence, system inventory in an integral facility such as MIST can change the course of a calculated transient to an extent sufficient to mask problems with input models or code models and correlations.

AFW BCM was underpredicted at times when the exposed tube area was about the same and the AFW flow was higher than the steady-state value in the facility. This may indicate a problem with the apportioning of liquid through the SG. It might, however, indicate a fundamental problem with the correlations used for heat transfer for the regimes occurring in the SG.

VII. LESSONS LEARNED AND CONCLUSIONS

The comparison of measured and calculated parameters for MIST Test 3109AA has shown that the physical phenomena that governed the course of these transients were also predicted in the calculation. The overall agreement between the tests and the calculation was reasonable: the major trends of the data were predicted correctly although TRAC values were frequently outside the range of data uncertainty because of minor code/model deficiencies. With reasonable agreement, valid conclusions should still be reached if the code were used in similar applications. Our lessons learned and key conclusions are further subdivided into the areas of (1) adequacy of facility knowledge, (2) adequacy of facility input model, (3) adequacy of code models and correlations, (4) scaling considerations, and (5) regulatory implications.

Specific differences between measured and calculated parameters can be attributed to one of three categories of factors that can affect the calculated results. First, uncertainty in the data necessary to fully describe the facility and test operation can lead to uncertainty in the calculated results. Second, approximations in the code input model such as the resolution of the nodalization, time-step size, or the selection of a one-dimensional component versus a three-dimensional component can affect calculated parameters. Third, the validity of the correlations and models in the code may affect the code calculations. Before conclusions can be drawn from code-data comparisons about the third category, code correlations and models, factors in the first two categories must be ruled out as possibly causing the differences

between measured and calculated parameters. Differences between MIST Test 3109AA data and calculation were caused by factors from each category.

A. Knowledge of the Facility

We identified one area where our knowledge of MIST facility operation was deficient. Uncertainty in the energy balance on the secondary side led to increases in calculated secondary pressure during the phase of the transient when the SGs were inactive (no loop flows and no AFW). The actual secondary pressure stayed constant during this period. In the calculation, the rise in secondary pressure during the inactive period caused set points to be reached early, which in turn caused the controlled SG-secondary depressurization to begin early. Consequently, the beginning of refill was calculated too early. In the calculation, fluid temperature in the SG secondary increased as the fluid came to thermal equilibrium with the SG metal mass. A B&W-suggested value of 1.5 kW of heat loss was imposed on each steam line for the calculation. This was not sufficient to offset the fluid-temperature gain. In the test, the SG-secondary fluid temperature, and hence pressure, was remarkably stable during the period with inactive SG. Apparently, energy losses, either heat losses and/or steam losses through the steam valve, were sufficient to prevent the SG-secondary temperatures and pressures from rising. These losses were apparently balanced such that the temperature and pressure did not decrease either. We believe that the guard heaters supplied sufficient energy to just offset the losses that would otherwise have caused the SG-secondary pressures and temperatures to drop.

This uncertainty in our knowledge of the facility did not cause large differences between test and calculation. It caused the timing of some calculated events to be shifted forward. This same phenomena occurred in other tests, so a definitive explanation of it would be desirable.

B. Input Model

We found the input model to be adequate for the nominal SBLOCA in the MIST facility. No differences between test data and calculation were found, suggesting that the input model was not an adequate representation of the facility. No noding study was conducted to determine the sensitivity of the calculation to noding.

C. Code Models and Correlations

Correlations and models in the code that cause differences between the test and calculation are often difficult to identify among the many factors that can affect the calculated parameters. The results of the Test 3109AA, however, indicated that the TRAC-PF1/MOD1 critical flow model may not properly account for changes in upstream subcooling. Also, the predicted BCM heat transfer was too low during the SG refill when AFW rates and exposed primary-side tube area were the same. This could be caused by a heat-transfer correlation error, SG nodalization that was too coarse, or by an incorrectly determined flow regime during the calculation.

D. Scaling Implications

The issue of scaling is one of the most difficult with which to deal. At the level of TRAC models and correlations, some effort has been made to deal with scaling in the TRAC-PF1/MOD1 models and correlations document.[8] However, it is difficult to review individual constitutive models and correlations and build a definitive statement about scalability for prediction of transients in a full-size plant. There is a large effort currently in progress to quantify the uncertainty of using TRAC-PF1/MOD1 for prediction of large-break loss-of-coolant accidents (LBLOCAs).[10] It is possible that a similar effort will follow to quantify the uncertainty of applying TRAC for predicting SBLOCA phenomena in full-size plants. The elements of the Code Scaling Applicability and Uncertainty (CSAU) method described in Ref. 11 include (1) availability of a full set of code-specific documentation, (2) a ranking of key components, processes, and phenomena, (3) review and use of separate-effects test data to determine uncertainty ranges on key parameters identified during the ranking process, (4) use of integral-effects test data directly where results can be considered to be scale independent, and (5) a combination of uncertainty contributions. Los Alamos supports addressing the scaling question through application of the CSAU or similar methodology.

There is one other activity within the MIST Phase-IV test program that will prove helpful in addressing scaling. A counterpart test to the Crystal River event of June 16, 1981, will be conducted.[12] Within the limitations of the MIST Test facility, every effort will be made to simulate the key events and phenomena in the transient at the Crystal River plant. TRAC calculations are planned for the MIST Crystal River scaling transient and for the full-size plant event. This activity should provide direct information about code scalability as the key transient phenomena are calculated in a model of both the full-size plant and the MIST facility with its scale factor of 1/817 for volume and power.

E. Regulatory Implications

The objective of this section is to summarize our understanding of issues, results, and conclusions that may be used in support of the regulatory process for B&W plants.

1. Background. Before 1979, most reactor safety research focused on LBLOCAs. LBLOCAs were recognized as limiting, worst-case accident scenarios. Understanding and predicting plant response to LBLOCAs was the object of the majority of the research planned and performed in the period 1973 to 1979.[13] In 1979, the TMI-2 accident, characterized as a SBLOCA that occurred when the PORV stuck open, changed perceptions about loss-of-coolant accidents. Much of the research emphasis shifted to the more probable SBLOCAs.

Because of their unique geometry and performance in possible SBLOCAs, B&W plants have been the object of much of the attention. The once-through SG (OTSG) has a much smaller inventory of secondary-side liquid than the inverted U-tube SGs in plants of Combustion Engineering and Westinghouse design. Thus, in loss-of-feedwater transients, the heat sink available in B&W designed plants is smaller. This can reduce the time available to take action. Reductions in primary inventory in B&W plants cause natural circulation to cease relatively early in a SBLOCA. Loss of natural circulation decouples the SGs as heat sinks and can lead to repressurization. BCM heat transfer is then important to re-establish the SGs as a heat sink when primary inventory further decreases. B&W plants also contain vent valves, unique to B&W designed plants, connecting the upper plenum and downcomer. These flapper valves allow flow from the upper plenum into the downcomer to promote reflood in LBLOCAs.

The effect of the RVVVs on plant thermal-hydraulic behavior was uncertain. There were other areas of concern as well. Reference 7 states (Appendix A.1, page I.A-1), "Due to the unique configuration of the B&W NSS, previous large integral test facilities did not model the unique B&W hot leg configuration or the OTSG and, as a result, did not simulate the appropriate natural circulation conditions. In particular, there was uncertainty about the effects of two-phase flow, non-condensable gases, and the validity of the boiler-condenser mode of heat removal. In addition, the hydraulic stability, effects of high point vents, and internal reactor vessel vent valves . . . were items of interest."

As a result of these and other issues, a Test Advisory Group (TAG) consisting of representatives from the Nuclear Regulatory Commission, B&W owners, B&W, and the Electric Power Research Institute was formed in September 1982 to[14]

1. identify experimental data needs related to B&W designed plants,
2. identify operating plant and experimental data available now or in the near future,
3. evaluate how well the data address the identified data needs, and
4. provide recommendations for future programs.

The TAG was, by their definition, successful in accomplishing these tasks. They produced a prioritized list of issues (reproduced as Table IV), and agreed on the design features and test matrix for the MIST facility. Table IV was produced after an extensive review. It consists of a list of 17 technical issues identified by the TAG as those that should be addressed through an integral systems test facility. Overall, the evaluation used ratings from A to D to represent a measure of the priority. An "A" rating was defined as top priority. A "D" rating was used to indicate a lower priority, although issues rated as "D" were still considered to be of sufficient importance to warrant investigation. The NRC representative to the TAG noted, for example, that the TAG issues list (Table IV) represented a culling from a more extensive list of potential issues. All issues remaining on the TAG list are thought to be important. A compromise on the priority was reached on all issues except the understanding of the HPVs as they affect natural circulation. The B&W owners rated this issue of "D" priority but the NRC rated this issue as "A" priority.

This section on regulatory implications attempts to evaluate the success of the tests in the MIST program in providing data on the TAG issues. Also, some closely related B&W plant calculations will be discussed to show the extent to which they also show the phenomena identified as TAG issues. A key element in discussing regulatory implications is to understand the relationship of the phenomena in the tests to the phenomena in full-scale plants. A step in achieving this is to understand differences between code calculations for scaled facilities, such as MIST, and full-scale plants. As noted in Ref. 6, the facility and tests were recommended by the TAG "...to provide a sufficient data base for use in computer code assessment. The assessed computer code is the link between the test data and the operating plant. Test facility results cannot be extrapolated to predict plant performance." More direct linkages of phenomena in tests and plants are desirable and, wherever possible, should be identified. Because of the lack of plant data, only three cases where codes have been tested against actual plant transients are identified here.

2. MIST SBLOCA Tests. Key SBLOCA events were also identified. A group of B&W personnel with extensive plant and thermal-hydraulic experience then reviewed the phenomena and ranked them by their relevance to the TAG issues. This B&W-produced priority ranking

of SBLOCA events by their relevance to the TAG issues is reproduced from Ref. 7 (Table 2.3, page I.2-10) as Table V.

A large number of MIST Tests were SBLOCAs, including test groups 31, 32, 35, and some tests in group 36. Test group 31 consisted of 12 (including repeats) tests where boundary conditions were varied. "The boundary system tests examined the adequacy and impact of the major boundary system simulations of MIST; namely, the RVVVs, guard heating, level controls of the SGs, and AFW wetting."[5] Group 32 tests varied leak and HPI conditions. Group 35 examined noncondensable gas and vent effects. Reactor coolant pump operations were the focus of group 36 tests. Test groups 33 and 34 examined feed-and-bleed cooling and SG tube ruptures, respectively.

The MIST nominal test (3109AA) exhibited over 60% of the phenomena listed in Table V, including the top-10 ranked items. It is particularly important in that it is the test to which parametric variations were to be compared.

3. Conclusions. It is possible to draw important conclusions regarding the regulatory implications of MIST Test 3109AA. Based on our analysis in Section VI.B of this report, we conclude that the phenomena of interest occurred and that the data were of high quality. The thermal-hydraulic phenomena were consistent; the cause and effect relationships were identified for what we believe are all of the major phenomena that occurred in the test (for the time period of the calculation). Therefore, the test data satisfy the objectives of this test as they relate to the TAG issues. As stated by the TAG and repeated here for further emphasis, the test results cannot be extrapolated to full-size B&W plants. The extension to full-size plants must be made through the use of assessed computer codes.

TRAC predicted the phenomena seen in the test with reasonable agreement. Since TRAC has also shown reasonable agreement with data from a number of other SBLOCA tests in a variety of other test facilities, we believe that correct conclusions about trends and phenomena would be drawn if the code were used in similar applications.

A plant-counterpart calculation was made with TRAC for the MIST nominal SBLOCA in a full-scale 177-fuel assembly, lowered-loop B&W plant.[15] The phenomena seen in this calculation were very similar to those of the MIST nominal test. The author also states that "the transient behavior was similar to other TRAC-calculated B&W SBLOCAs." A detailed examination of the MIST Test 3109AA test data and calculation and the plant-counterpart calculation showed differences in timing and in RVVV flow behavior. Although the events seen in the plant-counterpart calculation were similar, they were shifted forward in time. This comes, at least in part, from differences between scaled flow rates. At 2000 s, the integrated leak flow for the MIST Test 3109AA calculation times the scale factor (817) was about 63% of the integrated leak flow for the plant-counterpart calculation. Calculations using the TRAC model of the MIST facility have shown that using too high a leak flow will shift phenomena forward in time in a similar way. The TRAC calculation for MIST Test 3109AA used two-phase-flow multipliers of 0.86 and a geometrically correct input model of the piping upstream of the leak orifice to accurately model leak flow. The plant-counterpart calculation used a model for a 10-cm^2 pipe break following guidelines given in the TRAC User's Manual.

The RVVV flow in the plant-counterpart calculation shows a more oscillatory nature than seen in the MIST calculation. This should be expected since the degree of opening the plant valves is a function of the differential pressure across them. The actual plant RVVVs (which

are flapper valves) would be expected to flap open, then close as the differential pressure across them built up, was relieved, and then built up again. The RVVVs in the MIST facility, on the other hand, are either fully open or fully closed depending upon differential pressure and are not prototypical in this respect. This difference in behavior did not seem to affect the transient.

There is a paucity of data on full-scale plant transients that can be used to validate computer codes at full-scale operation. Calculations have been made for the 1979 Three Mile Island Unit 2 (TMI-2) transient that resulted in partial melting of the core, the Crystal River transient of February 26, 1980, and of the Davis-Besse event of June 9, 1985.

The accident at TMI-2 on March 28, 1979, was analyzed with an early version of TRAC (TRAC-P1A) in the earliest use of a thermal-hydraulics code for analysis of an actual event.[16] TMI-2 was a complex event; boundary flow values and timing were uncertain. The TRAC version under development at that time lacked many of the features of newer codes. It was much slower, as were the computers it was run on. The model was coarsely noded as necessitated by the slower running code and computers. With the assumptions used, the agreement was generally reasonable. The primary-system pressure and minimum core liquid coverage were in reasonable agreement. At the minimum water level, only about the bottom 25% of the length of the rods were immersed. This was predicted by TRAC and by a later analysis of radiation measurements and recently verified by the examination of the core remains. With differences between the early version of the TRAC code and the current version (TRAC-PF1/MOD1), and the simplified model used, it is difficult to draw general conclusions about the ability of TRAC to predict the phenomena that occurred in the TMI-2 accident.

This accident is being analyzed again as part of a test problem for TRAC-MELPROG, a severe core damage code integrated with TRAC. A developmental code version, TRAC-PF1/MOD2, is being used for the thermal-hydraulic version. When the results of this become available more definitive conclusions can be drawn about what phenomena were predicted by the code, and if the overall results are consistent with the plant data.

Another plant transient that was similar in its early stages and that has been analyzed with later code versions and more detailed models is the Crystal River-3 event of February 26, 1980. It was analyzed using two versions of the code, TRAC-PD2 and TRAC-PF1/MOD0 (Ref. 17). The event occurred when a power supply problem caused non-nuclear instrumentation to malfunction. This gave erroneous information to a control system, which reduced the feedwater flow, increased the reactor power, and opened the PORV. The reduced feedwater caused the pressure to rise, which caused the reactor and turbine to trip. The PORV stayed open. Pressure decreased, HPI was initiated, and the reactor coolant pumps tripped. Feedwater was re-established to the B loop and the PORV block valve was closed at an estimated 450 s. The primary repressurized such that safety relief valves relieved pressure spilling contaminated liquid into the containment. Unlike TMI-2, the HPIs kept the system inventory nearly full so that the core was never in danger.

Although there were instrumentation problems and boundary condition uncertainties, the Crystal River-3 transient gives a better test of phenomena than TMI-2. Phenomena included voiding in the A loop hot leg with natural circulation stalling. Natural circulation continued in the B loop as feedwater was available to cool that SG. A switch from main to auxiliary feedwater was made, with the AFW coming in at a much higher elevation than the main

feedwater. This increased the natural-circulation flow. Both versions of TRAC predicted the phenomena consistent with the data.

The early part of the Crystal River-3 transient was a SBLOCA caused by the stuck open PORV. Despite the uncertainty of the data and boundary conditions, it appears that TRAC was able to predict the phenomena, thus providing some evidence for the code's ability to predict SBLOCA phenomena in full-scale B&W plants.

Following the Davis-Besse event of June 9, 1985, TRAC (Ref. 18) and RELAP calculations were performed for the event and some parametric variations of it in a "rapid response" effort. At the time, there was significant uncertainty regarding key boundary conditions. A subsequent independent study of the Davis-Besse transient was conducted at the INEL.[18] It was concluded that a calculation of the Davis-Besse loss-of-feedwater transient was in good qualitative and quantitative agreement with the measured data. This agreement was attained for a calculation of the transient using RELAP5/MOD2. The maximum deviation between calculated and measured reactor-coolant-system pressure was about 0.3 MPa (50 psi). The deviations between calculated and measured reactor-coolant-system temperatures were generally less than 3 K (6°F). It was noted that the differences between an earlier RELAP5/MOD2 calculation, the TRAC-PF1/MOD1 calculation reported in Ref. 17, and the RELAP5/MOD2 (Ref. 19) calculation "were primarily because of the assumption of different core powers, feedwater flows, and pressurizer spray flows." The first RELAP5 calculation and the TRAC calculation were performed shortly after the Davis-Besse event; at this time there was significant uncertainty regarding key boundary conditions. The subsequent RELAP5 calculation used more accurate representations of these key boundary conditions resulting from additional study of the plant transient. We conclude that a TRAC-PF1/MOD1 calculation using the improved boundary conditions specification would have produced similar results.

The information from these calculations strengthens our confidence that the major trends to be expected during a transient in a full-size B&W plant, such as a SBLOCA, would be calculated using TRAC-PF1/MOD1.

REFERENCES

1. Safety Code Development Group, "TRAC-PF1/MOD1: An Advanced Best-Estimate Computer Program for Pressurized Water Thermal-Hydraulic Analysis," Los Alamos National Laboratory report LA-10157-MS and NUREG/CR-3858 (July 1986).
2. "Immediate Report, Test 3109AA: Group 31 (Boundary) Test 9, Nominal," Babcock & Wilcox document BAW-1925 (August 1986).
3. J. R. Gloudemans (principal author), "Group Report, MIST Test Group 31, Boundary Conditions," Babcock & Wilcox document BAW-1958 (March 1987).
4. D.A. Siebe and J. L. Steiner, "Pretest Analysis of MIST Test 310000," Los Alamos National Laboratory document LA-CP-87-52 (1987).
5. "Mist Test Specifications," Babcock & Wilcox document BAW-1985 (October 1985).
6. "Multi-Loop Integral System Test (MIST) Facility Specification," Babcock & Wilcox document RDD-84:4091-01-01:01 (1984).
7. J. A. Klingenfus, "Multi-Loop Integral System Test Design Verification Report," Babcock & Wilcox document NRC-04-83-168/RP 2399-1 (November 1984).

8. D. R. Liles, J. W. Spore, T. D. Knight, et al, "TRAC-PF1/MOD1 Correlations and Models," Los Alamos National Laboratory report LA-11208-MS and NUREG/CR-5069 (January 1989).
9. B. E. Boyack, H. Stumpf, and J. F. Lime, "TRAC User's Guide," Los Alamos National Laboratory report LA-10590-M and NUREG/CR-4442 (November 1985).
10. K. R. Katsma, R. A. Dimenna, and G. E. Wilson, "TRAC-PF1/MOD1 Uncertainty Quantification for LBLOCA Blowdown Peak Cladding Temperature," Idaho National Engineering Laboratory, Fifteenth Water Reactor Safety Information Meeting, October 26-30, 1987, Gaithersburg, Maryland, NUREG/CP-0090 (October 1987).
11. "Compendium of ECCS Research for Realistic LOCA Analysis," U.S. Nuclear Regulatory Commission report, NUREG-1230, Draft (April 1987).
12. "Test Specification for Rancho Seco Scaling Transient Test," MIST Program Management Group communication 4–7 (August 21, 1987).
13. B. W. Sheron, "SBLOCA - A Regulatory Perspective," Proceedings, Specialists Meeting on Small Break LOCA Analyses in LWRs, Vol. 2, Pisa, Italy, June 23–27, 1985.
14. "Test Advisory Group Final Report, Integral System Testing Program for the B&W-Designed NSS," Babcock & Wilcox document BAW-1787 (June 1983).
15. J. F. Lime, "TRAC Calculation of MIST Nominal-case SBLOCA in a Full-Scale B&W Lowered-Loop Plant," (report prepared in 1985) Los Alamos National Laboratory report LA-CP-92-293 (August 1992).
16. J. R. Ireland, P. K. Mast, T. R. Wehner, P. B. Bleiweis, W. L. Kirchner, and M. G. Stevenson, "Preliminary Calculations Related to the Accident at Three Mile Island," Los Alamos Scientific Laboratory report LA-8273-MS and NUREG/CR-1353 (March 1980).
17. P. Coddington and G. J. E. Willcutt, Jr., "TRAC Analysis of the Crystal River Unit-3 Plant Transient of February 26, 1980," Proceedings, ANS Topical Meeting on Anticipated and Abnormal Plant Transients in Light Water Reactors, Jackson, Wyoming, September 26–29, 1983.
18. J. F. Lime, B. Nassersharif, and B. E. Boyack, "Rapid-Response Analysis of the Davis-Besse Loss-of-Feedwater Event on June 9, 1985," Proceedings, ANS Topical Meeting on Reactor Physics and Safety, Saratoga Springs, New York, September 17–19, 1986.
19. C. B. Davis, "Davis-Besse Uncertainty Study," EG&G Idaho, Inc. document EGG-RTH-7453 (November 1986).

TABLE I

STEADY-STATE CONDITIONS FOR TEST 3109AA

Parameter	Unit	Test	TRAC
Core power	kW	128.6	126.6[a,b]
Pressurizer pressure	MPa	11.99	12.01
	psia	1739.	1742.
Hot-leg subcooling	K	13.3	13.8
	(°F)	23.9	24.8
Hot-leg temperatures	K	584.4	584.1
	(°F)	592.3	591.7
Cold-leg A1 pump suction temperature	K	561.5	560.3
	(°F)	551.0	548.9
Downcomer flow	kg/s	0.859	0.878
	(lbm/s)	1.894	1.936
Pressurizer water level	m	1.58	1.63[b]
	(ft)	5.17	5.35
Steam-generator A secondary level	m	1.42	1.49[c]
	(ft)	4.65	4.89
Steam-generator B secondary level	m	1.44	1.52[c]
	(ft)	4.74	4.99
Steam-generator A pressure	MPa	6.988	6.978
	(psia)	1014.	1012.
Steam-generator B pressure	MPa	6.997	6.979
	(psia)	1015.	1012.

[a] TRAC core power reduced to account for outside of core energy losses in facility.
[b] Specified in TRAC input.
[c] Control system controls to specified value.

TABLE II

TEST 3109AA TRANSIENT CONTROLS

Parameter	Control
PORV	Open when primary pressure = 16.2 MPa (2350 psia); remain open until primary pressure is within 0.69 MPa (100 psi) of secondary pressure.
Core power	SCRAM when pressurizer level = 0.305 m (1 ft)
RVVV	Before pressurized level = 0.305 m (1 ft) Closed After pressurizer level = 0.305 m (1 ft) Open when RVVV differential pressure > 861.8 Pa (0.125 psi) Close when RVVV differential pressure < 276 Pa (0.04 psi)
HPI	Scaled head-flow after pressurizer level = 0.305 m (1 ft)
CFT	Actuate at 4.14 MPa (600 psia) Manual isolation when: PORV open and HPI actuated and core exit > 27.8 K (50°F) for 30 min subcooling and primary pressure < 4.93 MPa (715 psia) and primary pressure not increasing Automatic isolation on low level
Primary pumps	Locked rotors
SG-secondary pressure	Initially controlled at 6.96 MPa (1010 psia). ATOG pressure control (Ref. 4) after pressurizer level = 0.305 m (1 ft)
AFW	Used to control SG-secondary level: set point = 1.524 m (5 ft) initially, set point = 9.631 m (31.6 ft) after pressurizer level = 0.305 m (1 ft)

TABLE III

EVENT TABLE FOR TEST 3109AA

Time (s) Test	Time (s) Calculation	Event Description
0.0	0.0	Start transient-break initiation.
150.	160.	Pressurizer level drops to 1.0 ft, core-power ramp, HPI, RVVV automatic control initiated, RVVV first opens, SG-secondary level reset.
185.	185.	Intact-loop hot leg saturates.
240.	310.	Intact-loop flow ends.
565.	565.	BCM begins in intact-loop SG as SG-secondary level settles in on set point.
1000.	1000.	BCM ends in intact-loop, broken-loop hot-leg level begins to decrease, broken-loop flow reaches minimum and then increases as voiding in upper head forces liquid into hot legs. Primary begins to repressurize.
1150.	1480.	RVVVs close in response to draining in vessel and downcomer.
1575.	1840.	RVVVs open, allowing core-generated steam to pass from vessel to downcomer, repressurization ends as steam passing through RVVVs contacts cold HPI water in downcomer and condenses. Intermittent broken-loop flow ends as steam no longer pushes liquid over hot-leg U-bend.
4000.	3400.	SG-secondary pressure set point decreases to intact-loop SG-secondary pressure. Steaming of SG-secondary begins, AFW comes on to maintain level, BCM heat-transfer event results. Primary depressurization rate increases. HPI flow exceeds leak flow for remainder of transient. Refill begins.
	7000.	Calculation terminated.

TABLE IV

TAG EVALUATION OF ISSUES

Natural Circulation	
Single-phase natural circulation	D
Two-phase natural circulation	C
Boiler-condenser natural circulation	A
Steam-generator-driven instabilities	B
Cold-leg oscillations	B
Interruption/re-establishment	B
High point vents	A/D
Noncondensable gases	B
Reactor vessel vent valves	C
Small Break Loss-of-Coolant Accident	
Break size	C
Emergency core cooling system operation	C
Reactor-coolant pump operation	B
Location of break	D
Break isolation	B
Reactor vessel vent valves	B
Feed and Bleed	D
Steam-Generator Tube Rupture	B

TABLE V

PRIORITY OF SBLOCA EVENTS

Rank	Rating	SBLOCA Event
1	8	Hot-leg U-bend saturation and voiding
2	8	RVVV activation
3	8	Leak-HPI cooling
4	7	Reinitiation of natural circulation
5	7	SG condensation of primary steam
6	7	Downcomer and cold-leg voiding and condensation
7	7	Leak flow
8	7	Reactor-vessel upper-head voiding
9	7	Decoupling of SG
10	6	Spillover circulation (hot-leg U-bend refilled)
11	6	Primary repressurization
12	6	Venting of primary fluid
13	5	Feed-and-bleed primary cooldown
14	5	Controlled SG depressurization and primary cooldown
15	5	Compression of primary fluid
16	5	Asymmetric conditions among cold legs
17	4	Single-phase natural circulation
18	4	"Pump bump"
19	4	Cooling of idle loop
20	4	Primary depressurization
21	4	Power and flow transient: reactor and coolant pump trip, feed transfer
22	3	Primary depressurization to core-flood tank/low-pressure injection pressures
23	3	Subcooling of primary components
24	3	SG repressurization
25	3	Pressurizer draining

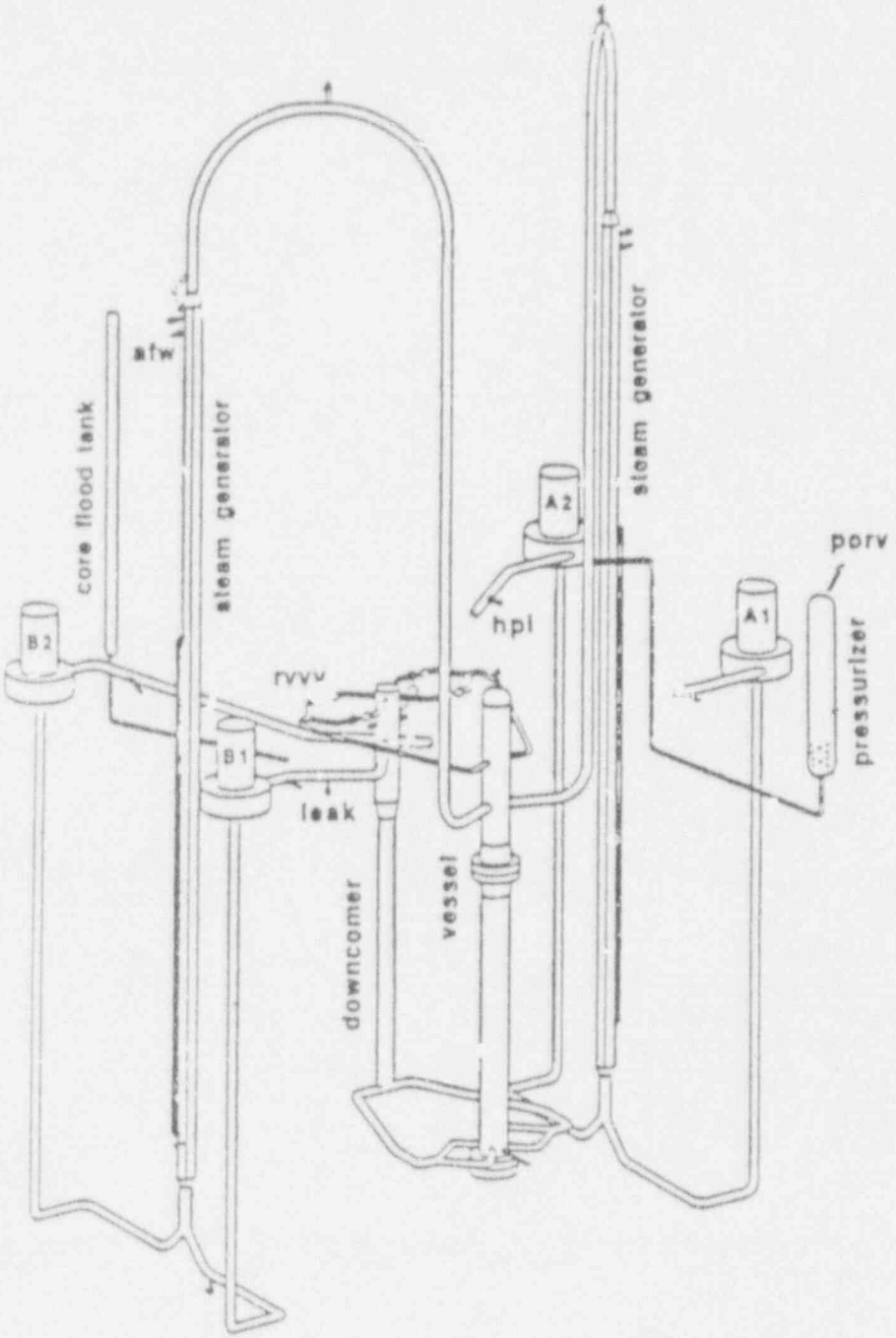

Fig. 1.
Overview of measured results for MIST Test 3109AA.

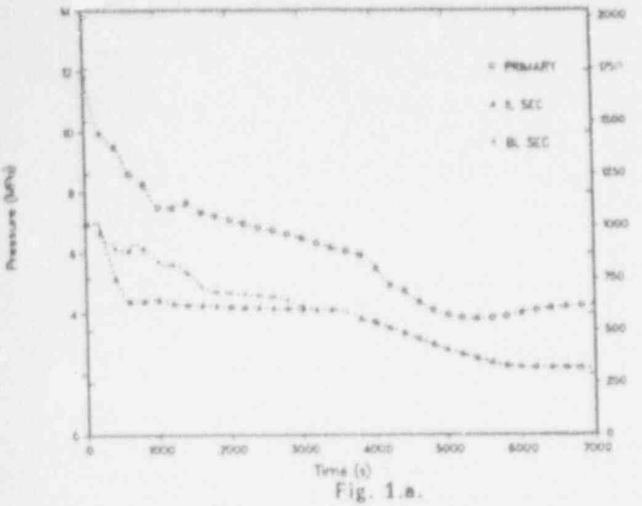

Fig. 1.a.
Primary and secondary pressures.

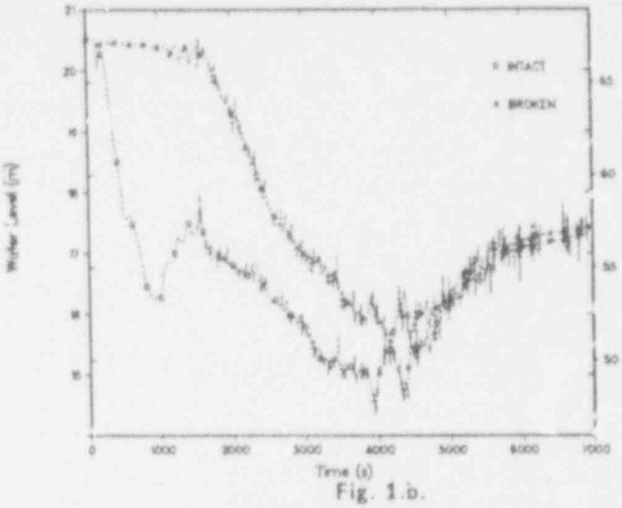

Fig. 1.b.
Hot-leg collapsed liquid levels.

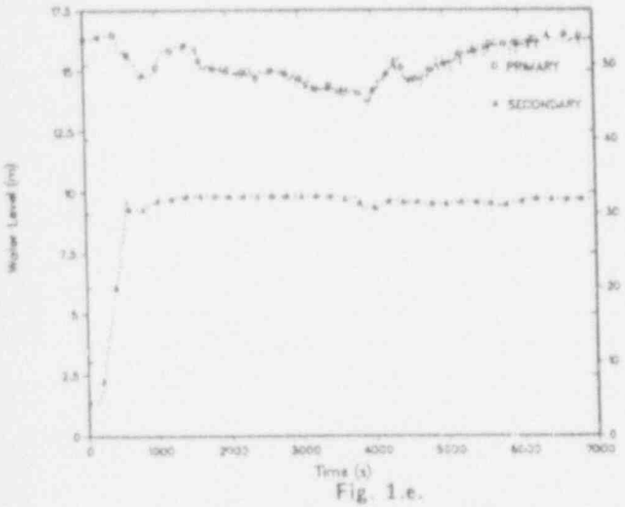

Fig. 1.e.
A-loop SG collapsed liquid levels.

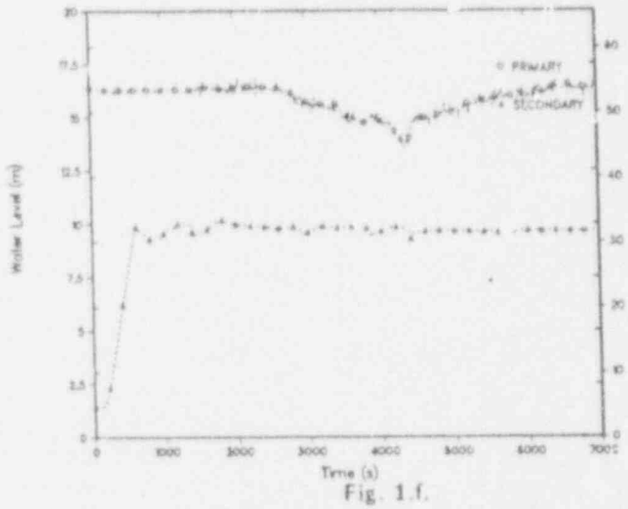

Fig. 1.f.
B-loop SG collapsed liquid levels.

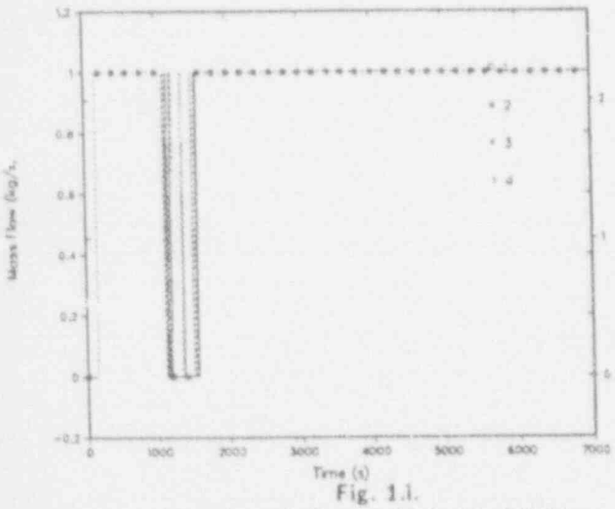

Fig. 1.i.
Full-closed indicators for facility RVVVs.

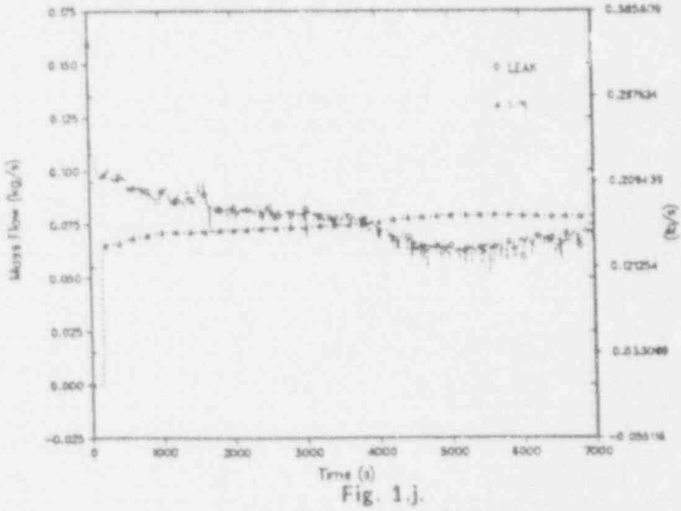

Fig. 1.j.
Cold-leg leak and HPI flows.

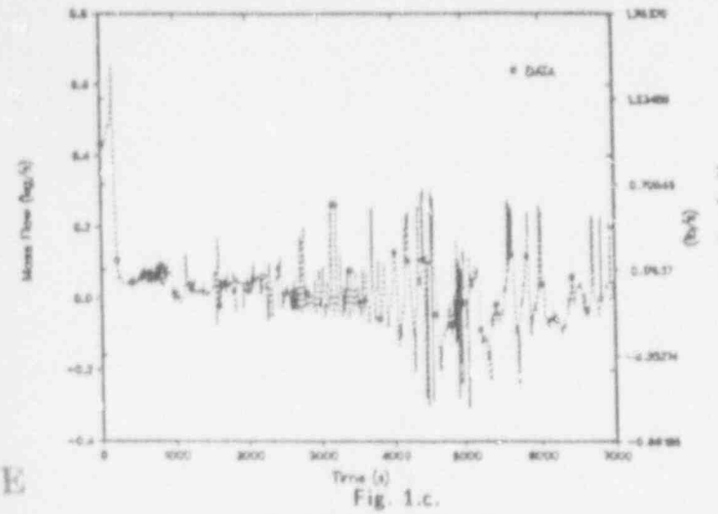

Fig. 1.c.
Total A-loop cold-leg flow.

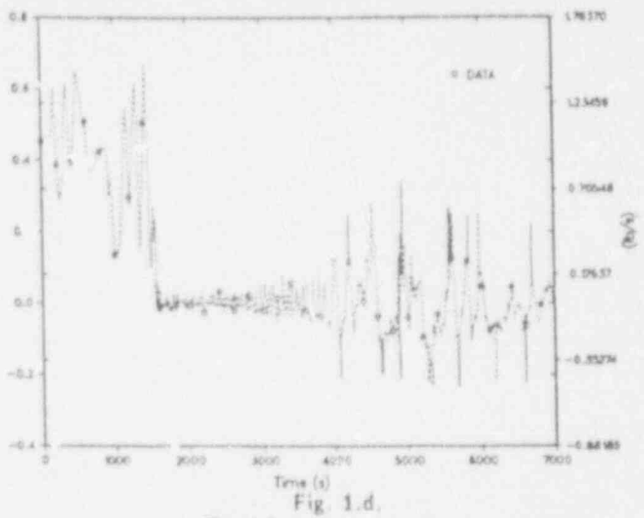

Fig. 1.d.
Total B-loop cold-leg flow.

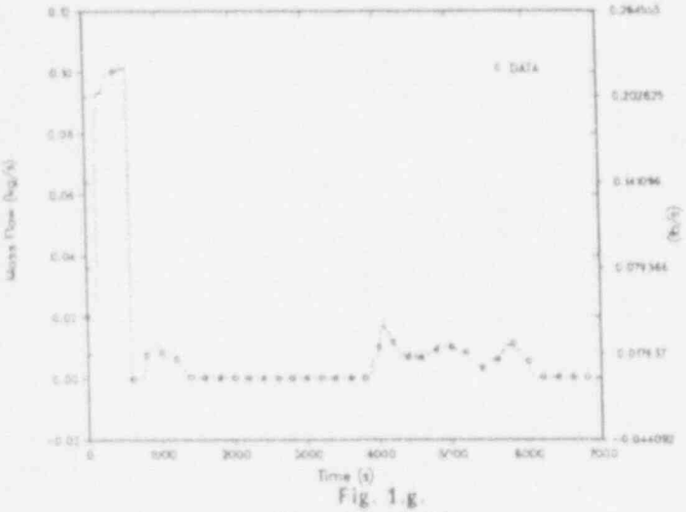

Fig. 1.g.
A-loop SG AFW flow.

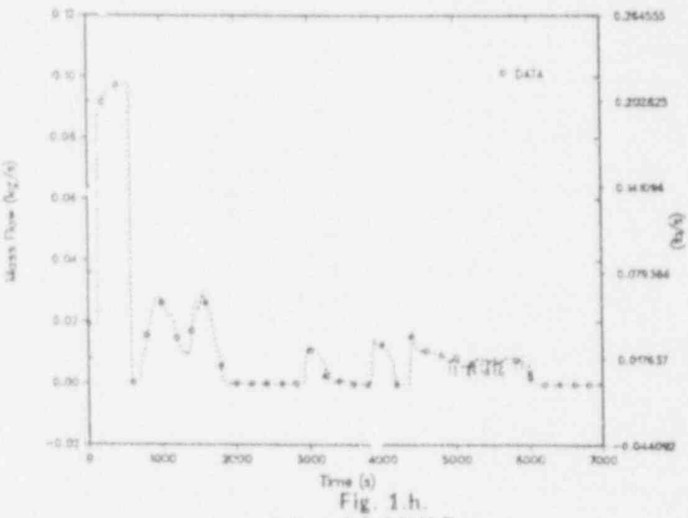

Fig. 1.h.
B-loop SG AFW flow.

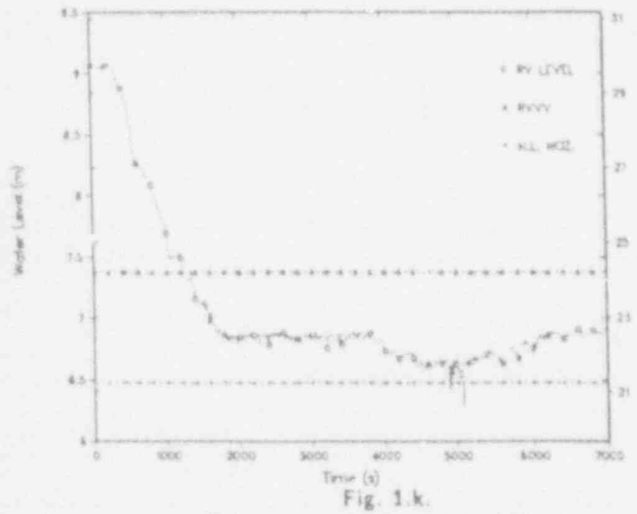

Fig. 1.k.
Reactor-vessel collapsed liquid level.

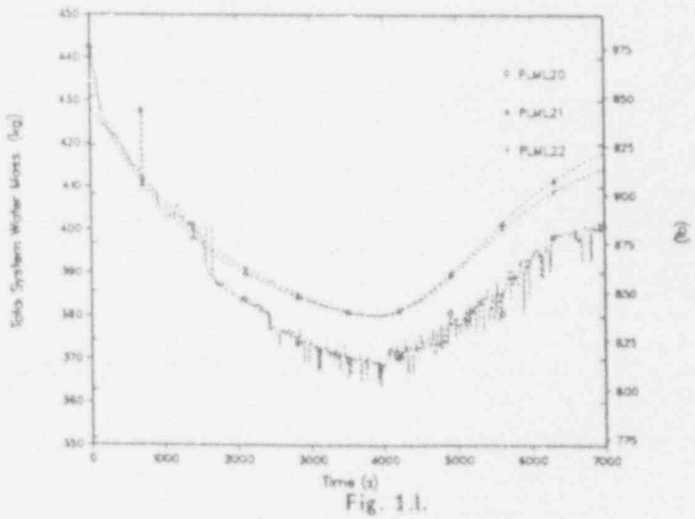

Fig. 1.l.
Primary system inventory.

40340-01

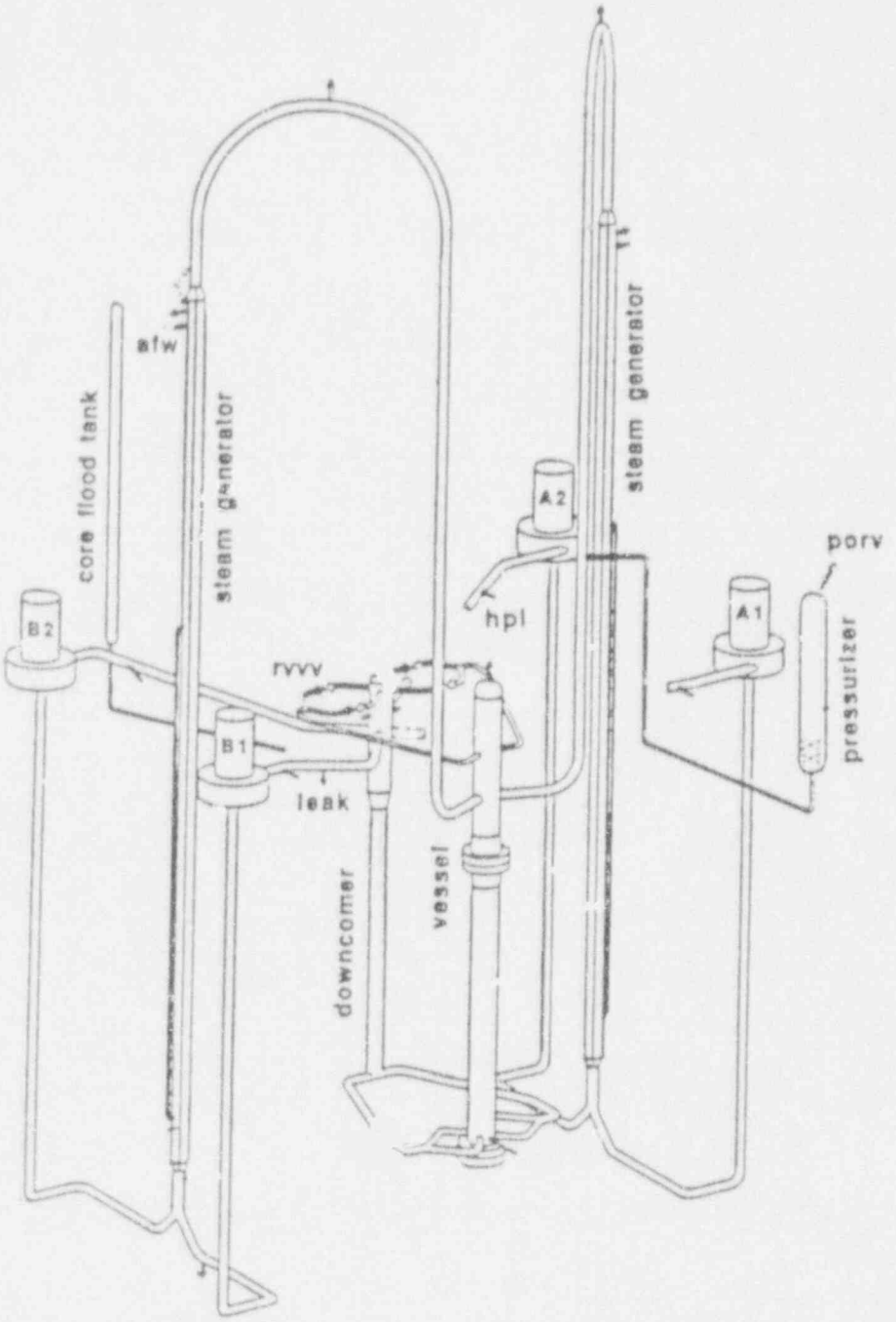

Fig. 2.
Overview of code-experiment comparisons for MIST Test 3109AA.

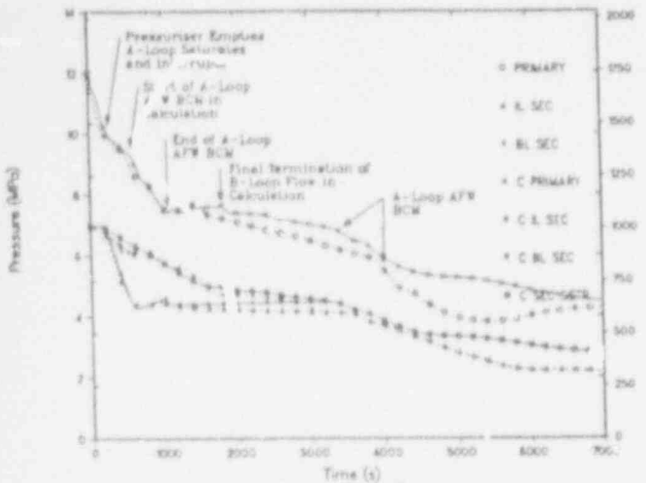

Fig. 2.a.
Primary and secondary pressures.

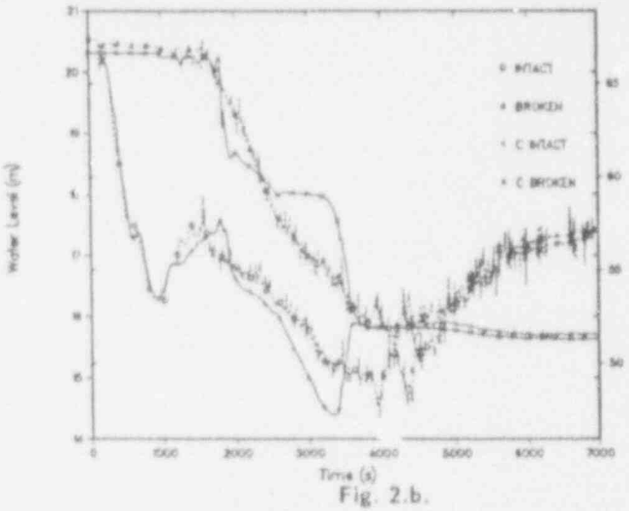

Fig. 2.b.
Hot-leg collapsed liquid levels.

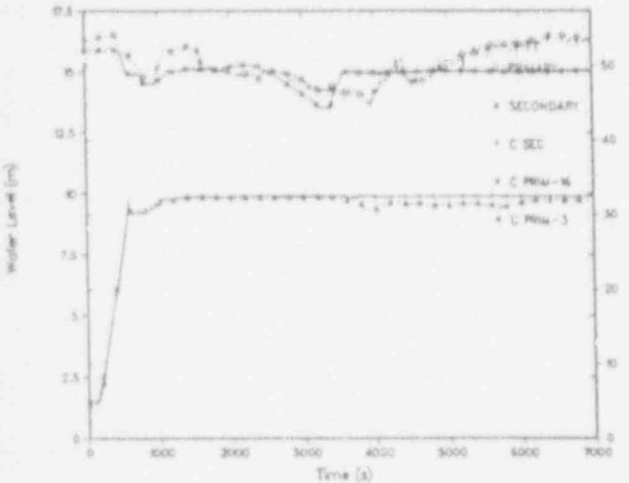

Fig. 2.e.
A-loop SG collapsed liquid levels.

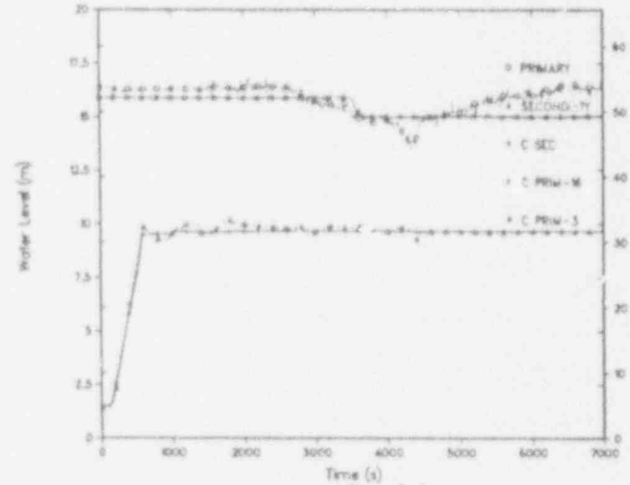

Fig. 2.f.
B-loop SG collapsed liquid levels.

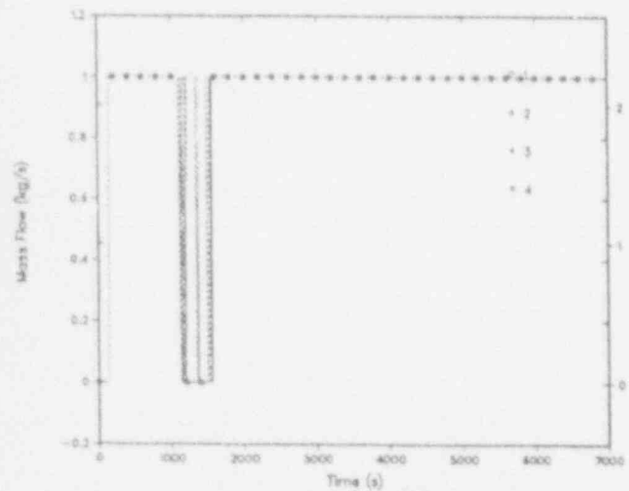

Fig. 2.i.
Full-closed indicators for facility RVVVs.

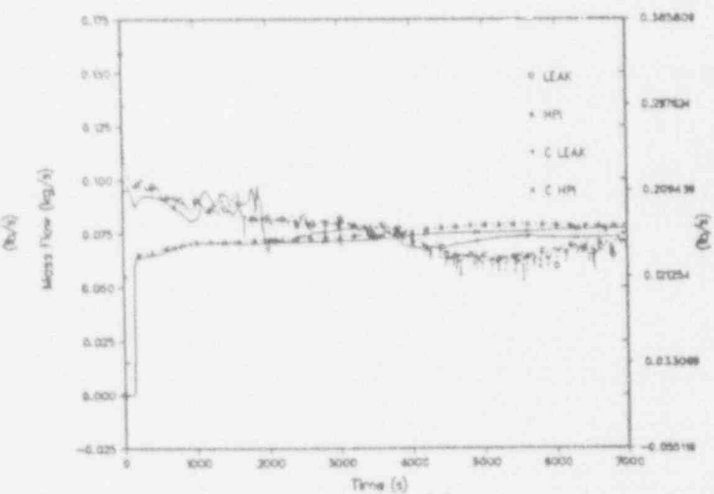

Fig. 2.j.
Cold-leg leak and HPI flows.

92

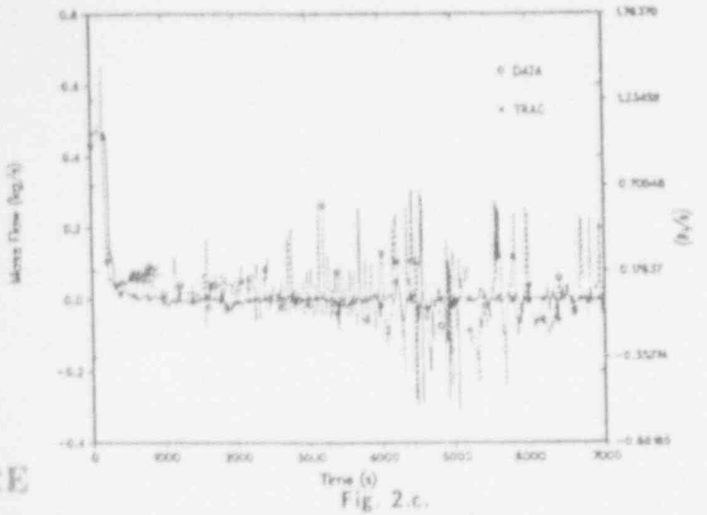

Fig. 2.c.
Total A-loop cold-leg flows.

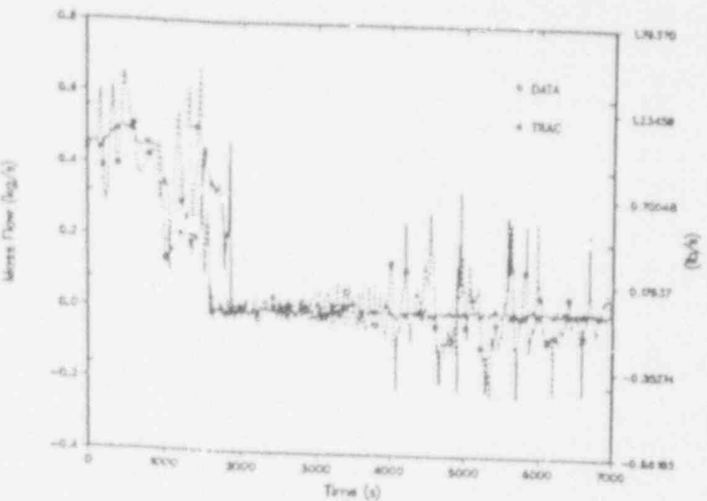

Fig. 2.d.
Total B-loop cold-leg flows.

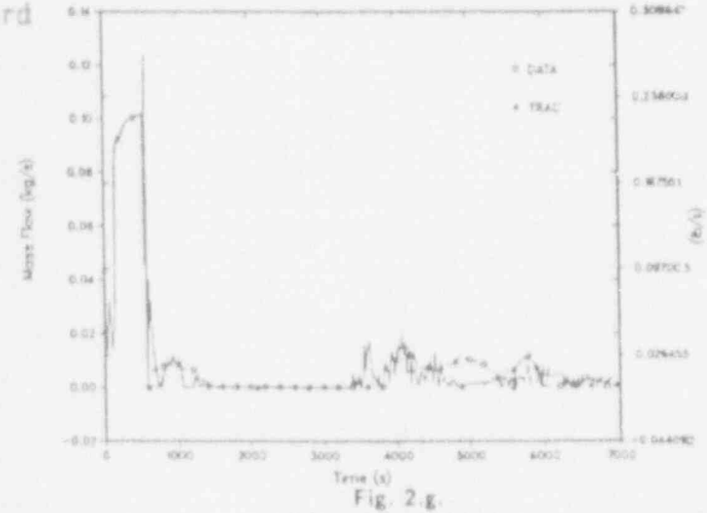

Fig. 2.g.
A-loop SG AFW flow.

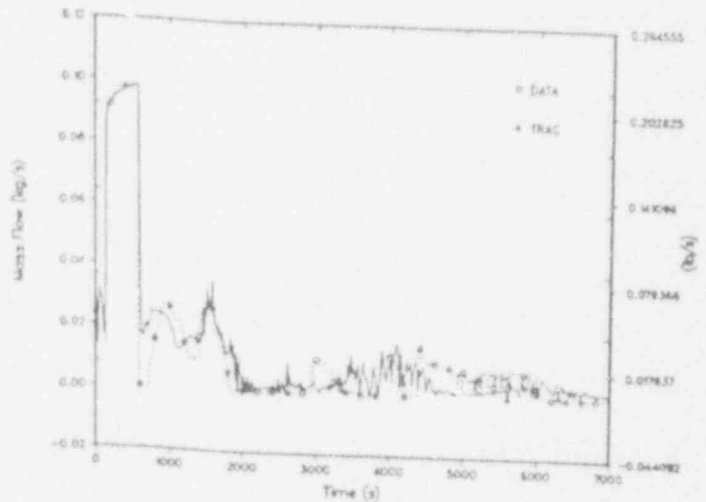

Fig. 2.h.
B-loop SG AFW flow.

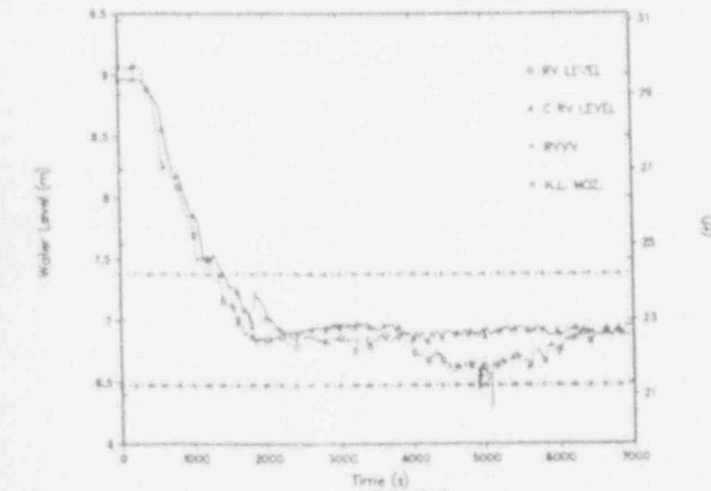

Fig. 2.k.
Reactor-vessel collapsed liquid level.

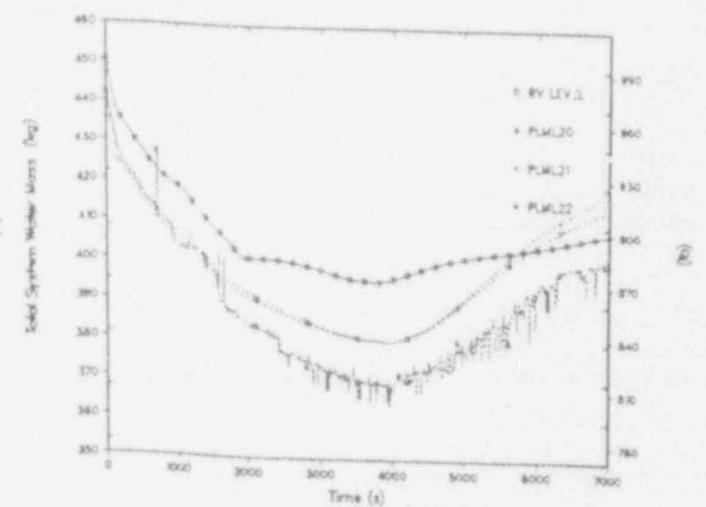

Fig. 2.l.
Primary system inventory.

2112403 40-02

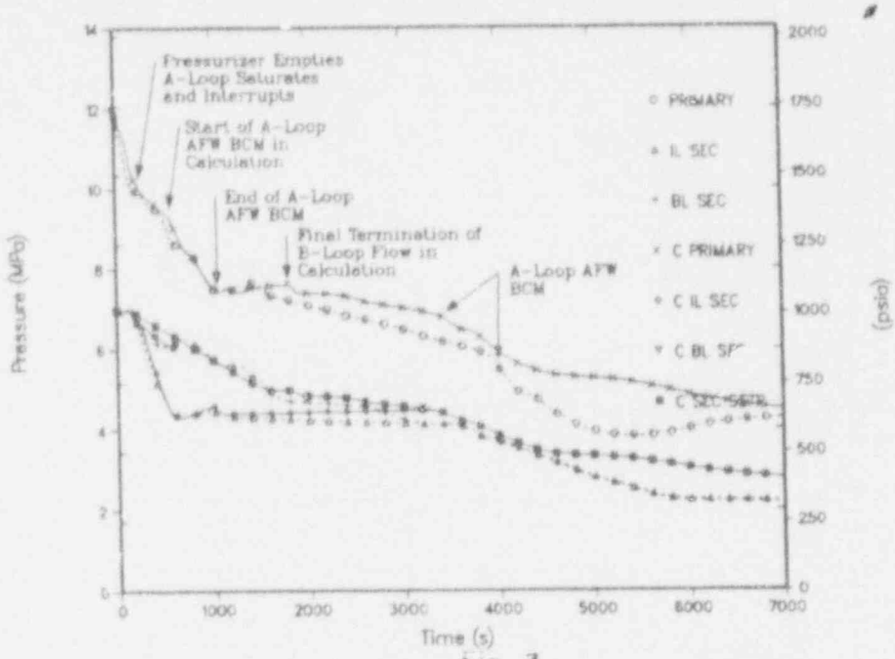

Fig. 3.
Primary and secondary pressures.

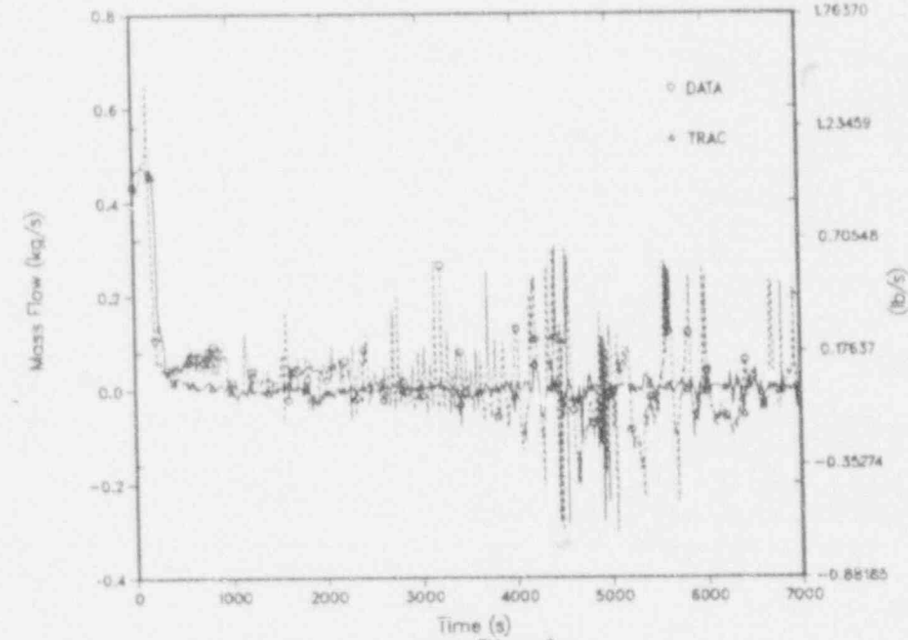

Fig. 4.
Total A-loop cold-leg flow.

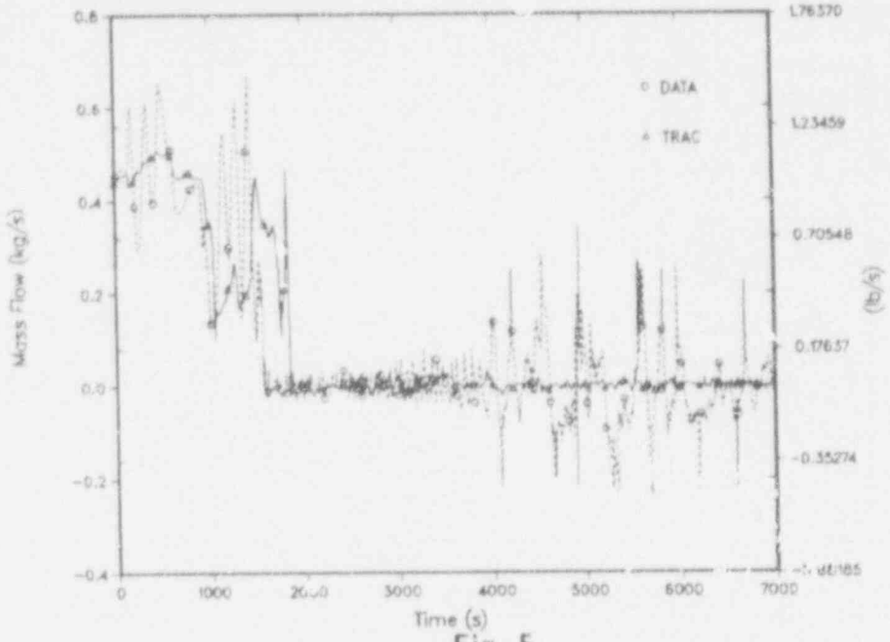

Fig. 5.
Total B-loop cold-leg flow.

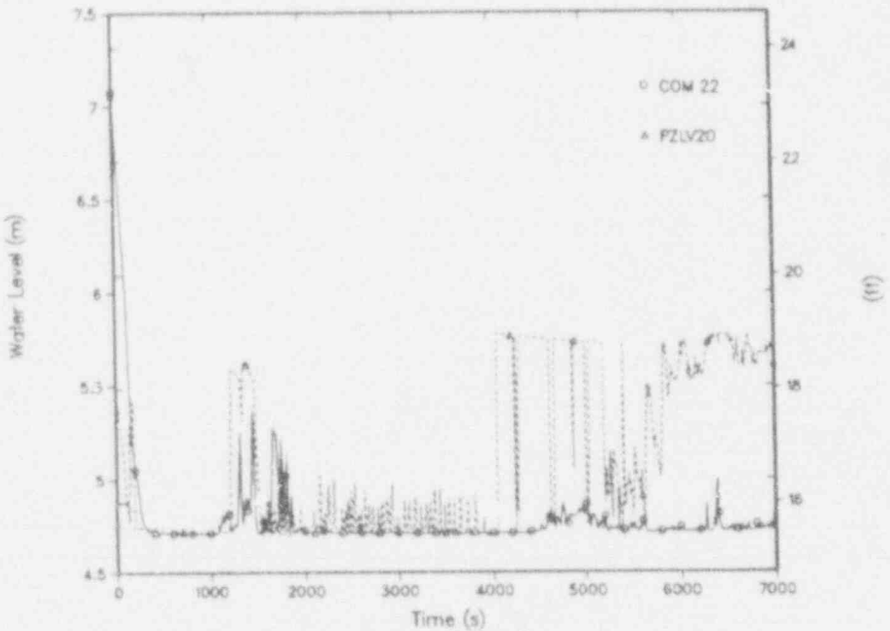

Fig. 6.
Pressurizer liquid level.

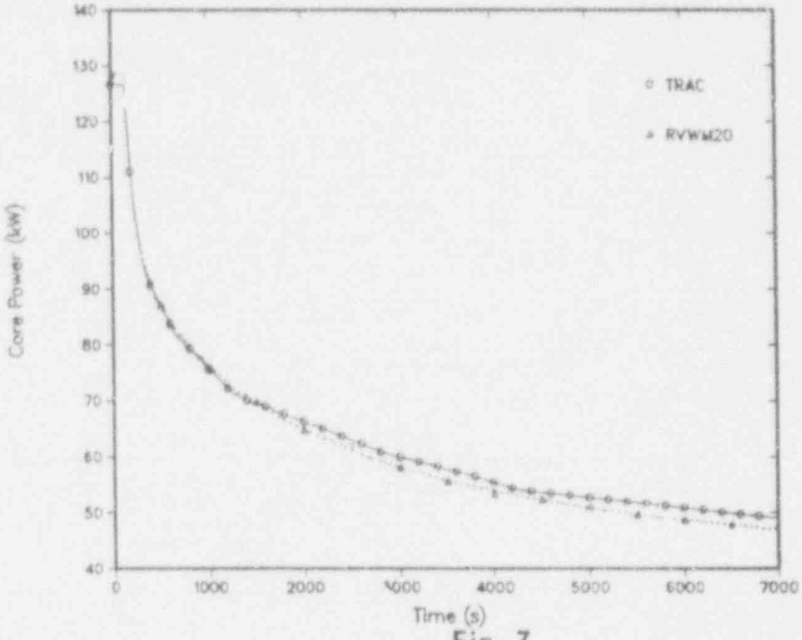

Fig. 7.
Core power.

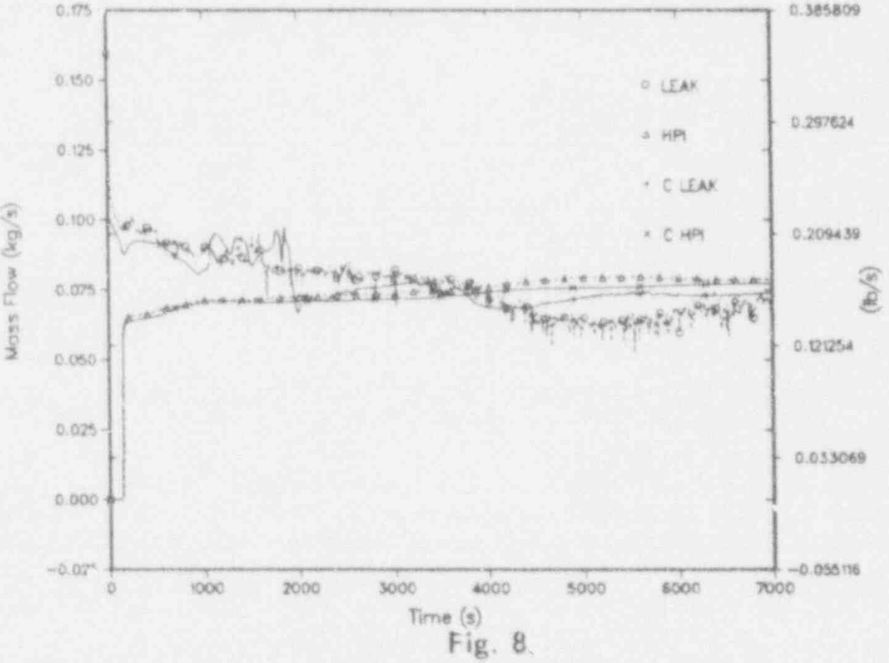

Fig. 8.
Cold-leg leak and HPI flows.

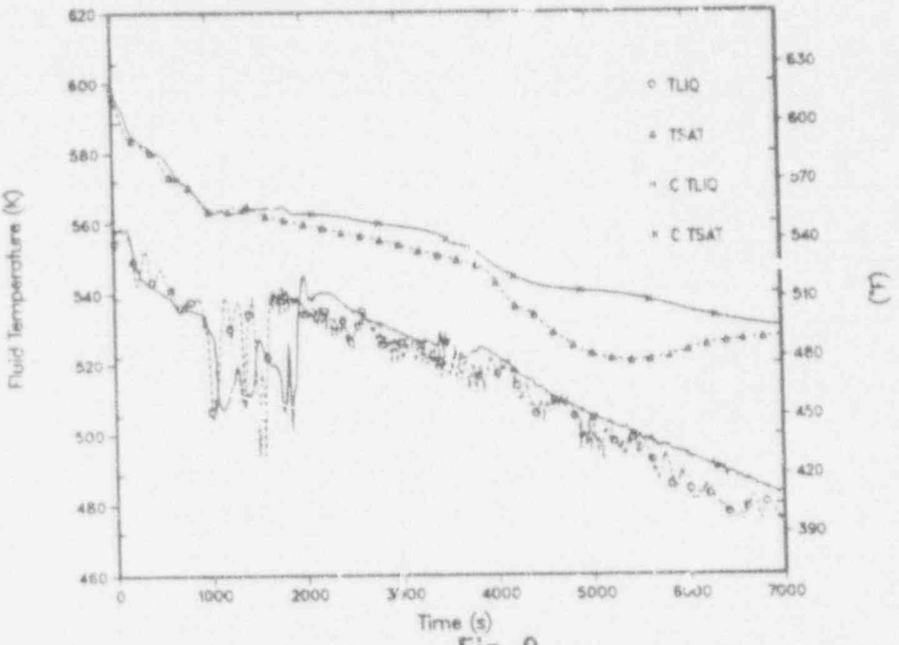

Fig. 9.
Leak upstream fluid temperatures.

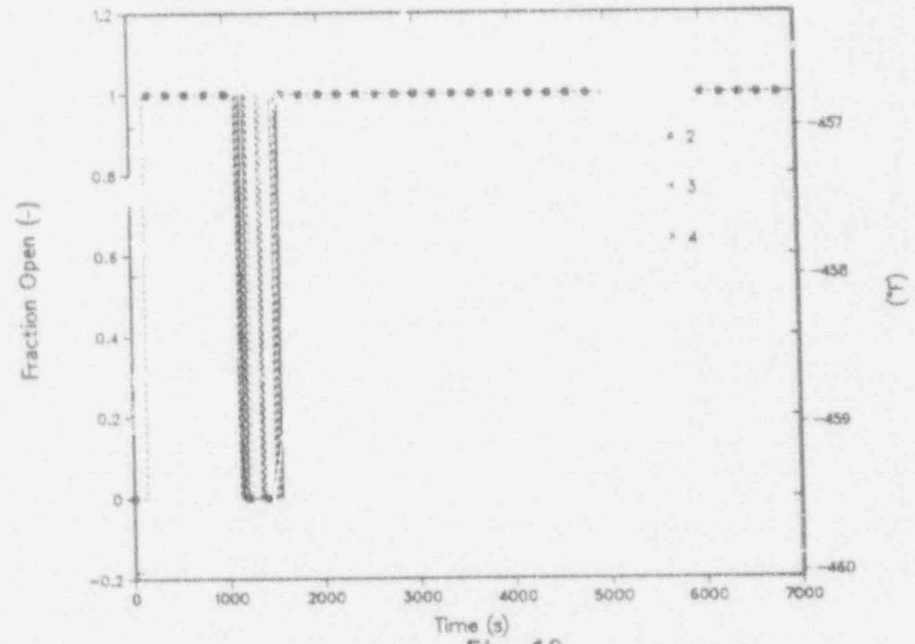

Fig. 10.
Full-closed indicators for facility RVVVs.

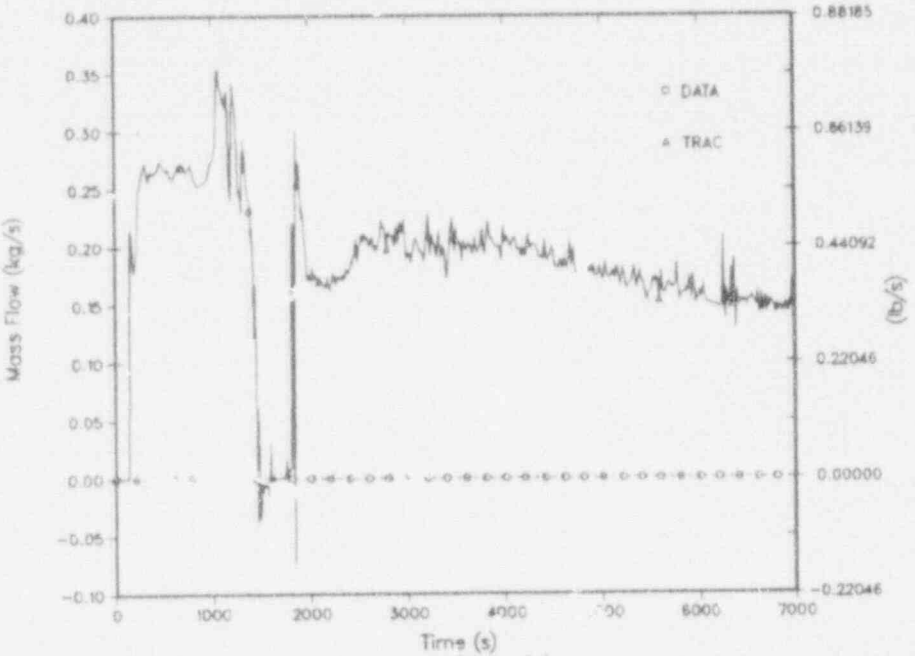

Fig. 11.
RVVV flows.

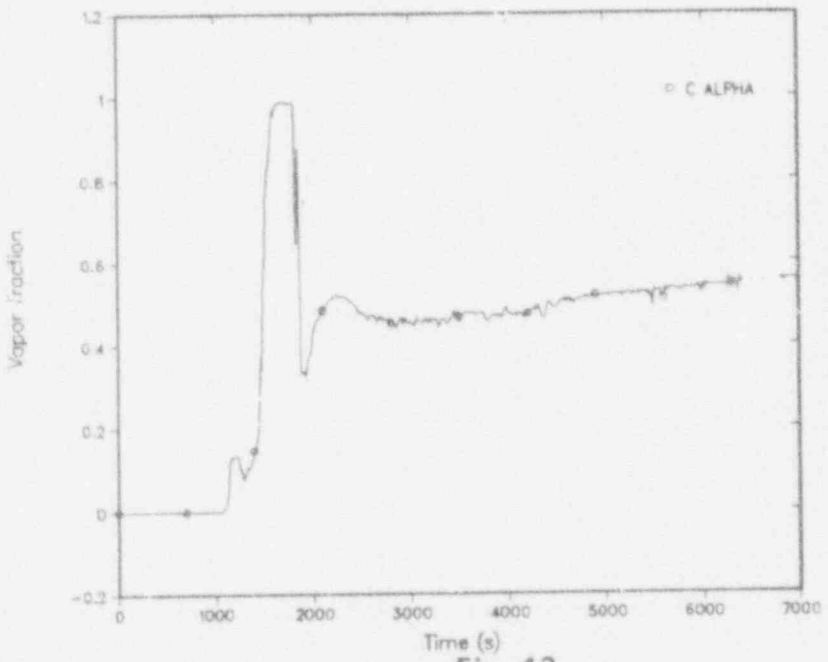

Fig. 12.
Vapor fraction upstream of RVVVs.

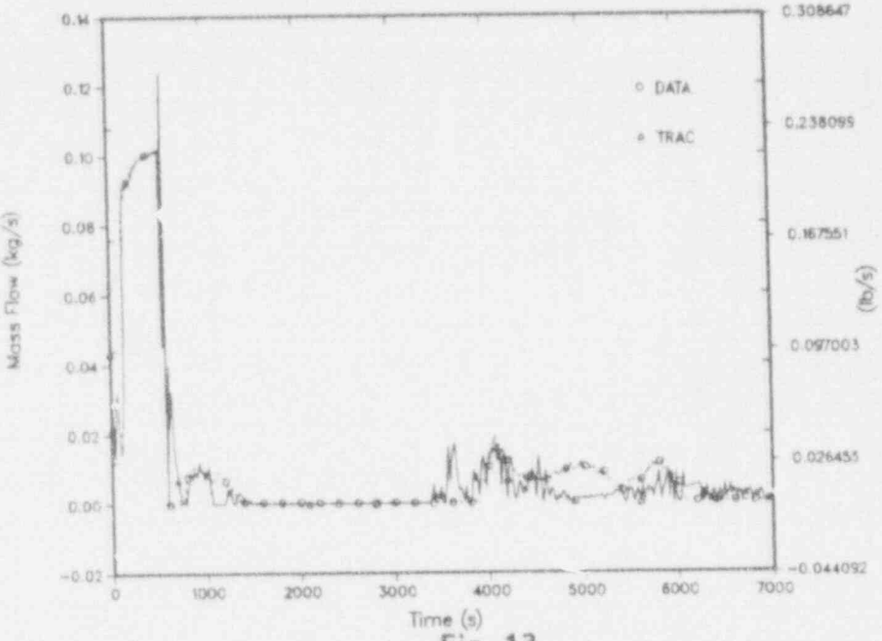

Fig. 13.
A-loop SG AFW flow.

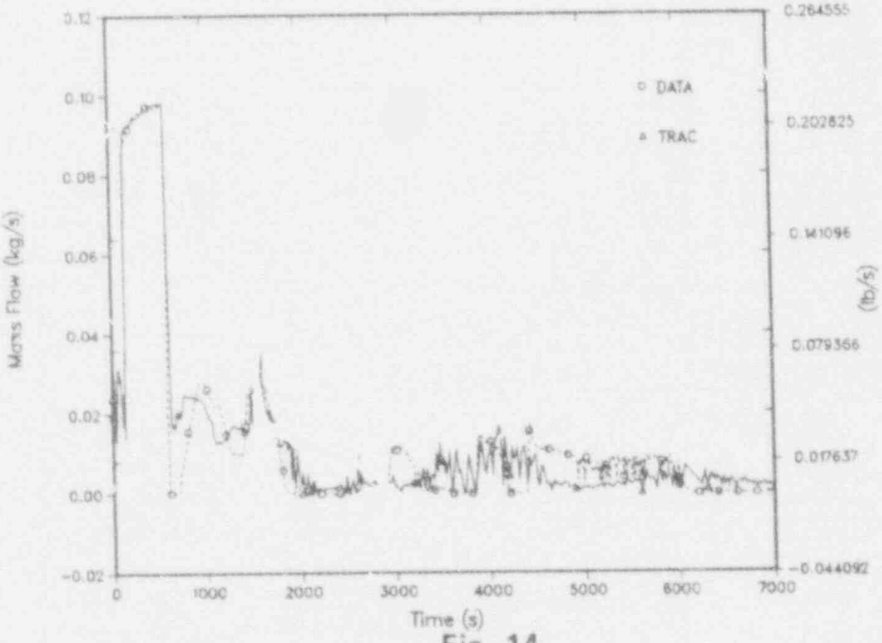

Fig. 14.
B-loop SG AFW flow.

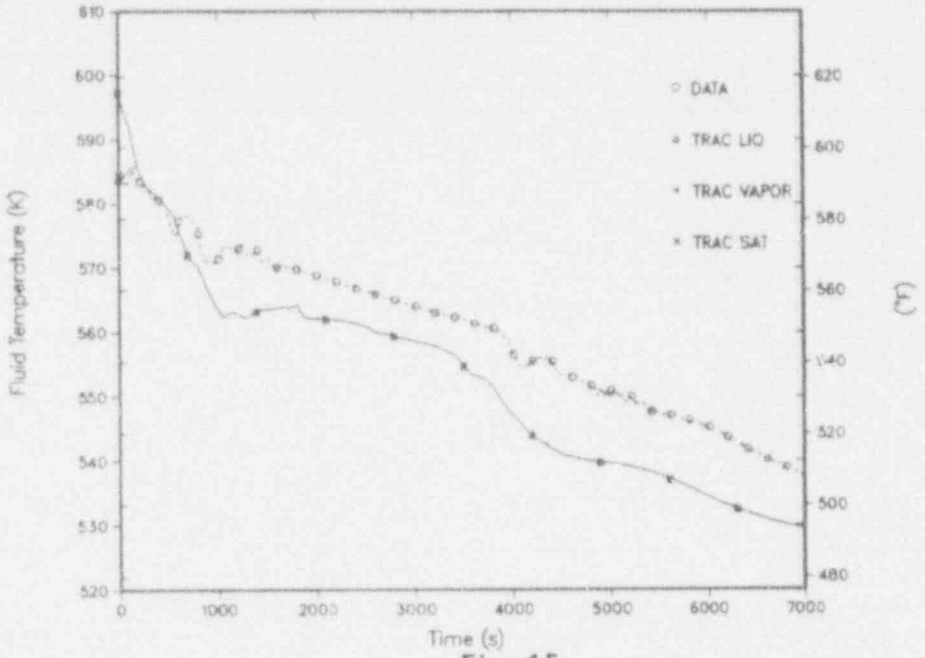

Fig. 15.
Hot-leg U-bend temperatures.

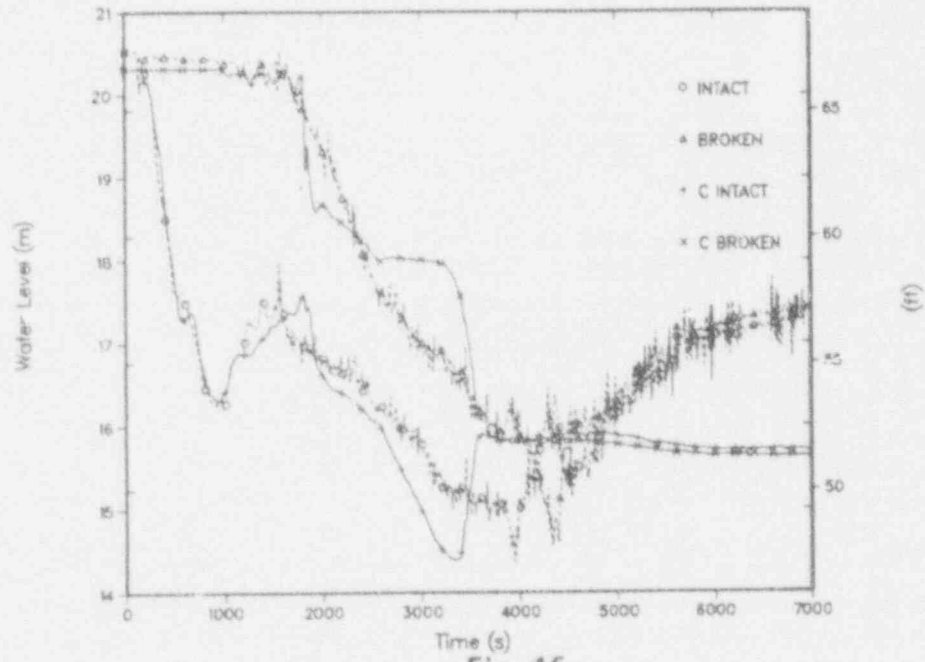

Fig. 16.
Hot-leg collapsed liquid levels.

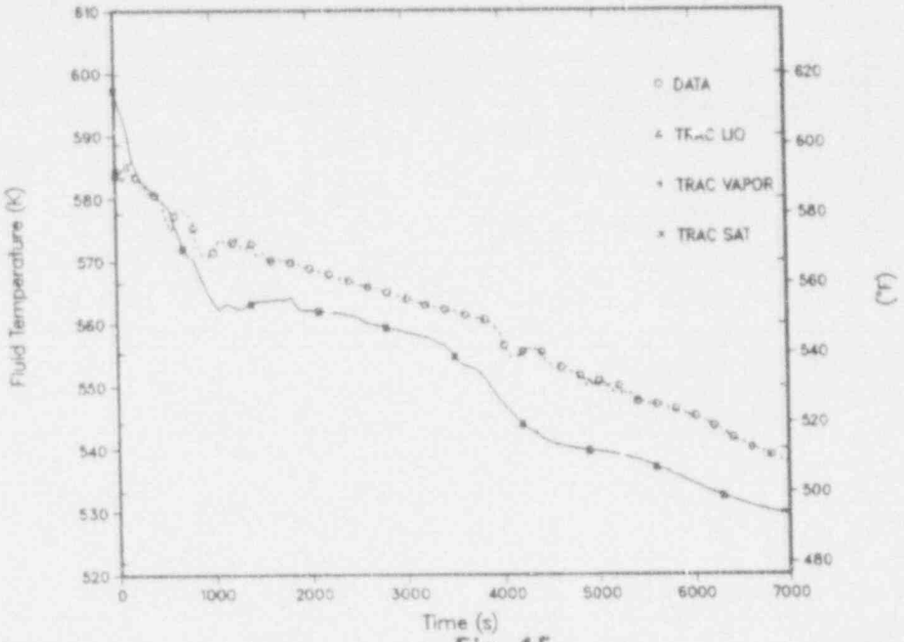

Fig. 15.
Hot-leg U-bend temperatures.

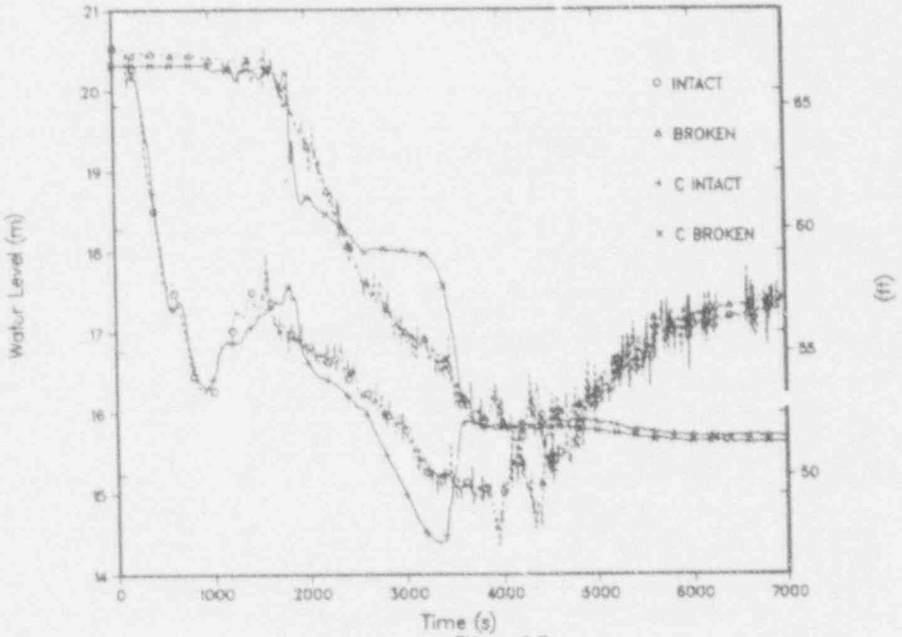

Fig. 16.
Hot-leg collapsed liquid levels.

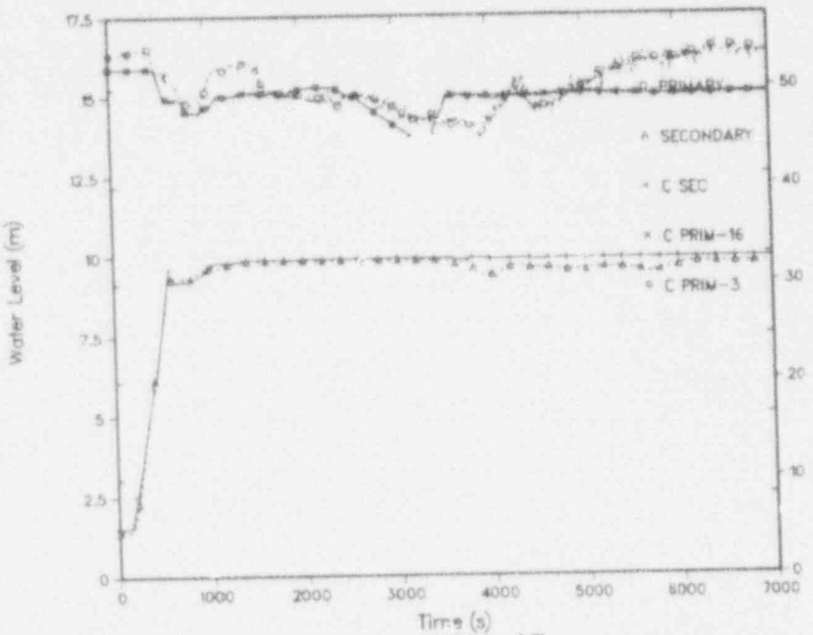

Fig. 17.
A-loop SG collapsed liquid levels.

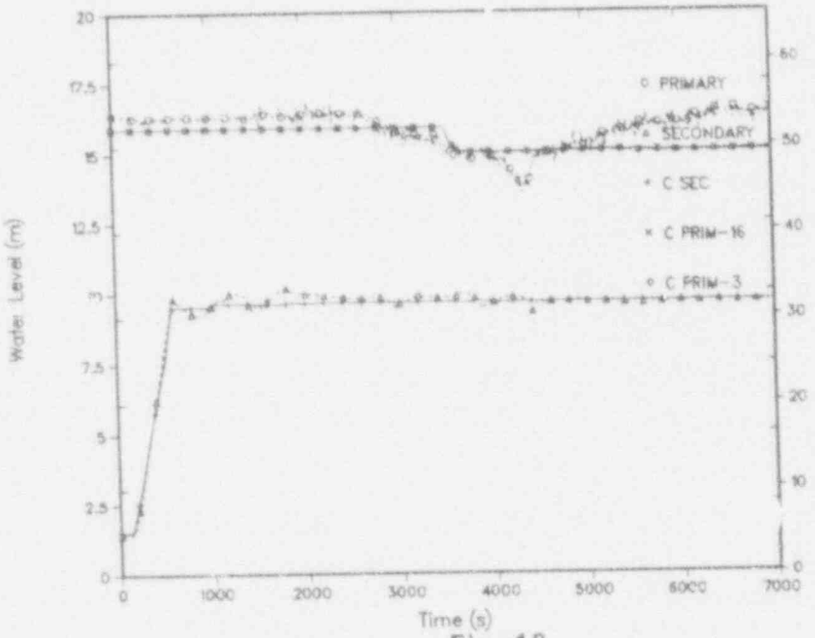

Fig. 18.
B-loop SG collapsed liquid levels.

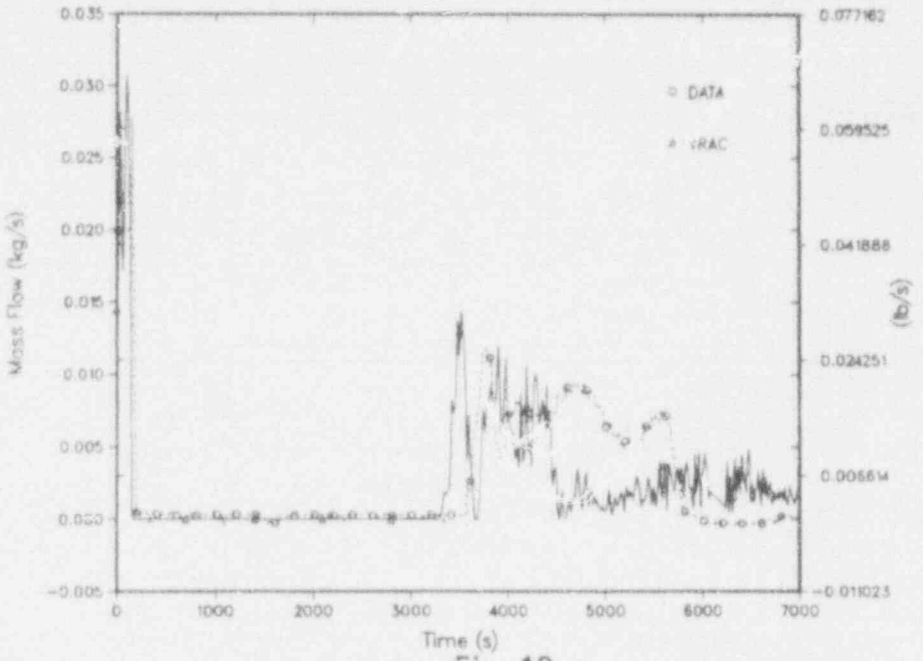

Fig. 19.

A-loop SG-secondary steam flow.

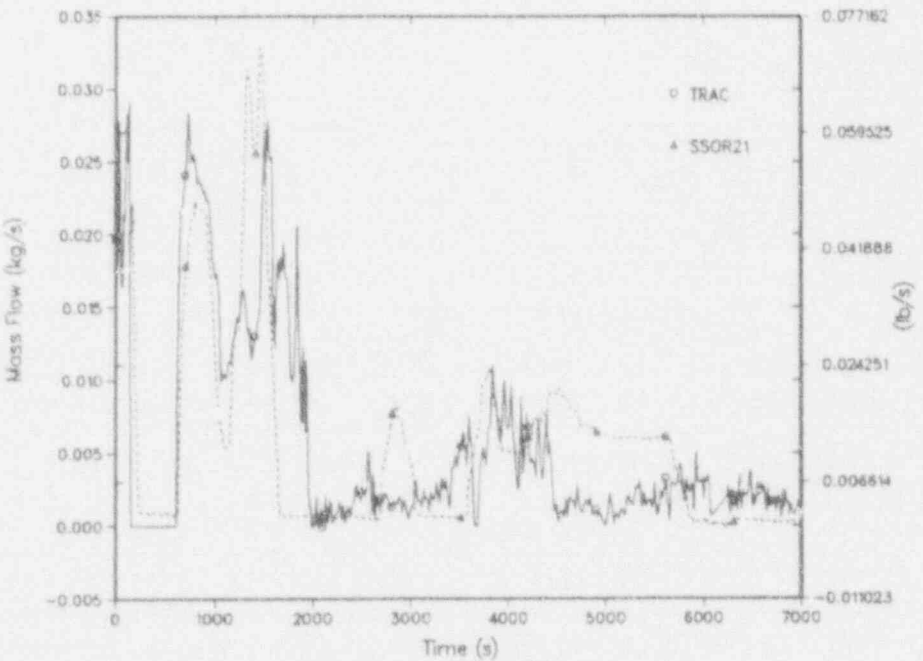

Fig. 20.

B-loop SG-secondary steam flow.

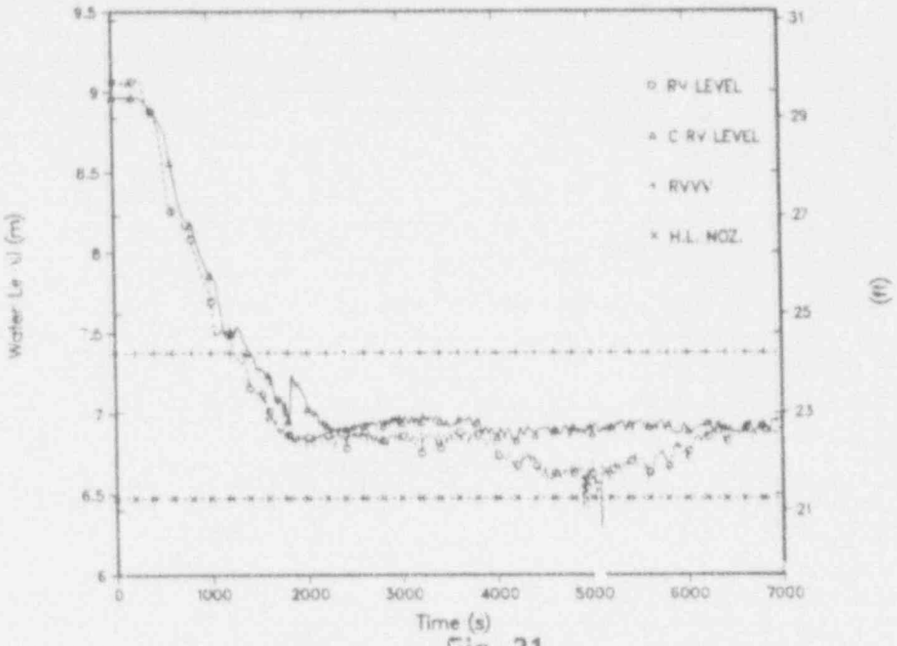

Fig. 21.
Reactor vessel collapsed liquid level.

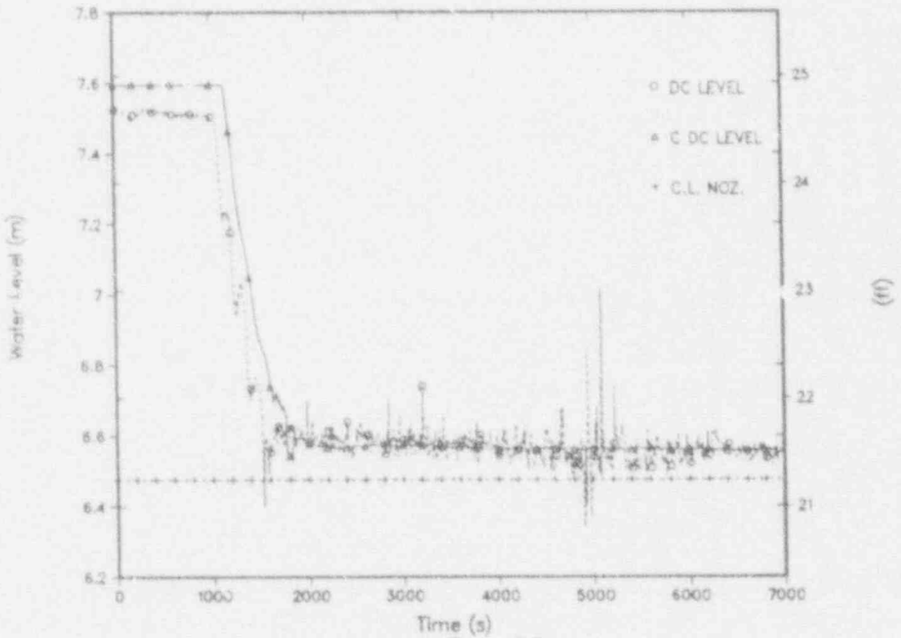

Fig. 22.
Downcomer collapsed liquid level.

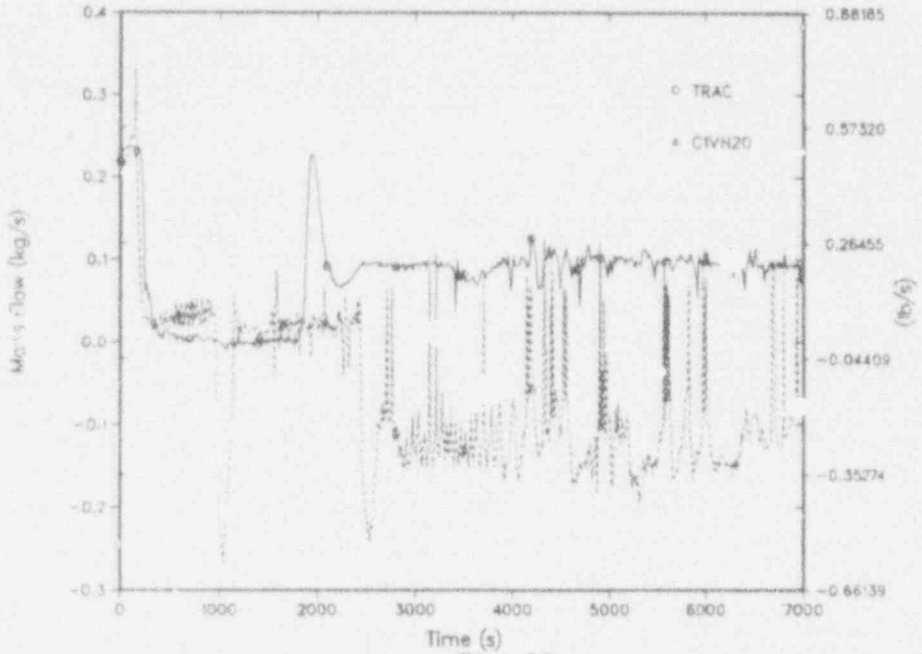

Fig. 23.
Cold leg A1 mass flow.

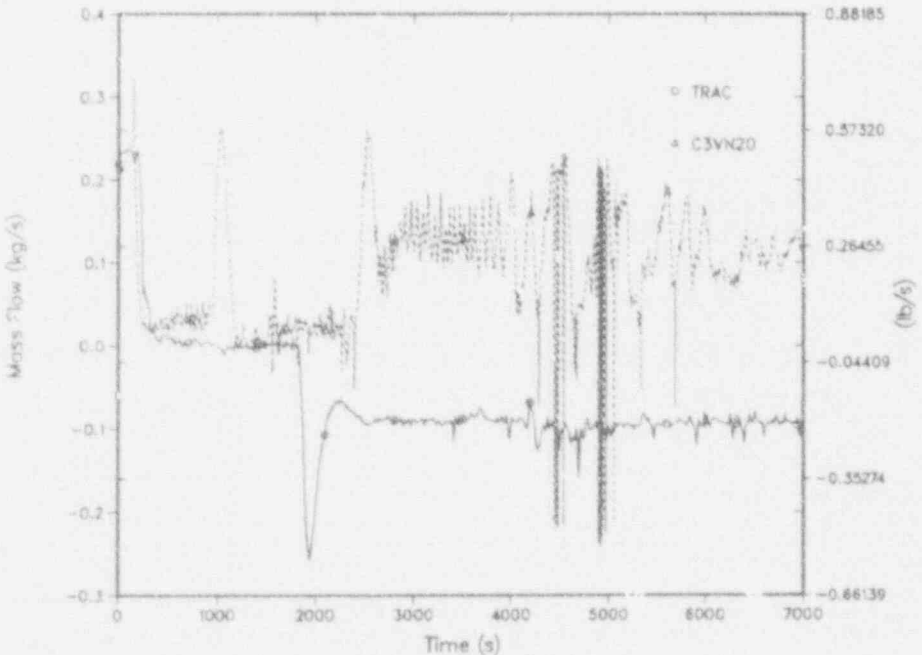

Fig. 24.
Cold-leg A2 mass flow.

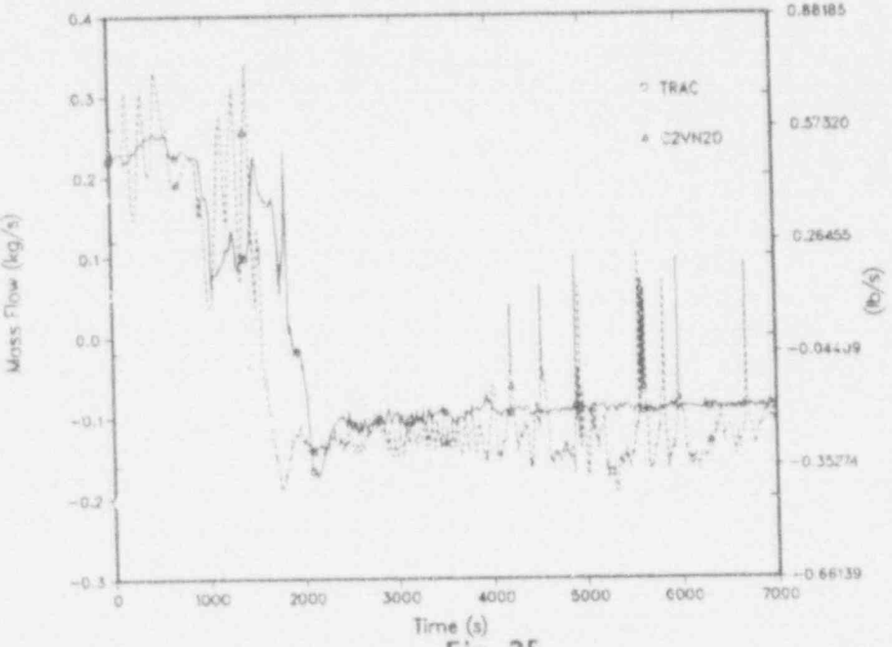

Fig. 25.
Cold-leg B1 mass flow.

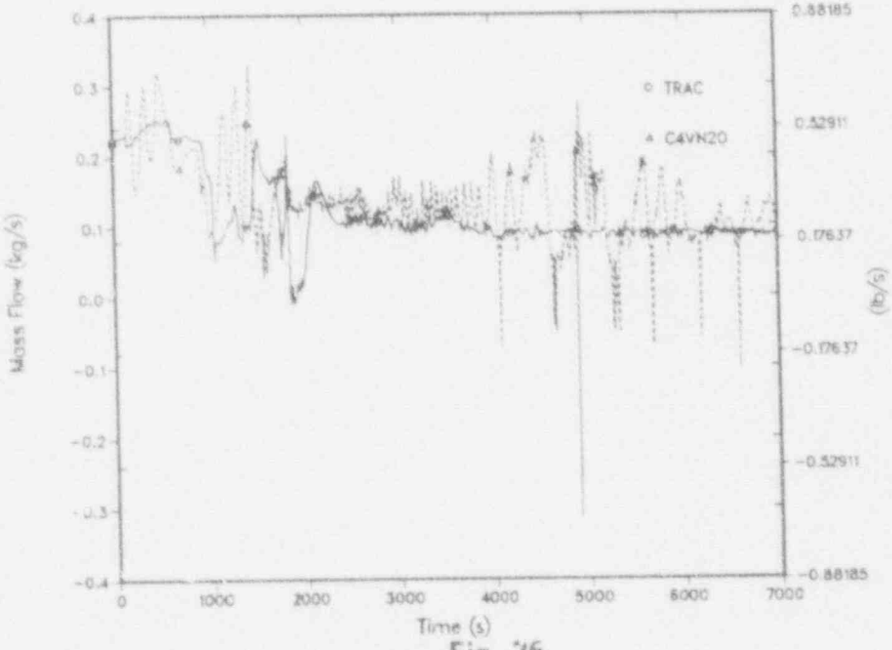

Fig. 26.
Cold-leg B2 mass flow.

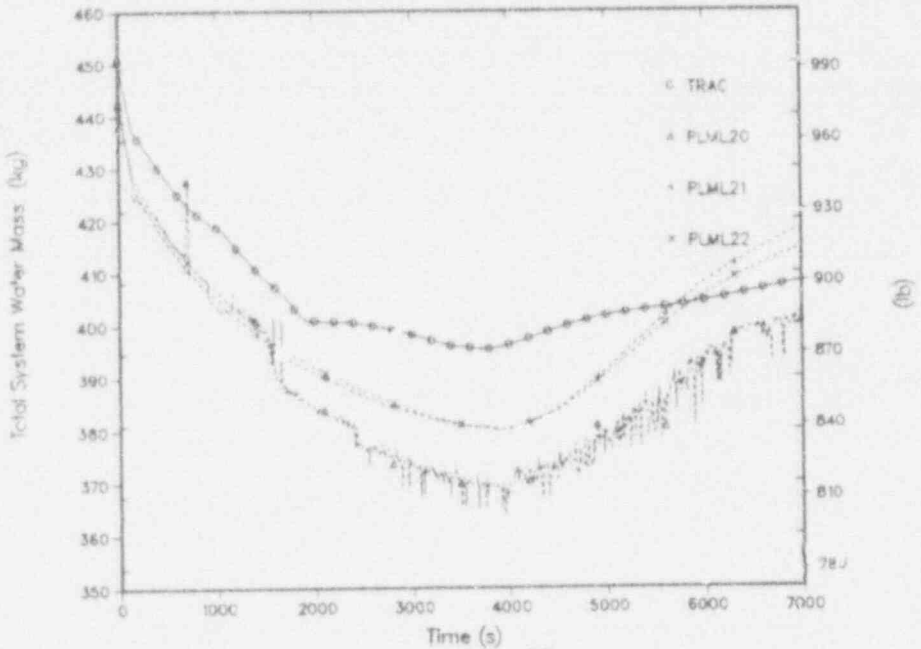

Fig. 27.
Primary liquid inventory.

APPENDIX A
TRAC MODEL OF MIST FACILITY

The MIST facility, shown in Fig. A-1, is a scale model of a B&W nuclear power plant. The facility is designed to investigate the effectiveness of plant automatic safety systems and operational procedures during postulated small-break and operational transients. The facility is primarily intended to investigate events occurring after reactor trip and reactor coolant-pump coast down. The MIST facility is scaled to a 2 x 4 lowered-loop prototype plant with 177 fuel assemblies. The scale factor is 1/817 for volume and power; component elevations are scaled one-to-one.

The TRAC model of the MIST facility has evolved over a period of time. The model was initially based on preliminary information provided in the MIST facility specifications (Ref. 5). It has progressed to its present form as available, as-built facility information was received from B&W. The final model compares very closely to the B&W REDBL5 model described in the MIST design verification report (Ref. 6). Archival information about the TRAC model used in this study is presented in Appendix A. A component schematic of the MIST model is shown in Fig. A-2. The model consists of 77 components that have been subdivided into 251 fluid cells. This model is considered to be finely noded and should be capable of providing reasonable results as shown in previous Once-Through Integral System (OTIS) calculations. Table A-I lists the components used for the MIST model and the number of fluid cells in each component. The outer walls of the vessel and loop-piping components are generally modeled as adiabatic boundaries since the MIST facility is guard heated to eliminate external heat losses. Localized uncompensated heat losses caused by cooled instruments are modeled using a constant heat-transfer coefficient at the component outer wall. The local heat-transfer coefficients were determined from heat-loss data provided by B&W. The following sections describe the modeling philosophy and actual modeling details of the various MIST facility components.

A. Reactor Vessel

A series of PIPE, TEE, PLENUM, and VALVE components has been connected to a 1-D CORE component to physically model the entire MIST reactor vessel (Fig. A-3). The 1-D CORE component (Component 3) is used to simulate the heated core region and a portion of the upper-plenum region from the core exit to an elevation slightly below the hot-leg nozzles. The heated core consists of a 7 x 7-rod array of which 45 rods are electrical heater rods and 4 rods simulate guide tubes. The axial power shape for the simulated rod is a chopped cosine profile and the radial power profile is flat. The hydraulic resistance from the rod-bundle grid spacers ($k = 0.57$) has been incorporated in the model. The core-power decay history is modeled using a trip-controlled table.

The upper-plenum and upper-head regions are modeled with Components 401–412, as shown in Fig. A-3. These one-dimensional components represent the geometry of the upper vessel region as follows: Components 401, 402, and 403 model the region inside the plenum cylinder; the annular region between the plenum cylinder and the vessel is modeled with Components 408–412; and the upper-head region above the plenum cylinder is represented by Components 404 and 405. RVVVs and vent-valve nozzles are modeled with a VALVE component (Component 7) that is connected to PLENUM Component 411.

The MIST RVVV system consists of four vent valves and connecting lines from the upper plenum to the upper downcomer. The actual system has been modeled as a single valve and associated piping. The valve-stroke time of 2.0 s and hydraulic-loss coefficient of 95.0 have been modeled. A trip-control system controls the opening and closing of the valve based on opening the valve when the pressure drop across the valve is 861.8 Pa (0.125 psi) and closing at 275.8 Pa (0.040 psi). An outer heat-transfer coefficient was applied to the valve to model the uncompensated localized heat loss of the valves of 1480 W (5.05×10^3 Btu/h).

The primary tube of TEE Component 2 represents the lower-plenum region, whereas the secondary tube models all the piping configuration connecting the lower plenum and the vertical downcomer. Components 103 and 104 model the 0.076-m (3-in.) sch 80 piping and the lower portion of the downcomer annulus region slightly below the cold-leg nozzles. Component 103 represents the piping that contains the cooled thermocouple (TC) and includes an outer heat-loss coefficient to model the TC's uncompensated heat loss of 1100 W (3.855×10^3 Btu/h). Component 8 is a PLENUM component used to model the connections of the cold-leg nozzles to the downcomer annulus. The upper portion of the downcomer annulus, RVVV nozzle, and CFT nozzle are sim[illegible] with TEE Component 9.

The fluid in the do[illegible]ner annulus region was initially assumed to follow one-dimensional behavior, and this was later verified in a sensitivity study that incorporated a three-dimensional model of the downcomer annulus region. The results of this study showed that, although small multidimensional effects were present in the downcomer annulus, they did not affect vessel and loop behavior as compared to results obtained with the one-dimensional downcomer model.

An ACCUM and a VALVE component were used to model the CFT system (Components 10 and 11). The CFT is initially 75% full of 316.5 K (110.3°F) water at a pressure of 4.137 MPa (600 psi). The surge line and valve are connected to the upper-downcomer region at the 7.087-m (23.25-ft) elevation. The VALVE component models the CFT isolation valve, which is dependent on calculated system conditions.

B. Intact Loop

In the MIST facility, the intact loop was designated as the loop containing the pressurizer. All components of the intact loop are shown in Fig. A-4 and described in Table A-1. The hot-leg nozzle and piping to the pressurizer surge line are simulated by the primary tube of Component 21. Also, an outer heat loss of 640 W (2.18×10^3 Btu/h) was modeled to simulate the heat loss of the viewports and densitometer located near the hot-leg nozzle region. The secondary tube represents the pressurizer surge line. Components 22 and 23 model the pressurizer and PORV, respectively. The balance of the hot leg is represented by Components 108, 25, and 109. Component 25 included a connection to the HPV valve and an outer heat-transfer coefficient to model an uncompensated heat loss of 170 W (0.58×10^3 Btu/h) through a viewport in the U-bend.

The MIST intact-loop SG was modeled with an STGEN component (Component 29) and two PLENUM components (Components 28 and 30) as shown in Fig. A-5. Considerable effort was expended on the SG model during the OTIS posttest calculations and in preliminary MIST posttest calculations. The STGEN Component 29 includes two parallel fluid channels to represent the primary side of the intact-loop MIST SG. The first channel represents the 16 tubes not wetted on the outside by the AFW, and the second channel represents the 3 tubes adjacent to the AFW injection nozzle on the secondary. Both of the primary channels

are divided into 12 axial cells. The secondary side of the MIST intact loop SG was modeled with a single fluid channel, also consisting of 12 axial cells. Three TEEs and a PIPE were used for the secondary side . Two TEE side legs were used for the SG downcomer. The falling-film heat transfer from the AFW is calculated using a code update that redistributes the liquid in each of the secondary cells to the heat slabs connected to the three-tube primary channel. In addition to the liquid redistribution, a multiplier is applied to the Chen correlation heat-transfer coefficient for the wetted channel heat slabs. The head-versus-flow curve for the SG AFW is modeled with FILL Component 31.

Components 28 and 30 model the inlet and exit plena, respectively, and provide the connection between the loop piping and SG-primary tubes. The lower tube sheet and outer shell wall have been included in the heat-transfer data. No special code models have been used to vary the tube wetted areas or the heat-transfer coefficients based on AFW flow.

The split cold legs from the SG exit plenum to the downcomer consist of Components 34, 117, 118, 36, 38, 115, 116, and 40. The pump-suction piping, pump-discharge piping, and HPI por are modeled by these components. Each pump suction and discharge line is constructed of 0.051-m (2-in.) sch 80 piping, 10.82 m (35.5 ft) and 1.75 m (5.74 ft) in length, respectively. The two primary-coolant pumps located in the intact-loop cold legs are modeled with PUMP Components 35 and 39. Each of the identical PUMP components represents a fluid volume of 0.007334 m^3 (0.26 ft^3) and a flow length of 1.608 m (5.28 ft) and models the locked-rotor resistance of the MIST pumps. Uncompensated local heat losses of 1350 W (4.61×10^3 Btu/h) per pump are modeled by outer heat-transfer coefficients in the PUMP components.

C. Broken Loop

The broken-loop piping and SG components are shown in Figs. A-6 and A-7. These components are described in Table A-1, and they are identical to the corresponding intact-loop components, except that there is no pressurizer connection to the broken loop. Thus, PIPE Component 105 in the broken-loop hot leg is identical to the primary side of TEE Component 21 in the intact-loop hot leg. The broken-loop SG is modeled in exactly the same manner as the intact-loop SG with STGEN Component 54 and PLENUM Components 53 and 55.

D. HPI System

The HPI system is modeled with Components 41, 59, and 37. FILL Component 41 is used to model the HPI fluid conditions and flow rate. The HPI flow rate used in Component 41 is determined in a series of control blocks, which monitor the calculated cold-leg pressure, pressurizer level, and core-exit subcooling. Using these parameters, the control blocks model the head-flow characteristics of the HPI pump and the logic for the HPI actuation and throttling of the HPI flow. The HPI flow rate determined in the control blocks is then used in FILL Component 41. The HPI piping and manifold are modeled with PIPE Component 59 and PLENUM Component 37, the latter of which is connected to each cold-leg pump discharge.

E. Controls

The steady-state and transient-control functions are modeled using signal variables, control blocks, and trips. These control parameters are used to control the core power, SG AFW and discharge flows, HPI flow, RVVVs, the PORV, and the CFT isolation valve. The transient

control logic is implemented in the input for the steady-state calculation, thus simplifying the transient restart input. Most of the control logic is modeled using control blocks; the control parameters are evaluated once each time step.

TABLE A-I
COMPONENT DESCRIPTION OF MIST MODEL

Component Numbers	Component Description	Number of Cells
1	Bottom of reactor vessel	1
2	Lower plenum and lower downcomer	3
3	Core and upper plenum	7
401	Upper plenum, hot-leg elevation	3
402	Upper plenum, middle section	2
403	Upper plenum, upper section	2
404	Upper head, lower section	1
405	Upper head, upper section	1
406	Top of reactor vessel	1
407	Upper-plenum cylinder, bottom cap	1
408	Upper-plenum cylinder, lower section	1
409	Upper-plenum cylinder, hot leg connections	1
410	Upper-plenum cylinder, middle section	1
411	Upper-plenum cylinder, vent valve connections	1
412	Upper-plenum cylinder, upper section	1
7	Reactor vessel vent valve	4
8	Downcomer (cold-leg nozzle connections)	1
9	Upper downcomer	5
103	Lower downcomer	1
104	Lower downcomer	4
10	Core flood tank valve	2
11	Core flood tank	3
21	Loop A hot leg (lower section)	8
22	Pressurizer	4
23	PORV	2
24	Pressurizer atmospheric boundary	1
108	Loop A hot leg	4
25	Loop A hot leg (upper section)	2
26	Loop A high-point vent valve	2
27	Loop A high-point vent atmospheric boundary	1
109	Loop A hot leg	3
28	Loop A STGEN inlet plenum	1
29	Loop A STGEN	42
30	Loop A STGEN exit plenum	1
31	Loop A STGEN high AFW fill	1

TABLE A-I (cont.)

COMPONENT DESCRIPTION OF MIST MODEL

Component Numbers	Component Description	Number of Cells
91	Steam Line	2
32	Loop A STGEN secondary atm. boundary	1
34	Cold-leg A1 pump suction	2
117	Cold-leg pump suction	1
118	Cold-leg pump suction	3
35	Cold-leg A1 pump	2
36	Cold-leg A1 pump discharge	5
38	Cold-leg A2 pump suction	2
115	Cold-leg pump suction	1
116	Cold-leg pump suction	3
39	Cold-leg A2 pump	2
40	Cold-leg A2 pump discharge	5
105	Loop B hot leg (lower section)	4
106	Loop B hot leg (upper section)	4
50	Loop B hot leg	2
51	Loop B high-point vent valve	2
52	Loop B high-point vent atmospheric boundary	1
107	Loop B hot leg	3
53	Loop B STGEN inlet plenum	1
54	Loop B STGEN	42
95	Steam line	2
69	Loop B STGEN secondary atmospheric boundary	1
68	Loop B STGEN upper auxiliary feed	1
55	Loop B STGEN exit plenum	1
56	Cold-leg B2 pump suction	2
119	Cold-leg B2 pump suction	1
120	Cold-leg B2 pump suction	3
57	Cold-leg B2 pump	2
58	Cold-leg B2 pump discharge	5
60	Cold-leg B1 pump suction	3
61	Cold-leg B1 pump-suction leak valve	2
62	Leak atmospheric boundary	1
121	Cold-leg B1 pump suction	1
63	Cold-leg B1 pump	2
122	Cold-leg B1 pump suction	3
64	Cold-leg B1 pump discharge (upper)	4
66	Cold-leg B1 pump discharge (lower)	2

TABLE A-I (cont.)
COMPONENT DESCRIPTION OF MIST MODEL

Component Numbers	Component Description	Number of Cells
67	Cold-leg B1 pump-discharge leak valve	2
80	Leak atmospheric boundary	1
37	HPI manifold	1
41	HPI fill	1
59	Connection between HPI fill and manifold	1
	Components	77
	Fluid cells	276

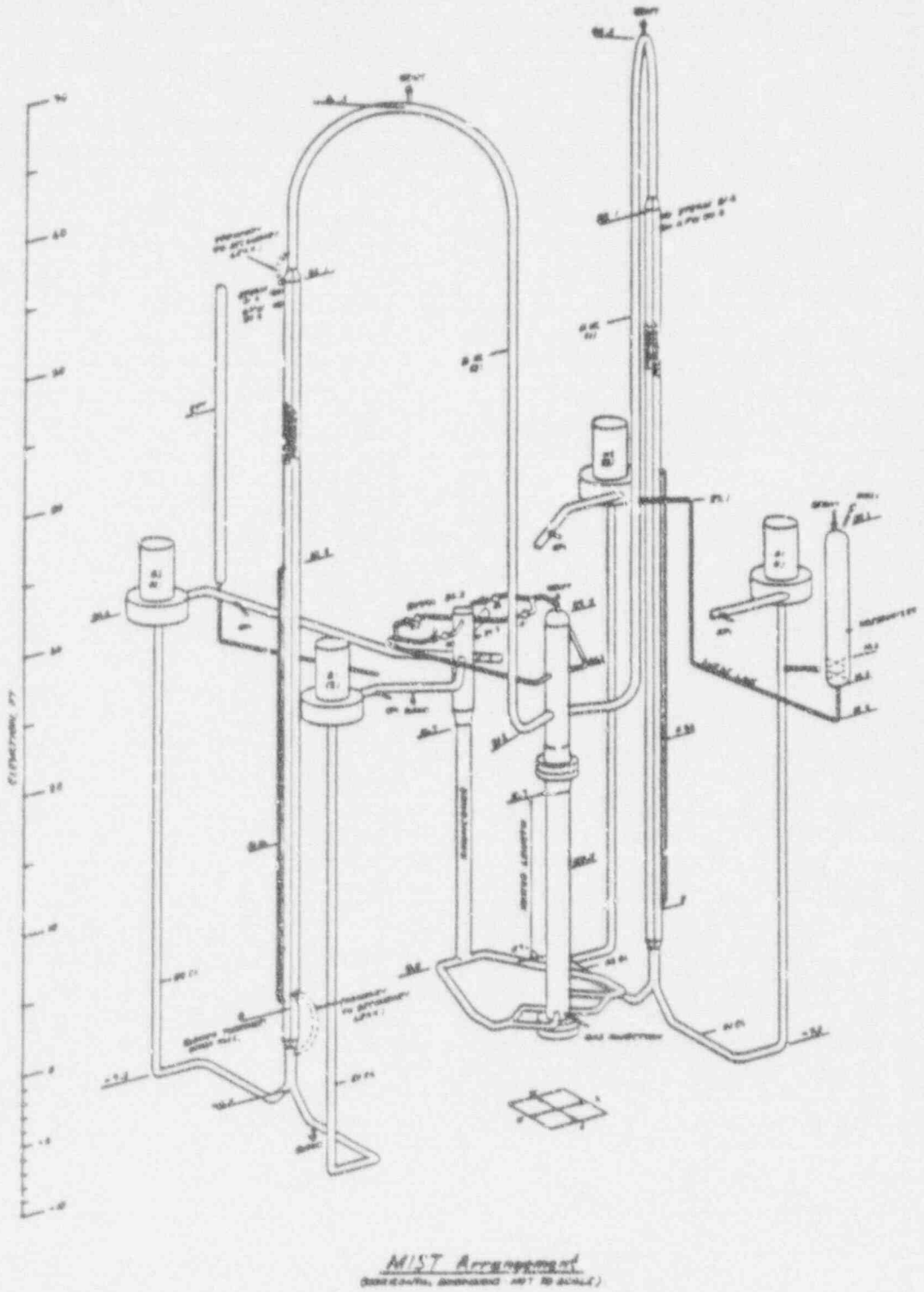

Fig. A-1.
MIST facility isometric.

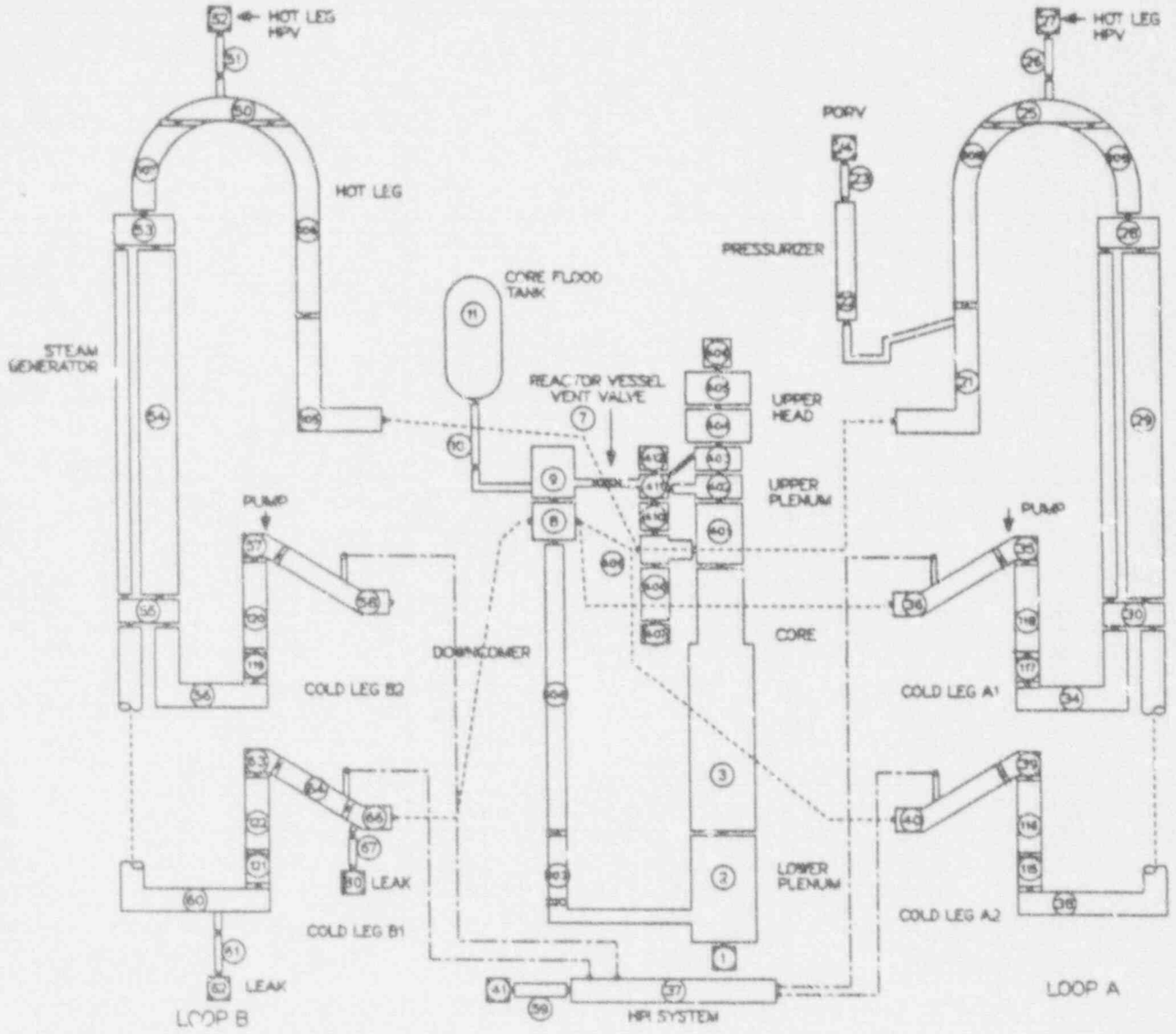

Fig. A-2.
TRAC component noding schematic of MIST facility.

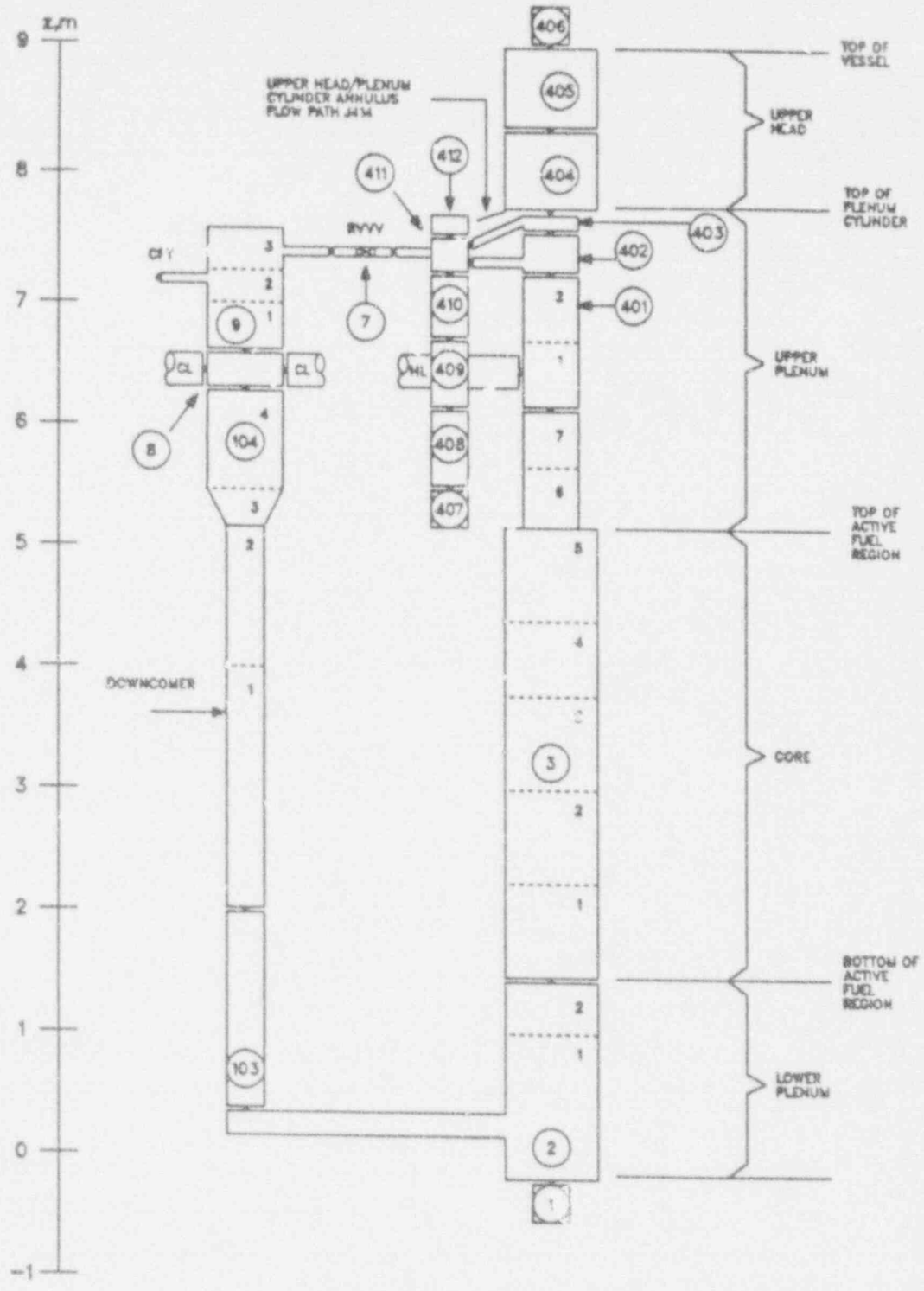

Fig. A-3.
TRAC reactor vessel noding schematic of MIST facility.

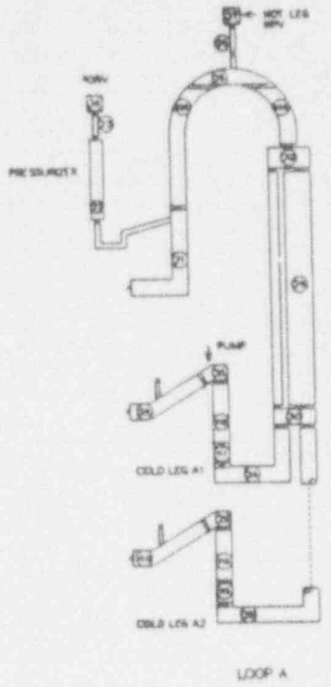

Fig. A-4.
TRAC A-loop noding schematic of MIST facility.

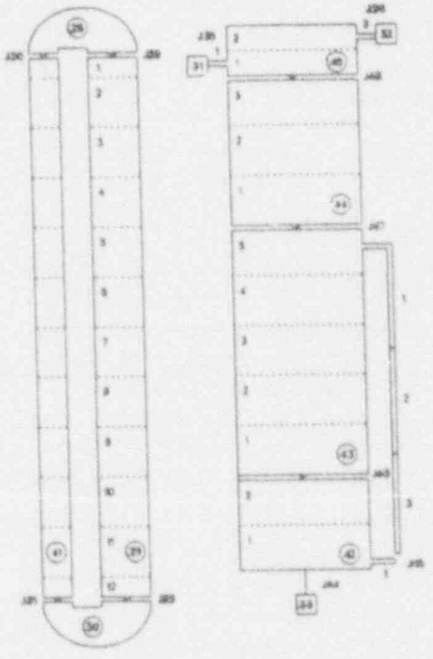

Fig. A-5.
TRAC A-loop SG noding schematic.

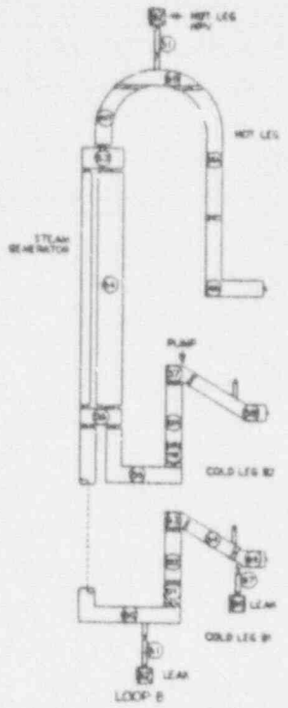

Fig. A-6.
TRAC B-loop noding schematic of MIST facility.

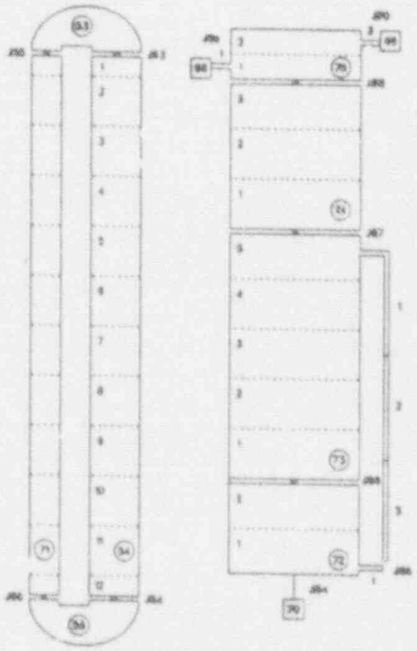

Fig. A-7.
TRAC B-loop SG noding schematic.

APPENDIX B
ARCHIVAL INFORMATION

I. CODE IDENTIFICATION AND STORAGE

TRAC-PF1/MOD1 with error correction sets through 12.7 was used for the posttest calculation of MIST Test 3109AA. The program library and updates required to recreate this code are stored on the Los Alamos Central File System (CFS) and may be accessed through the following path:

/Q9TRAC/ARCHIVES/12.7

In addition, a MIST-specific code update named STGN1X was used. Initialization of the MIST facility in natural circulation rather than pumped flow caused modeling difficulties unique to this facility. An accurate prediction of SG heat-transfer distribution is necessary to correctly predict steady-state loop flows and hence initial system pressure and temperatures. Code modifications were required to achieve this. A list of this update is provided at the end of this appendix.

II. INPUT DECK STORAGE

The TRAC input deck, which contains the model of the MIST facility, is permanently stored in the TRAC Input Deck Archive (TIDA) on the Los Alamos CFS and may be accessed through the following path:

/TIDA/EXPERIMENT/MIST/number of this report, *e.g.*, LA-CP-XX-XXXX

III. CALCULATION FILE STORAGE

The output (TRCMSG, TRCOUT, TRCGRF, TRCDMP) files generated by TRAC during the calculation of MIST Test 330302 are stored on the Los Alamos CFS and may be accessed through the following path:

/ISTP/MIST/POSTTEST/3109AA

These files will be maintained for a minimum of one year from the publication date of this report.

IV. UPDATE STGN1X LISTING

This update is a hardwired change to the code logic for distributing high-elevation AFW between wetted and unwetted tube regions on the SG secondary. This update is specific to the MIST facility and will not be incorporated into a released version of TRAC-PF1/MOD1. This update is permanently stored in the TIDA on the Los Alamos CFS and may be accessed through the following path:

/TIDA/EXPERIMENT/MIST/number of this report, *e.g.*, LA-CP-XX-XXXX

```
*id mistcu
*i stgn1x.15                    stgn1x
c
c  iflgw is flag to detect steam generator tube heat
c            structure which is wetted by the afw
c
c  iflgwc is flag to detect a wetted steam generator tube heat
c            structure to which the chen muitiplier is applied
c
c  iflgd is flag to detect steam generator tube heat
c            structure which is not wetted by the afw
c
c  hlc1 and hlc0 are the multiplier and additive constant for
c  the liquid heat transfer coefficient
c
c  hvc1 and hvc0 are the multiplier and additive constant for
c            the vapor heat transfer coefficient
c
c  alphamw is the maximum void fraction used to determine
c            the heat transfer coefficients for the wetted
c            steam generator tubes above the pool
c
c  alphad is the void fraction used to determine the heat
c            transfer coefficients for the unwetted steam
c            generator tubes above the pool
c
c  alpha0 is the minimum void fraction for identifying steam
c            generator secondary cells which are above the liquid pool
c
c  alpha1 is the minimum void fraction for reducing the void
c            fraction used to determine the heat transfer coefficients
c            for the wetted steam generator tubes above the pool
c
c            alpha2 is the maximum void fraction for reducing the void
c  fraction used to determine the heat transfer coefficients
c  for the wetted steam generator tubes above the pool
c
      data iflgw    ,iflgwc   ,iflgd   / 0.0 , 0.0     , 0.0    /
      data alpha0   ,alpha1   ,alpha2  / 0.9 , 0.95    , 0.9999 /
      data alphamw  ,alphad            / 1.0 , 0.9965  /
      data hlc0     ,hlc1              / 0.0 , 1.8     /
      data hvc0     ,hvc1              / 0.0 , 1.0     /
c
*i uphgam.144
c
c  check for slab which is wetted by the afw
c
   if(i .ge. (ncell1 + 1) .and. i .le. (2*ncell1-1)) iflgw = 1
c
c  check wetted slab to determine whether to apply chen multiplier
c
   if(iflgw .eq. 1 .and. a(lalp+io) .ge. alpha0
   +          .and. a(lalp+io) .lt. alpha2) iflgwc = 1
c
c  check for slab which is not wetted by the afw
c
   if(i .ge. 1 .and. i .le. (ncell1-1)) iflgd = 1
c
c
   alpha = a(lalp+io)
c
c
c  reset alpha for dry slabs above pool
c
```

```
      if(iflgd .eq. 1 .and. a(lalp+io) .ge. alpha0) then
        if(a(lalp+io) .le. alpha2) alpha = alphad
        if(a(lalp+io) .gt. alpha2) alpha = amax1(a(lalp+io),alpha4)
      endif
c
c
c     reset alpha for wetted slabs above pool
c
      if(iflgw .eq. 1 .and. a(lalp+io) .ge. alpha0) then
        if(a(lalp+io) .gt. alpha2) alphamw = 1.
        if(a(lalp+io) .le. alpha2) alphamw = alpha1
        alpha = amin1(a(lalp+io),alphamw)
      endif
c
c
*d stgn1x.86
      * alpha,a(lsig+io),grvg,vlz,vlz,zero,vvz,zero,zero,
*i uphgam.146
c
c     apply chen multiplier for slab with iflgwc = 1
c     and heat transfer mode = 7
c
      if (iflgwc .eq. 1 .and. a(lidgho+im1) .eq. 2.) then
        a(lholgn+im1) = a(lholgn+im1) * hlc1 + hlc0
        a(lhovgn+im1) = a(lhovgn+im1) * hvc1 + hvc0
      endif
c
      iflgw = 0
      iflgwc = 0
      iflgd = 0
c
```

APPENDIX C

CODE ASSESSMENT DESCRIPTOR DEFINITIONS

The code assessment descriptors are used to provide an overall characterization of how TRAC predicted the thermal-hydraulic behavior in the MIST facility. Four descriptors are used to characterize the degree of agreement and the application consequences of either the agreement or lack of agreement. The four descriptors are **excellent agreement, reasonable agreement, minimal agreement,** and **insufficient agreement**. Each of these descriptions is defined below along with the consequences for future application of the code in the given area being characterized and the perceived need for additional code development.

Excellent agreement is an appropriate descriptor when the code exhibits no deficiencies in modeling a given behavior. Major and minor phenomena and trends are correctly predicted. The calculated results are judged by the analyst to be close to the data with which a comparison is being made. If the uncertainty of the data has been identified and made available to the analyst, the calculation will, with few exceptions, lie within the uncertainty band of the data. The code may be used with confidence in similar applications. Neither code models nor the facility noding model require examination or change.

Reasonable agreement is an appropriate descriptor when the code exhibits deficiencies, but the deficiencies are minor; that is, the deficiencies are acceptable because the code provides an acceptable prediction of the test. All major trends and phenomena are correctly predicted. Differences between the test and calculated traces of parameters identified as important by the analyst are greater than those deemed necessary for excellent agreement. If uncertainty data are available, the calculation will frequently lie outside the uncertainty band. However, the analyst believes that the discrepancies are not sufficiently large to require a warning to potential users of the code in similar applications. The assessment analyst believes that the correct conclusions about trends and phenomena would be reached if the code were used in similar applications. The code models and/or facility noding model should be reviewed to see if improvements can be made.

Minimal agreement is an appropriate descriptor when the code exhibits deficiencies and the deficiencies are significant; that is, the deficiencies are such that the code provides a prediction of the test that is only conditionally acceptable. Some major trends or phenomena are not predicted correctly while others are predicted correctly. Some TRAC calculated values lie far outside the uncertainty band of the data with which a comparison is being made. The assessment analyst believes that incorrect conclusions about trends and phenomena may be reached if the code were used in similar applications. The analyst believes that certain code models and/or the facility noding model must be reviewed, corrections made, and a limited assessment of the revised code or input models made before the code can be used with confidence for similar applications. A warning should be issued to the TRAC user community that the user applying the code in similar applications risks drawing incorrect conclusions. This warning should stay in force until the identified review, modification, and limited assessment activities are completed and the resultant characterization descriptor is "reasonable" or better.

Insufficient agreement is an appropriate descriptor when the code exhibits major deficiencies; that is, the deficiencies are such that the code provides a prediction of the test that is unacceptable. Major trends are not predicted correctly. Most TRAC calculated values lie far

outside the uncertainty band of the data with which a comparison is being made. The assessment analyst believes that incorrect conclusions about trends and phenomena are probable if the code is used in similar applications. The analyst believes that certain code models and/or the facility noding model must be reviewed, corrections made, and a limited assessment of the revised code or facility noding model made before the code can be used with confidence for similar applications. A warning should be issued to the TRAC user community that the code must not be used for similar applications until the identified review, modification, and limited assessment activities are completed and the resultant characterization descriptor is "reasonable" or better.

APPENDIX D

PERFORMANCE INDICATORS

A comparison of CPU time versus transient time for the calculation of MIST Test 3109AA on a CRAY-1S computer at Los Alamos National Laboratory is presented in Fig. D-1. Plots of time-step size versus real time and number of time steps versus real time are presented in Figs. D-2 and D-3, respectively. The time-step data presented in Fig. D-2 illustrate that larger time steps up to the input limit of 0.15 s were possible when the primary system was in single-phase natural circulation. After the liquid level decreased to about the RVVV elevation, the code selected reduced time-step sizes because of changing void fractions in the small cells used for the plenum cylinder at the vent valve elevation. The time step after this occurred at about 2000 s was in the range of about 0.03 to 0.04.

The "grind" time for this calculation is calculated from the equation:

$$\text{Time} = (\text{CPU} \times 10^3) / (\text{C} \times \text{DT}) \ ,$$

where CPU = total execution time in seconds,
C = total number of volumes in the model, and
DT = total number of time steps.

The resultant time is expressed in milliseconds per computational volume per time step.

For the MIST Test 3109AA, the CPU time was 75 000 s, the total number of volumes in the MIST facility model was 251, and the total number of time steps was 165 000. Thus,

$$\text{Time} = (7.5 \times 10^4 \times 10^3) / (251 \times 1.65 \times 10^4)$$

Time = 18.1 milliseconds per volume per time step.

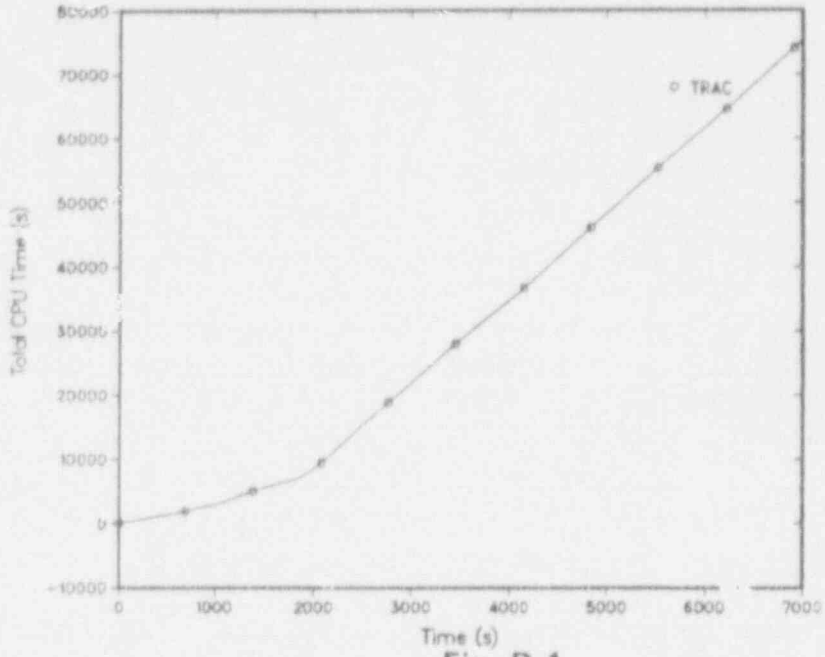

Fig. D-1.
CPU time vs real time for Test 3109AA

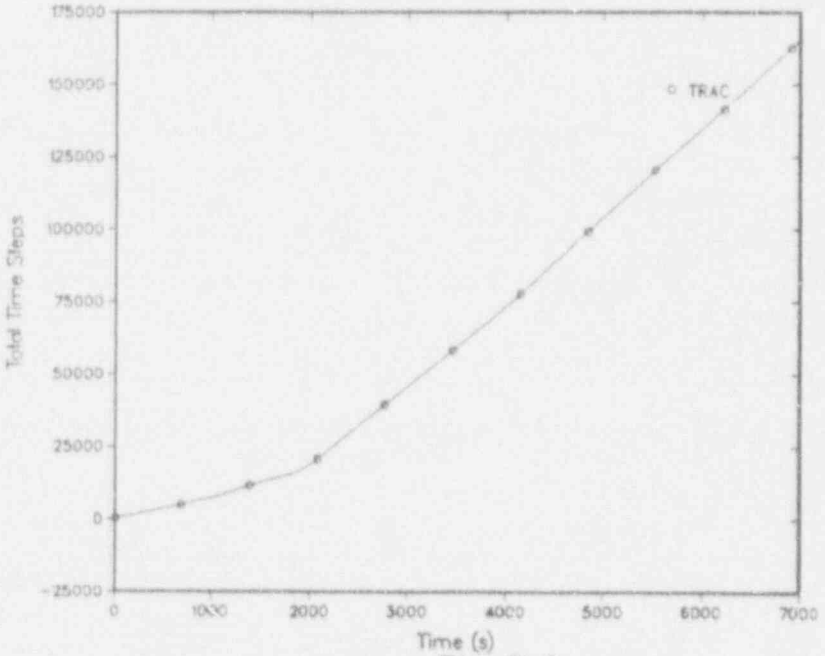

Fig. D-2.
Time-step size vs real time for Test 3109AA

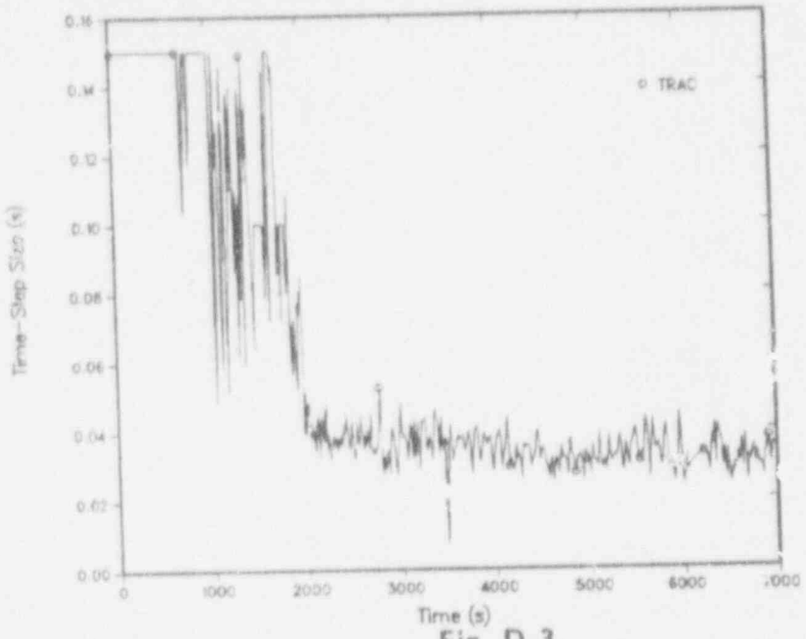

Fig. D-3.
Number of time steps vs real time for Test 3109AA

NRC FORM 335 (2-89) NRCM 1102, 3201, 3202

U.S. NUCLEAR REGULATORY COMMISSION

BIBLIOGRAPHIC DATA SHEET

1. REPORT NUMBER (Assigned by NRC, Add Vol., Supp., Rev., and Addendum Numbers, if any.)

NUREG/CR-5887
LA-UR-89-2158

2. TITLE AND SUBTITLE

Posttest Analysis of MIST Test 3109AA Using TRAC-PF1/MOD1

3. DATE REPORT PUBLISHED

MONTH: September | YEAR: 1992

4. FIN OR GRANT NUMBER

A7311

5. AUTHOR(S)

James L. Steiner, Donald A. Siebe, Brent E. Boyack

6. TYPE OF REPORT

Technical

7. PERIOD COVERED (Inclusive Dates)

8. PERFORMING ORGANIZATION – NAME AND ADDRESS (If NRC, provide Division, Office or Region, U.S. Nuclear Regulatory Commission, and mailing address; if contractor, provide name and mailing address.)

Los Alamos National Laboratory
Los Alamos, NM 87545

9. SPONSORING ORGANIZATION – NAME AND ADDRESS (If NRC, type "Same as above"; if contractor, provide NRC Division, Office or Region, U.S. Nuclear Regulatory Commission, and mailing address.)

Division of Systems Research
Office of Nuclear Regulatory Research
U. S. Nuclear Regulatory Commission
Washington, DC 20555

10. SUPPLEMENTARY NOTES

None

11. ABSTRACT (200 words or less)

We have completed a posttest calculation and analysis of Multi-loop Integral System Test (MIST) 3109AA as the nominal test for the MIST program. It is a test of a small-break loss-of-coolant accident (SBLOCA) with a scaled 10-cm^2 break in the B1 cold leg. The test exhibited the major post-SBLOCA phenomena, as expected, including depressurization to saturation, intermittent and interrupted loop flow, boiler-condenser mode cooling, refill, and postrefill cooldown. Full high-pressure injection and auxiliary feedwater were available, reactor coolant pumps were not available, and reactor-vessel vent valves and guard heaters were automatically controlled. Constant level control in the steam-generator secondaries was used after steam-generator secondary refill and symmetric steam-generator pressure control was used. We performed the calculation using TRAC-PF1/MOD1. We found that agreement between test data and the calculation was generally reasonable. All major trends and phenomena were correctly predicted. We believe that the correct conclusions about trends and phenomena will be reached if the code is used in similar applications.

12. KEY WORDS/DESCRIPTORS (List words or phrases that will assist researchers in locating the report.)

Thermal Hydraulic Analysis
Multi-Loop Integral System Test (MIST)
Small-break loss of coolant accident (SBLOCA)
TRAC-PF1/MOD1
MIST Test 3109AA

13. AVAILABILITY STATEMENT

Unlimited

14. SECURITY CLASSIFICATION

(This Page) Unclassified

(This Report) Unclassified

15. NUMBER OF PAGES

16. PRICE

NRC FORM 335 (2-89)

Federal Recycling Program

UNITED STATES
NUCLEAR REGULATORY COMMISSION
WASHINGTON, D.C. 20555-0001

OFFICIAL BUSINESS
PENALTY FOR PRIVATE USE, $300

FIRST CLASS MAIL
POSTAGE AND FEES PAID
USNRC
PERMIT NO. G-67

ISBN 0-16-038195-9

UNITED STATES
NUCLEAR REGULATORY COMMISSION
WASHINGTON, D.C. 20555-0001

OFFICIAL BUSINESS
PENALTY FOR PRIVATE USE, $300

FIRST CLASS MAIL
POSTAGE AND FEES PAID
USNRC
PERMIT NO. G-67

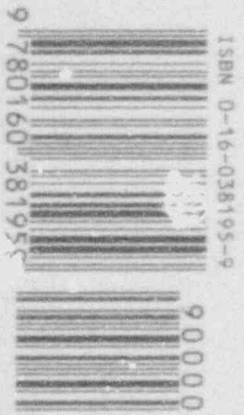

ISBN 0-16-038195-9